# Power Flow and Structure-Borne Noise

*in medium frequency range*

Wachulec, Marcin

*Publication date:*
2002

*Document Version*
Publisher's PDF, also known as Version of record

# Power Flow and Structure-Borne Noise

## in Medium Frequency Range

**Marcin Wachulec**

**PhD Thesis**

Structural Dynamics Group
Department of Civil Engineering
Aalborg University 2002

# Power Flow and Structure-Borne Noise in Medium Frequency Range

Marcin Wachulec

Department of Civil Engineering
Aalborg University

December 2001

Ph.D. Thesis
The European Doctoral School
of Technology and Science
at Aalborg University, DENMARK

# Abstract

The method of power flow analysis within a structure depends on the frequency considered. For the low frequencies the standard Finite Element Method (FEM) can be used efficiently. In the high frequencies the Statistical Energy Analysis (SEA) proved its usefulness. The distinction between low and high frequency is not straightforward and depends on such factors like geometry, material properties or level of uncertainty of these parameters. In built-up structures the definition of low and high frequency ranges becomes increasingly difficult, because the members might differ in terms of their dynamic properties. The term medium frequency range is used to describe the range of frequencies where it is not possible to use a single method to describe the behaviour of the structure. The assembly of thin plates is a good example of built-up structure because of the differences between the properties in plane and out of plane of the plate.

For the reasons mentioned there is a need for development alternative methods for power flow estimation that could be applied in the medium frequency range. In this thesis the idea of coupling FEM and SEA in a hybrid formulation is explored. The hybrid formulation requires partition of co-ordinates into sets corresponding with global and local motions. The hierarchical formulation of FEM is used to implement the hybrid approach. This gives the possibility to modify the calculations without making changes in the model. The hierarchical formulation has also additional properties that the high order co-ordinates behave in similar manner as the high order normal modes.

The hierarchical formulation is developed in this thesis that allows for modelling plate assemblies in an efficient way. The implementation is verified versus standard results, both numerical (FEM) and analytical.

In the last part the expressions that define the interaction between deterministic and statistical description are defined based on the hierarchical formulation. The definition of coupling is a crucial step in the application of hybrid method for analysis of plate assemblies. An example of analysis of the simple structure by the hybrid method is also presented.

# Acknowledgement

The present thesis has been prepared in connection with a Ph.D. study carried out in the period October 1998 to November 2001 at the Department of Building Technology and Structural Engineering and the Department of Civil Engineering, Aalborg University, Denmark. The financial support provided by The Danish Technical Research Council within the project: 'Damping Mechanisms in Dynamics of Structures and Materials' is highly appreciated.

I would like to thank Poul H. Kikegaard, my supervisor and Søren R.K. Nielsen for the supervision and guidance during my study at Aalborg University, DK. I would also like to thank Robin S. Langley for his help during my visit at the Department of Engineering, University of Cambridge, UK.

I would like to thank my friends at the Structural Dynamics Laboratory at Aalborg University and Dynamics and Vibration Group at University of Cambridge for the fruitful discussions and support. I am grateful to Solveig Hesselvang for proof reading of the thesis.

Finally, I would like to thank Aneta and Malgosia for their patience and my parents for their support.

# Contents

# List of Figures

# List of Tables

# List of Symbols

## Greek Symbols

| | |
|---|---|
| $\Pi$ | power |
| $\mathbf{\Pi}^{ext}$ | vector of power supplied by external loading |
| $\Pi^{ext}$ | power supplied by external loading |
| $\Pi^{diss}$ | power dissipated |
| $\Pi_{ij}$ | power transmitted from subsystem $i$ to subsystem $j$ |
| $\boldsymbol{\Phi}$ | vector potential of displacement field |
| $\tilde{\mathbf{\Psi}}$ | vector of mode shapes |
| $\tilde{\mathbf{\Psi}}_i$ | mode shape |
| $\mathbf{\Psi}$ | vector of shape functions |
| $\mathbf{\Psi}^{(e)}$ | vector of shape functions for element $e$ |
| $\mathbf{\Psi}_i$ | 2-D or 3-D shape function |
| $\mathbf{\Psi}_i^{(e)}$ | 2-D or 3-D shape function for element $e$ |
| $\Psi_i$ | 1-D shape function |
| $\Omega$ | frequency band, usually octave or one/third octave band |
| $\Omega_i$ | non-dimensional frequency parameter |
| $\alpha$ | mass proportional damping factor in Rayleigh damping model |
| $\alpha_{ij}$ | continuity condition between co-ordinate $i$ and $j$ |
| $\beta$ | stiffness proportional damping factor in Rayleigh damping model |
| $\gamma$ | power flow proportionality constant |
| $\delta$ | Kronecker's delta function |
| $\overline{\boldsymbol{\epsilon}}$ | virtual strains |
| $\overline{\boldsymbol{\epsilon}}^{(e)}$ | virtual strains of element $e$ |

| | |
|---|---|
| $\epsilon$ | stiffness-proportional dissipation factor in Raileigh model |
| $\boldsymbol{\varepsilon}$ | vector of modal energies |
| $\varepsilon_i$ | energy of mode $i$, (oscillator $i$) |
| $\zeta_i$ | modal damping factor |
| $\zeta_i^{app}$ | approximate modal damping factor |
| $\zeta_{ij}$ | modal coupling coefficient |
| $\boldsymbol{\eta}$ | coupling matrix |
| $\eta_i$ | damping loss factor of subsystem $i$ |
| $\eta^{(e)}$ | damping loss factor of element $e$ |
| $\eta_{ij}$ | coupling loss factor between systems $i$ and $j$ |
| $\lambda_{trans}^{(s)}$ | wavelength of bending wave in subsystem $s$ at 'transition frequency' $\omega_{trans}^{(s)}$ |
| $\mu$ | Lamé constant |
| $\nu$ | Poisson ratio |
| $\boldsymbol{\xi}^{(e)}$ | local co-ordinate system of element $e$ |
| $\rho$ | mass density |
| $\rho^{(e)}$ | mass density of element $e$ |
| $\boldsymbol{\sigma}$ | stress tensor |
| $\boldsymbol{\sigma}^{I(e)}$ | initial stress tensor of element $e$ |
| $\boldsymbol{\sigma}^{(e)}$ | stress tensor of element $e$ |
| $\boldsymbol{\upsilon}$ | displacement field in local co-ordinate system |
| $\upsilon$ | displacement field in local 1-D co-ordinate system |
| $\upsilon_i$ | component of the displacement field in local co-ordinate system |
| $\phi$ | scalar potential of displacement field |
| $\omega$ | frequency, central frequency of frequency band $\Omega$ (angular) |
| $\omega_{max}$ | maximum frequency in analysis (angular) |
| $\omega_r$ | resonant frequency (angular) |
| $\tilde{\omega}_i$ | natural frequency of mode $i$ (angular) |
| $\omega_{trans}^{(s)}$ | 'transition frequency' for subsystem $s$ (angular) |

## Latin Symbols

| | |
|---|---|
| $A$ | cross section area |
| $A^{(e)}$ | cross section area of element $e$ |
| $\mathbf{B}$ | strain displacement relation matrix |
| $B$ | bending stiffness of the plate |
| $\mathbf{C}$ | damping matrix |
| $\mathbf{C}_v$ | matrix of viscous damping coefficients |
| $\mathbf{D}$ | dynamic stiffness matrix |
| $\mathbf{D}_{gg}$ | global dynamic stiffness matrix |
| $\mathbf{D}_{ll}$ | local dynamic stiffness matrix |
| $\mathbf{D}_{gl}$ | global local dynamic stiffness matrix |
| $\mathbf{D}_{l^s l^s}$ | local dynamic stiffness matrix of subsystem $s$ |
| $\Delta\mathbf{D}$ | additional dynamic stiffness matrix in hybrid formulation |
| $\mathbf{E}$ | elasticity matrix, stress-strain relation |
| $\mathbf{E}^{(e)}$ | elasticity matrix of element $e$ |
| $E$ | elasticity (Young) module |
| $E^{(e)}$ | elasticity (Young) module of element $e$ |
| $\hat{E}$ | complex elasticity module |
| $E_i$ | energy of subsystem $i$ |
| $E_{Bi}$ | energy of bending (out-of-plane) motions of subsystem $i$ |
| $E_{Ii}$ | energy of in-plane motions of subsystem $i$ |
| $\mathbf{F}$ | vector of force amplitudes, Fourier transform of $\mathbf{F}$ |
| $\tilde{\mathbf{F}}$ | vector of modal force amplitudes |
| $\mathbf{F}_g$ | vector of force amplitudes acting on global co-ordinates |
| $\mathbf{F}_l$ | vector of force amplitudes acting on local co-ordinates |
| $\Delta\mathbf{F}$ | vector of additional forces in hybrid formulation |
| $\boldsymbol{F}$ | vector potential of force vector |
| $\mathbf{G}(\mathbf{x}, \mathbf{y}, \omega)$ | Green's function relating response at location $\mathbf{x}$ to harmonic point force of frequency $\omega$ in location $\mathbf{y}$ |
| $H$ | Heaviside function |
| $\mathbf{K}$ | stiffness matrix |
| $\tilde{\mathbf{K}}$ | modal stiffness matrix |

| | |
|---|---|
| $\mathbf{K}^{(e)}$ | stiffness matrix of element, part etc. $e$ |
| $\hat{\mathbf{K}}$ | complex stiffness matrix |
| $\bar{\mathbf{K}}$ | condensed stiffness matrix |
| $K_i^{(e)}$ | highest order of interpolation function in element $e$ in direction $i$ |
| $\tilde{K}_i$ | modal stiffness of mode $i$ |
| $K_{ij}$ | element $ij$ of the stiffness matrix |
| $\bar{K}_{ij}$ | element $ij$ of the condensed stiffness matrix |
| $\mathbf{M}$ | mass matrix |
| $\tilde{\mathbf{M}}$ | modal mass matrix |
| $\mathbf{M}^{(e)}$ | mass matrix of element, part etc. $e$ |
| $\bar{\mathbf{M}}$ | condensed mass matrix |
| $\tilde{M}_i$ | modal mass of mode $i$ |
| $M_{ij}$ | element $ij$ of the mass matrix |
| $\bar{M}_{ij}$ | element $ij$ of the condensed mass matrix |
| $\mathcal{M}^{(s)}$ | modal overlap in subsystem $s$ |
| $N_{glob}$ | number of global modes |
| $N_i(\Omega)$ | number of modes in frequency band $\Omega$ |
| $N_{loc}^{(s)}$ | number of local modes in subsystem $s$ |
| $N_{sub}$ | number of subsystems |
| $\mathbf{Q}(i\omega)$ | vector of co-ordinate amplitudes (frequency domain) |
| $\tilde{\mathbf{Q}}(i\omega)$ | vector of modal co-ordinate amplitudes (frequency domain) |
| $\mathbf{Q}^{(e)}$ | vector of co-ordinate amplitudes (frequency domain) corresponding to element, part etc. $e$ |
| $\mathbf{Q}_g$ | vector of global co-ordinate amplitudes (frequency domain) |
| $\mathbf{Q}_l$ | vector of local co-ordinate amplitudes (frequency domain) |
| $\mathbf{Q}_{l^s}$ | vector of local co-ordinate amplitudes in subsystem $s$, (frequency domain) |
| $S$ | surface of the body |
| $S_u$ | surface with predefined surface displacement |
| $S_f$ | surface with predefined surface traction |
| $S^{(e)}$ | surface of element $e$ |
| $T^{(e)}$ | kinetic energy of element $e$ |

| | |
|---|---|
| $U^B$ | displacement amplitude of a 'blocked' system |
| $U_s^B$ | displacement amplitude of a 'blocked' subsystem $s$ |
| $U^{(i)}$ | displacement amplitude in 1-D co-ordinate system (frequency domain) |
| $V$ | volume occupied by the elastic body |
| $V^{(e)}$ | volume of element $e$ |
| $W^{(e)}$ | potential energy of element $e$ |
| $Y_{point}$ | point mobility |
| $Y_{point}^{\infty}$ | point mobility of infinite structure |
| $b_r$ | bandwidth of a resonance curve |
| $c_B$ | propagation velocity of bending waves |
| $c_T$ | propagation velocity of transverse (shear) waves |
| $c_L$ | propagation velocity of longitudinal waves |
| $\mathbf{f}$ | vector of forces |
| $\mathbf{f}^B$ | body forces per unit volume |
| $\mathbf{f}_B$ | vector of element body forces |
| $\mathbf{f}_C^i$ | concentrated forces acting at locations $\mathbf{x}_i$ |
| $\mathbf{f}_I$ | vector of element initial stresses forces |
| $\mathbf{f}_S$ | vector of element surface forces |
| $f$ | scalar potential of force vector |
| $f_{trans}^{(s)}$ | 'transition frequency' for subsystem $s$ |
| $\mathbf{g}(\mathbf{x}, \mathbf{y}, t)$ | Green's function relating response at location $\mathbf{x}$ to point force in location $\mathbf{y}$ |
| $k$ | wave number |
| $\hat{k}$ | complex wave number |
| $k_{trans}^{(s)}$ | wave number of bending wave in subsystem $s$ at 'transition frequency' $\omega_{trans}^{(s)}$ |
| $m^{(e)}$ | mass of element (subsystem) |
| $n_i(\omega)$ | modal density of subsystem $i$ at frequency $\omega$ |
| $n_{in}$ | number of local modes with natural frequencies below frequency of interest |
| $n_{int}^{(e)}$ | number of internal co-ordinates in element $e$ |
| $n_{intg}$ | number of internal co-ordinates in element $e$ in global description |

| | |
|---|---|
| $\boldsymbol{q}(t)$ | vector of co-ordinates (time domain) |
| $\tilde{\boldsymbol{q}}(t)$ | vector of modal co-ordinates (time domain) |
| $\overline{\boldsymbol{q}}(t)$ | vector of virtual co-ordinates (time domain) |
| $q_i$ | co-ordinate $i$ (time domain) |
| $t$ | time |
| $\mathbf{u}(\mathbf{x}, t)$ | displacement field |
| $\mathbf{u}^{(e)}(\mathbf{x}^{(e)}, t)$ | displacement field of element $e$ |
| $\overline{\mathbf{u}}$ | virtual displacement field |
| $\dot{\mathbf{u}}(\mathbf{x}, t)$ | velocity field |
| $\ddot{\mathbf{u}}(\mathbf{x}, t)$ | acceleration field |
| $u^{(i)}$ | displacement in 1-D co-ordinate system (time domain) |
| $\mathbf{x}$ | co-ordinate system |
| $\mathbf{x}^{(e)}$ | co-ordinate system of element $e$ |
| $\mathbf{x}_{(i)}$ | position of point $i$ in multidimensional co-ordinate system |
| $x_i$ | co-ordinate $i$ in co-ordinate system $\mathbf{x}$ |
| $x_{(i)}$ | position of point $i$ in one-dimensional co-ordinate system |
| $\mathbf{y}$ | alternative co-ordinate system |
| $y_i$ | co-ordinate $i$ in co-ordinate system $\mathbf{y}$ |

## Operations

| | |
|---|---|
| $\lvert\ \rvert$ | absolute value |
| $(\ )^*$ | complex conjugate |
| $\langle\ \rangle_S$ | spatially averaged value |
| $\langle\ \rangle_t$ | time average value |
| $\langle\ \rangle_i$ | value averaged over index $i$ |
| $\Im(\ )$ | imaginary part |
| $\Re(\ )$ | real part |
| $(\ )^H$ | Hermitian transpose of the matrix |
| $(\ )^T$ | transpose of the matrix |
| $\nabla$ | gradient |
| $\nabla^2$ | Laplace operator |

## Abbreviations

| | |
|---|---|
| 1-D | one-dimensional |
| 2-D | two-dimensional |
| 3-D | three-dimensional |
| DOF | degree of freedom |
| DSM | dynamic stiffness method |
| EFEA | energy finite element analysis |
| EOM | equation of motion |
| FEM | finite element method |
| MDOF | multi-degree-of-freedom system |
| PDE | partial differential equation |
| SEA | statistical energy analysis |

# Chapter 1

# Introduction

> Many of the acoustic events that reach our ear such as the sound of violin, the squeaking of breaks, or a noisy conversation in the next apartment- are either produced or conducted by vibrating solid bodies [21].

This sentence opens one of the major publications in the field of structure-borne sound. It indicates the mechanical background of sound or noise. The term sound usually indicates the positive outcome of an action. Action that is performed to generate sound, play music etc. The term noise, although related to similar fluctuations of pressure field reaching human ear, is used when the audio effect is present but not desirable. Drummer hitting the drum with the stick generates vibrations of the drum membrane. These vibrations cause the movements of the fluid which cause changes in the pressure field. Hitting the roof of the car with the stick or fingers will also generate sound. If, instead of the hit, the roof of the car is excited by the vibrations of the engine or the suspension system, similar audio effect can appear. The main difference is that hitting the roof results in response in wide frequency range, so that part of it will usually be audible. Continuous harmonic excitation, like from another car components would rather excite narrow frequency range. So the results are not always audible, even if they are present.

Not all sounds or noises are, of course, generated by mechanical vibrations. However, this work is focused on mechanically induced (or structure-borne) noise. Clearly some conditions are necessary for the structure-borne sound to appear, namely the vibrating structure and the medium where the sound can propagate. The vibrations of the structure have to fulfil certain conditions for the radiation to take place. The surrounding medium has no shear stiffness so that only the component normal to the surface is of importance. The fluctuations of the medium surrounding structure have the same frequency as the vibrations of the surface. Therefore, the vibrations in audible (for human) frequencies are of main interest. The audible frequency range for a human is defined as a range from 16 Hz to 16

kHz, which for the mechanical engineering is a very wide range.

Vibrating surface of the structure acts as loading to the surrounding medium and generates the fluctuations of the pressure level. Fluctuations of pressure in the medium can have either local or global character, which means that they can either disappear in the nearest vicinity of the surface, or propagate through the medium. The interaction between structure and surrounding medium does not only have impact on the medium. Also the motions of the structure are influenced. This effect depends on many factors including the properties of medium (density, pressure), the properties of the structure and the frequencies of interest. If the structure is submerged in dense fluid, for example water or oil, then the effect on the structure will generally have to be considered. However, if the radiation of sound from mechanical system to air is considered, then the load from the air can usually be omitted.

Structural members differ in terms of sound radiation efficiency. In any case the emitted sound is proportional to the energy of the member. For these reasons the prediction of structure-borne sound requires the knowledge of energy distribution in the structure. However, in the vibro-acoustic analysis, the assessment of the structure-borne noise is not the aim per se. The aim is usually to modify the structure in order to reduce the amount of sound radiated. In that case the knowledge of the energy distribution is not sufficient. It is desirable to assess the transmission paths and to reduce the amount of energy flowing into the members that radiate sound most efficiently. Also the amount of power that excites the structure should be controlled and minimized and this can in some cases be achieved by structural modifications.

Calculating the energy distribution in the continuous mechanical system requires setting up a mathematical model. It can be achieved by considering the motions of the structure under excitation. The energy distribution can then be derived from response quantities, like displacement (velocity) fields, intensity vectors etc. The motions of the continuous mechanical system can be described by the system of partial differential equations (PDE) with corresponding boundary conditions and initial conditions. Closed-form solution of PDE is the most desirable, since they allow to understand the behaviour of the system and the influence that systems' parameters have on the solution. The second property is especially valuable for the purposes of any kind of optimization, reduction of vibrations and reduction of energy flow including. Unfortunately, the closed-form solutions are only available for the narrow class of systems with appropriate boundary conditions.

A method that allows coupling of some domains for which the closed-form solution of differential equation exists, is called dynamic stiffness method (DSM) [54]. Each homogeneous domain forms one element denoted by number in Figure 1.1. The solution of the PDE for each element is presented in the form of a dynamic stiffness matrix where the relations between loads and displacements, i.e. the nodal variables

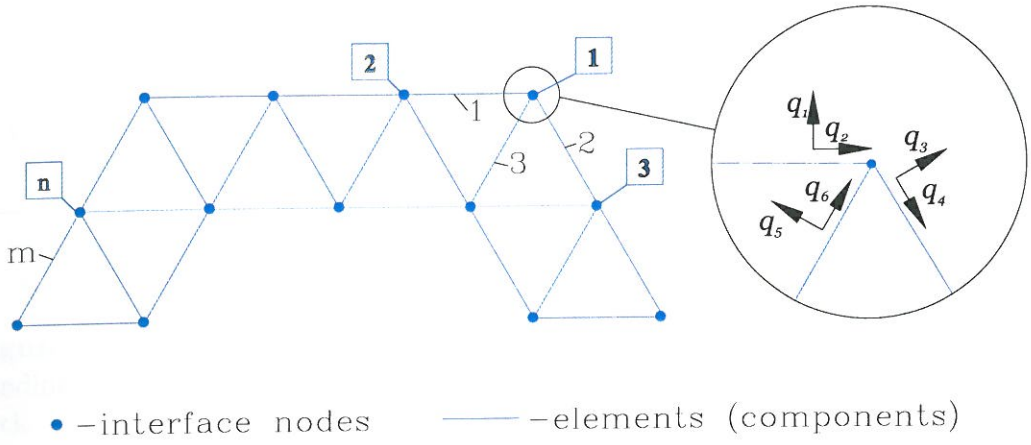


**Figure 1.1**: Scheme of a DSM model of 2-D beam truss.

$q_i$ are defined. In the assembly procedure the elements are coupled through appropriate definition of continuity conditions at interface nodes, denoted by framed numbers in Figure 1.1. The variables $q_i$ are the quantities used for the definition of continuity and boundary conditions. In this way the multi-degree-of-freedom (MDOF) system is created from the continuous one providing there is a discrete number of variables necessary to define the continuity. Then the sum of variables at the junctions determines the size of the problem. For that reason the DSM can only be used when considering discretely connected 1-D elements (like beams or rods) [9,15,22,54,90], or in the case of line coupling of 2-D elements if a separable solution is available (like plate or shell simply supported at two opposite edges, [7,8,52,56,62], because then the MDOF system can be identified. The DSM introduces spatial partition of the structure. The results are exact in the case of point connected elements and the size of the problem depends on the number of coupling variables but not on frequency considered.

The similar approach has also been used in an approximate way. Again the structure is subdivided into elements, which are coupled by discrete number of variables at coupling points. The approximation results from the use of approximate dynamic stiffness matrix within elements, [18,37,49,65,80,86,88,92,99]. Figure 1.2a presents an example of structure that can be divided into three elements (or substructures). These are combined at the coupling points. The dynamic stiffness matrices of each element can be approximated for example by truncated set of natural modes of the element or other approximate description. In Figure 1.2b the additional approximation follows from discretization of the line junction into the set of points.

The properties of the method depend of the type of approximation used for single elements. Usually, like in the case of modal approximation, the size of the problem

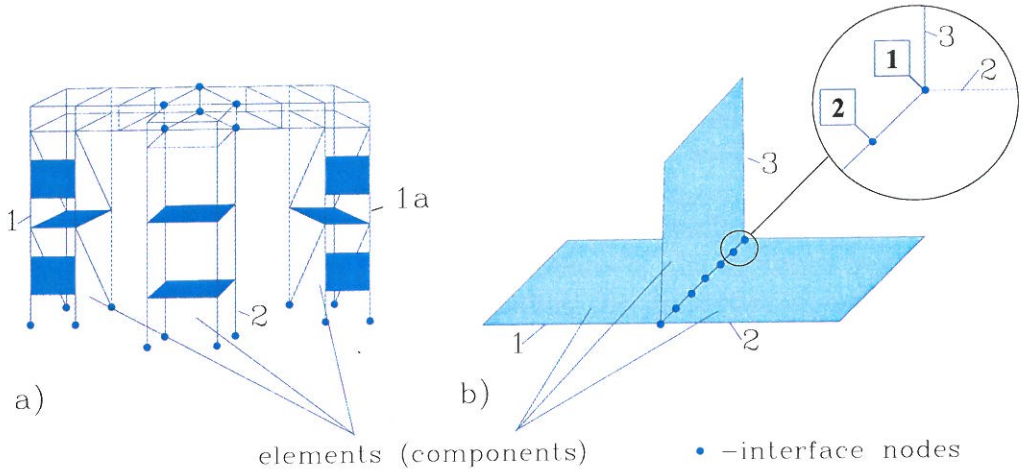


**Figure 1.2**: Scheme of a DSM model using approximate description of elements.

increases with frequency. This is because each element is an MDOF system and the number of internal degrees of freedom (DOF) within each element, (modes in modal expansion) have to be increased with frequency. The reduction in the description can be achieved if the structure is built up of the same elements, like element 1 and $1a$ because the internal properties are the same and the element can be used multiple.

For some structures, like beams, plates, shells or unbounded media the PDE can be transformed into the form of wave equation. The motions can then be decomposed in terms of different wave types or wave components and these considered separately. The reflection and transmission of the wave at the discontinuity are studied. Figure 1.3 presents a scheme of a beam junction (a) and plate junction (b) with the wave components. The energy variables can be defined in terms of wave amplitudes and propagation velocities. The considerations of wave propagation leading to power flow assessment can be found in [42,44,57,59,60,70,84,85,100,101]. In most of the cases only one structural discontinuity can be considered at a time. The exception from this rule is the considerations of power flow in one dimensional (1-D) elements, like beams. For 1-D structures the countable number of continuity conditions between members can be defined and an MDOF system created. The procedure is similar to one used with DSM but the continuity is defined through wave amplitudes, see [5, 79, 94]. The common practice in solving the wave equation is disregarding the evanescent wave components, i.e. the components with imaginary wave numbers. This assumption is based on the fact that the amplitude of evanescent wave decays exponentially with the distance.

If the solution of the wave equation can be found then the results are independent of frequency. This is because at certain frequency only one component of each

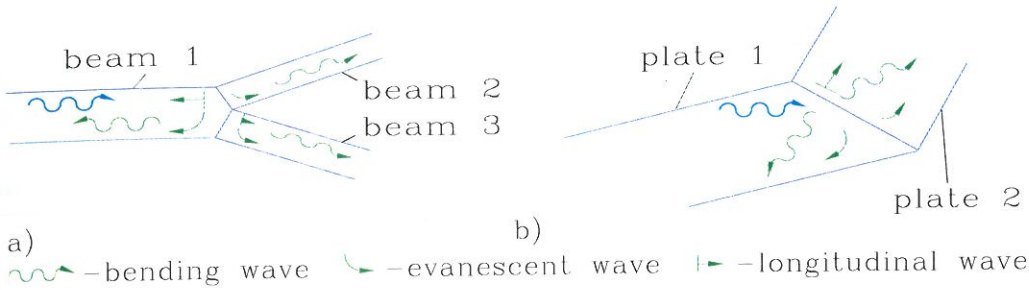


**Figure 1.3**: Scheme of a) three beams junction; b) two plates junction. The incident bending wave is partially transmitted into other elements and partially reflected back.

type will be present. However, apart from the previously mentioned assumption regarding evanescent filed, the additional assumptions are used in case of 2-D and 3-D structures. These concern the distribution of angels from which the incident wave hits the junction, and the phase shifts between different wave components [72]. Usually a reverberant wave field is assumed (resulting in equally possible incidence from each angle and equally possible phase shift) but this is only true at high frequencies.

In both exact DSM and wave approach the partition of the structure was introduced in this way that the element properties could have been evaluated in an analytical way. Certain restrictions applied to the definition of continuity conditions and the elements itself. In more general cases the approximate solutions of PDE must be sought for.

> The difficulties in obtaining closed-form solutions to problems of distributed parameter systems can be traced to the inherent difficulty of solving PDE, with or without space dependent coefficients, and in satisfying boundary conditions, particularly for two and three-dimensional problems. These difficulties can be circumvented by eliminating the spatial dependence from the problems through discretization in space, but this implies certain approximations [77].

The discretization process transforms the continuous mechanical system to an MDOF system. Consequently the description by set of PDE is transformed into the description by the set of ordinary differential equations. The 'certain approximations' in the spatial discretization often involve the approximation of the displacement field. This leads to the formulation of finite element method (FEM). The method has been used for assessment of energy distribution or power flow among others in [29, 30, 33–36, 73, 91, 95, 98]. The response of the structure due to applied loading is calculated in deterministic sense in terms of displacement (velocity) field. Energy

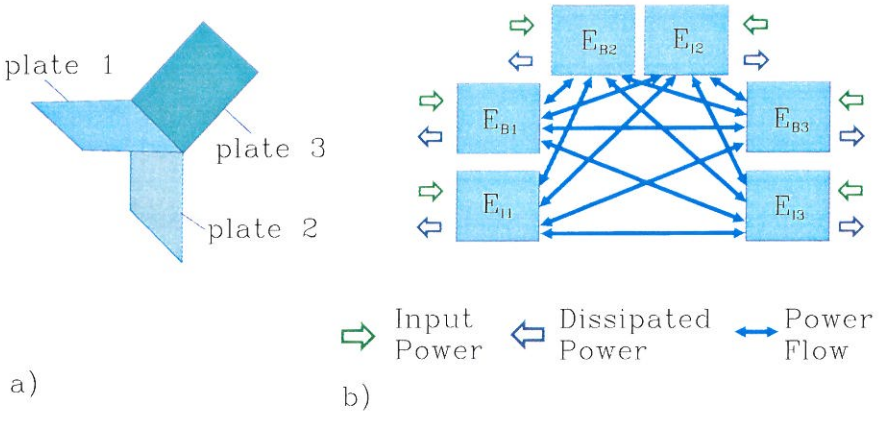


**Figure 1.4**: Scheme of a) three plates structure and b) its SEA model.

variables are derived from this solution either at particular locations or averaged in space. Displacement and its spatial derivatives are used to fulfil continuity conditions. The main drawback of the FEM to the power flow calculations is that the approximation of the displacement field must be accurate for accurate results. This means that as the frequency of interest increases the system becomes bigger and bigger. The computational costs of solving the system of equations increase beyond the possibilities of computers.

Another disadvantage of the methods like DSM or FEM is that they describe a certain idealization of the real structure. This is because in reality the system parameters are uncertain and so the response to the loading would also be uncertain. The presence of uncertainties is sometimes used in the wave approach. The influence of uncertainties becomes more important in the higher frequencies (apart from the uncertainties in boundary conditions that affect mainly the lowest modes). This fact should be kept in mind when applying deterministic methods to the noise and vibration problems.

The models of energy flow within the structure can also be worked out directly from the energy balance. The energy is used as a primary variable. The transformation of continuous mechanical system into an MDOF system is performed by identifying elements (subsystems). One of the methods using the power balance as a start point for development of mathematical model is the statistical energy analysis (SEA). In SEA the system is divided into subsystems, see Figure 1.4 , and the average energy of the subsystem ($E_i$) is a single variable. In the example two subsystems are defined for each of the plates, containing bending energy $E_{Bi}$ and in-plane energy $E_{Ii}$. The use of average energy as a variable reduces the influence of uncertainties on the results of analysis. The examples of SEA applications can be found in [20, 38, 40, 45, 46, 97, 103].

Another method that uses energy as a variable is the energy finite element analysis (EFEA) [12, 13, 81, 102]. The main difference between SEA and EFEA is that the former one describes the average energy in subsystem whereas the latter one describes the energy density averaged over wavelength and time, and therefore presents spatial distribution of energy.

The necessity of introducing continuity conditions is inherent in all discretization schemes. The continuity conditions assure that after division the structure remains continuous. In energy-based descriptions, like SEA and EFEA the power transfer between elements has to be defined based on the energy of subsystems. This is somehow difficult and not straightforward and certain assumptions must be used before such energy transfer can be described. Usually an analogy between mechanical and thermal energy is assumed and the energy transfer is related to the difference between energies of joined subsystems. The assumption of energy flow proportionality to the energy differences has been criticized in [71]. Carcaterra in [14] reviews the methods based on thermal analogy and finds that:

> Although the intuition contained in the thermal analogy is fascinating, it is likely that the thermal power flow takes into account only first order contribution of a more complicated phenomenon.

The structures to be analysed can differ considerably in terms of structural complexity. Single members of uniform or non uniform properties, assemblies of similar members in 2-D and 3-D, finally assemblies of different members. The members can differ in terms of their dynamic properties so that even members of the same type can behave differently at some frequency. The power flow calculations are usually performed in frequency domain, i.e. at certain discrete frequencies. At low frequencies all members can usually be modelled by some deterministic method, like FEM. That is when all members behave according to the assumptions of the method. Similarly, when each member fulfils the assumptions of the statistical method like SEA then the structure can be modelled that way. Because of the differences in structural members of a built-up structure at the same frequency one component can have low mode count (i.e. only few modes resonating in the frequency band) and another one high mode count, the components can be damped at different levels, etc. That means that neither the deterministic methods (like FEM) nor the statistical methods (like SEA) are appropriate for the modelling of all members of the built-up system (see [27, 83]). The frequency range where such difficulty appears is usually called the medium frequency range. The definition of the medium frequency range is not straightforward and there are no exact limits of that frequency range. It can only be described by the system's properties.

The definition of medium frequency range indicates that a special method should be applied for power flow calculations. Some authors propose modifications of the existing and well-known methods in order to make them applicable for the medium

frequency range analysis of built-up structures. Methods used to reduce FEM calculations will be presented in Section 2.1.4 and methods used to take the uncertainties into consideration when performing finite element analysis will be presented in Section 2.1.5.

The combination of two general methods, the FEM and SEA is often proposed. The different ways of combining FEM and SEA are:

- Deriving the coupling loss factors for separate junctions, i.e. modelling only part of the structure was proposed in [68, 89, 95]
- By deriving the coupling loss factors (or deterministic energy influence coefficients [93]) from the FEM energy flow model. The method has been used in [75, 92].
- Wilson in [104] proposed a coupling of the two descriptions by describing elements of the structure by either FEM or SEA and minimizing the differences in the coupling terms in an iterative procedure.
- Langley and Bremner in [63] proposed hybrid formulation where the system co-ordinates are partitioned and the FEM and SEA description is used for the sets of co-ordinates.

Other methods proposed for the medium frequency range analysis of the built-up structures include:

- Fuzzy structure theory [83] which deals with the description of structures composed of main structure ('master structure' in the method terminology) and the 'fuzzy attachments' coupled to the 'master structure'. The 'fuzzy attachments' do not take part in energy transmission, and from the point of view of the coupled system the 'fuzzy attachments' act as additional damping applied to the 'master structure'. An example of 'master structure' could be a ship hull and 'fuzzy attachments' would include the small equipment attached inside the hull. 'Fuzzy structure' is often pictured as a set of oscillators coupled with the 'master structure'.
- Set of parabolic equations to model the propagation of waves in built-up structures has been presented in [6]. The vibrational field is split into highly oscillating components that describe substructures and slowly varying function that describes the displacement of primary structure. The local components act on the primary structure by adding damping, i.e. in a similar manner as in fuzzy structure theory.

With the aim of the thesis on the development of the prediction method that will be applicable for the general built-up structures yet focused on the structural

radiation the main focus should be on the structures containing plates and shells. Therefore, the methods specific for the beams and rods will not be further considered and the hybrid FEM-SEA method will be investigated.

## 1.1 Scope of the Thesis

This thesis is focused on power flow calculations in linear mechanical systems subjected to dynamic loading. The special interest lies in the noise generated by the structures. The wide range of frequencies in which generation of sound can take place exhibits a pronounce difficulty. The range of techniques used for prediction of the system vibrations and structure-borne sound generation is equally wide. Low frequency methods include the FEM in stationary and non-stationary problems, the wave approach for transient problems. In high frequencies SEA is mainly used. The medium frequencies are not equipped with well developed method yet, and the aim of this thesis is to develop a numerical method capable of modelling the systems in medium frequency range.

Since the generation of structure-borne noise is of importance the elements of big area to volume ratio should be considered, like plates and shells, the 1-D and 3-D elements being less important.

## 1.2 Thesis Outline

In Chapter 2 methods used in the power flow analysis, including FEM, wave approach and SEA are described. The applicability of methods to the medium frequency range analysis is discussed. The hybrid FEM-SEA method is introduced that spans the two approaches into a method applicable in medium frequencies. Finally an example of application of the various approaches is presented.

In Chapter 3 the formulation of the hierarchical version of FEM for the thin plates is presented. The properties of the method are described and the applicability of the method as a base for the development of hybrid FEM-SEA for the plate assemblies is discussed.

In Chapter 4 the implementation of the hierarchical FEM is presented. The procedures for assembly of the model, including imposing of continuity conditions, are described. The validation of the method is presented by comparison with results of other analysis.

In Chapter 5 the implementation of the hybrid FEM-SEA approach to the thin plate assemblies is presented. The definition of global and local sets of co-ordinates and the coupling between them is presented. The algorithm developed for the analysis

is described and an example application is presented.

In Chapter 6 the conclusions are summarized. The contribution of this thesis is mentioned and the areas that require further research are pointed out.

# Chapter 2

# Methods of Power Flow Analysis

The methods used for power flow analysis, as indicated in the introduction, will be presented in this chapter. The focus is on the methods that lie foundation for the development of the hybrid FEM-SEA method. These are both the FEM and SEA, as well as some extensions of either method. The wave approach is also presented as it is a main approach for calculating the coupling loss factors in SEA. Also the concept of hybrid FEM-SEA as presented in [63] will be presented.

The presentation is not very detailed but the basic concepts used latter for the development of general hybrid FEM-SEA are included. These will be referred to in the later chapters.

## 2.1 Finite Element Method

The FEM is 'the numerical method' for many engineering calculations including dynamic analysis. Detailed derivation of FEM can be found in many books on the subject including [4, 16, 77]. Here only the necessary basics of the method will be presented and the limitations of the method are pointed out. Also some methods of overtaking the limitations are suggested.

### 2.1.1 Formulation of FEM

Several formulations lead to the basic MDOF description of continuous mechanical system. Among them there is the displacement-based method using the principle of virtual displacements which is one of the methods used in derivation of FEM.

Let us consider the elastic body occupying the volume $V$. The boundary conditions are prescribed at the surface $S$ of the body in terms of surface displacements $\mathbf{u}^{S_u}$ defined at the surface $S_u$ and the surface traction $\mathbf{f}^{S_f}$ defined at the surface

$S_f$. The body is subjected to concentrated loads $\mathbf{f}_C^i$ at position $\mathbf{x}_i$ and external body forces $\mathbf{f}^B$ (per unit volume). The latter one include inertia forces and damping forces, according to d'Alembert's principle.

The principle of virtual displacements states that the equilibrium of the body requires that the internal work (due to stresses $\boldsymbol{\sigma}$) is equal to the total external virtual work, i.e. [4]

$$\int_V (\overline{\boldsymbol{\epsilon}})^T \boldsymbol{\sigma} dV = \int_V (\overline{\mathbf{u}})^T \mathbf{f}^B dV + \int_{S_f} (\overline{\mathbf{u}}^{S_f})^T \mathbf{f}^{S_f} dS + \sum_i (\overline{\mathbf{u}}^i)^T \mathbf{f}_C^i \tag{2.1}$$

where the line over the symbol denotes virtual quantity. In (2.1) $\overline{\boldsymbol{\epsilon}}$ is the virtual strains due to the virtual displacements $\overline{\mathbf{u}}$.

The FEM assumes division of the domain into elements. The elements are connected by nodal points at their boundaries. Performing the partition into elements yield equation (2.1) to have the form

$$\sum_e \int_{V^{(e)}} (\overline{\boldsymbol{\epsilon}}^{(e)})^T \boldsymbol{\sigma}^{(e)} dV^{(e)} = \sum_e \int_{V^{(e)}} (\overline{\mathbf{u}}^{(e)})^T \mathbf{f}^{B(e)} dV^{(e)} + \sum_e \int_{S_1^{(e)},\ldots,S_q^{(e)}} (\overline{\mathbf{u}}^{S(e)})^T \mathbf{f}^{S(e)} dS^{(e)} + \sum_i (\overline{\mathbf{u}}^i)^T \mathbf{f}_C^i. \tag{2.2}$$

The summation covers all elements of the volume, and the surfaces of the element $e$ which are the surface of the body are denoted by $S_1^{(e)}, \ldots, S_q^{(e)}$. The displacement field of single element $e$ is described as

$$\mathbf{u}^{(e)}(\mathbf{x}^{(e)},\ t) = \boldsymbol{\Psi}^{(e)}(\mathbf{x}^{(e)})\boldsymbol{q}(t) \tag{2.3}$$

where $\boldsymbol{\Psi}^{(e)}$ is the displacement interpolation matrix with the superscript $e$ denoting the $e^{\text{th}}$ element; $\boldsymbol{q}$ is a vector of co-ordinates, i.e. $\boldsymbol{q}^T = [q_1\ q_2\ \ldots\ q_n]$ where $n$ is a number of co-ordinates. The element strains may be evaluated as

$$\boldsymbol{\epsilon}^{(e)}(\mathbf{x}^{(e)},\ t) = \mathbf{B}^{(e)}(\mathbf{x}^{(e)})\boldsymbol{q}(t) \tag{2.4}$$

where $\mathbf{B}^{(e)}$ is the strain displacement relation following choice of $\boldsymbol{\Psi}^{(e)}$. The stresses are related to strains and initial stresses, i.e.

$$\boldsymbol{\sigma}^{(e)}(\mathbf{x}^{(e)},\ t) = \mathbf{E}^{(e)}\boldsymbol{\epsilon}^{(e)}(\mathbf{x}^{(e)},\ t) + \boldsymbol{\sigma}^{I(e)}(\mathbf{x}^{(e)},\ t_0) \tag{2.5}$$

where $\mathbf{E}^{(e)}$ is the elasticity matrix of element $e$, $\boldsymbol{\sigma}^{I(e)}(\mathbf{x}^{(e)},\ t_0)$ are the known initial stresses in element $e$.

Using the same description as in (2.3, 2.4) for the virtual element displacements $\overline{\mathbf{u}}^{(e)}$ and strains $\overline{\boldsymbol{\epsilon}}^{(e)}$, i.e.

$$\overline{\mathbf{u}}^{(e)}(\mathbf{x}^{(e)},\ t) = \boldsymbol{\Psi}^{(e)}(\mathbf{x}^{(e)})\overline{\boldsymbol{q}}(t) \tag{2.6}$$

$$\overline{\boldsymbol{\epsilon}}^{(e)}(\mathbf{x}^{(e)},\ t) = \mathbf{B}^{(e)}(\mathbf{x}^{(e)})\overline{\boldsymbol{q}}(t) \tag{2.7}$$

and substituting into (2.2) one obtain:

$$\overline{\boldsymbol{q}}^T \left[ \sum_e \int_{V^{(e)}} (\mathbf{B}^{(e)})^T \mathbf{E}^{(e)} \mathbf{B}^{(e)} dV^{(e)} \right] \boldsymbol{q} = (\overline{\boldsymbol{q}})^T \left[ \sum_e \int_{V^{(e)}} (\boldsymbol{\Psi}^{(e)})^T \mathbf{f}^{B(e)} dV^{(e)} \right.$$
$$\left. + \sum_e \int_{S_1^{(e)},\ldots,S_q^{(e)}} (\boldsymbol{\Psi}^{S(e)})^T \mathbf{f}^{S(e)} dS^{(e)} - \sum_e \int_{V^{(e)}} (\mathbf{B}^{(e)})^T \boldsymbol{\sigma}^{I(e)} dV^{(e)} + \mathbf{f}_C \right]. \quad (2.8)$$

This can be simplified by defining the stiffness matrix:

$$\mathbf{K} = \sum_e \mathbf{K}^{(e)} = \sum_e \int_{V^{(e)}} (\mathbf{B}^{(e)})^T \mathbf{E}^{(e)} \mathbf{B}^{(e)} dV^{(e)}; \quad (2.9)$$

the element body forces vector, the surface forces vector and the initial stresses:

$$\mathbf{f}_B = \sum_e \int_{V^{(e)}} (\boldsymbol{\Psi}^{(e)})^T \mathbf{f}^{B(e)} dV^{(e)} \quad (2.10)$$

$$\mathbf{f}_S = \sum_e \int_{S_1^{(e)},\ldots,S_q^{(e)}} (\boldsymbol{\Psi}^{S(e)})^T \mathbf{f}^{S(e)} dS^{(e)} \quad (2.11)$$

$$\mathbf{f}_I = \sum_e \int_{V^{(e)}} (\mathbf{B}^{(e)})^T \boldsymbol{\sigma}^{I(e)} dV^{(e)}. \quad (2.12)$$

One may combine (2.10) - (2.12) and nodal concentrated loads $\mathbf{f}_C$ into load vector $\mathbf{f}$:

$$\mathbf{f} = \mathbf{f}_B + \mathbf{f}_S - \mathbf{f}_I + \mathbf{f}_C \quad (2.13)$$

and rewrite (2.8) as:

$$\mathbf{K}\boldsymbol{q} = \mathbf{f}. \quad (2.14)$$

### FEM applied to dynamic analysis in time domain

In the dynamic analysis the inertia forces can be included in the body force vector. Then equation (2.10) has to be rewritten as

$$\mathbf{f}_B^{(e)} = \sum_e \int_{V^{(e)}} (\boldsymbol{\Psi}^{(e)})^T \left[ \mathbf{f}^{B(e)} - \rho^{(e)} \boldsymbol{\Psi}^{(e)} \ddot{\boldsymbol{q}}(t) \right] dV^{(e)} \quad (2.15)$$

where using d'Alembert's principle the inertia forces are proportional to the acceleration $\ddot{\mathbf{u}}(t)$ and the mass density $\rho^{(e)}$ of the element. By substituting

$$\mathbf{M} = \sum_e \mathbf{M}^{(e)} = \sum_e \int_{V^{(e)}} \rho^{(e)} (\boldsymbol{\Psi}^{(e)})^T \boldsymbol{\Psi}^{(e)} dV^{(e)} \quad (2.16)$$

one obtains the equilibrium equation in the form:

$$\mathbf{M}\ddot{\boldsymbol{q}}(t) + \mathbf{K}\boldsymbol{q}(t) = \mathbf{f}(t) \tag{2.17}$$

So far the damping was not included in the description. The reason for that is that there are several ways in which the dissipation of energy can be described. The frequently used approximations include:

- Viscous damping. The velocity proportional damping factor. This measure is most often used to describe one-degree-of-freedom systems. It can also be extended to multi-degree-of-freedom systems. Then the effect of damping may be included in the analysis, in similar way as the one of mass, i.e.

$$\mathbf{M}\ddot{\boldsymbol{q}}(t) + \mathbf{C}_{\mathbf{v}}\dot{\boldsymbol{q}}(t) + \mathbf{K}\boldsymbol{q}(t) = \mathbf{f}(t) \tag{2.18}$$

  where $\mathbf{C}_{\mathbf{v}}$ is the matrix of viscous damping coefficients.
- Damping loss factor. In the continuous systems dissipation of energy is assumed to be caused by thermoelasticity. Therefore, the structural damping model is used and the dissipation is included by use of imaginary part of modulus of elasticity, i.e. $\hat{E} = E(1 + i\eta)$, where $\eta$ is the loss factor. This leads to complex stiffness matrix in FEM description. Similarly, it causes the wave number to be complex. This description of damping is used in FEM analysis in frequency domain and in SEA. This damping model does not fulfil the casualty condition, but it can be used for the steady state problems.
- Rayleigh Model. Also called proportional damping is mostly used in MDOF systems. It is widely used in FEM formulations. The damping matrix $\mathbf{C}$ is defined as: $\mathbf{C} = \alpha\mathbf{M} + \beta\mathbf{K}$. This description is a simplification of the modal damping model. The simplification in the sense that the modal damping factor $\zeta_i$ is approximated by $\zeta_i^{app} = (\alpha + \beta\omega_i^2)/2\omega_i$.

### FEM applied to dynamic analysis in frequency domain

By taking the Fourier transform of equation (2.18) one obtains the equation of motion (EOM) for the viscous damping model in the form

$$[-\omega^2\mathbf{M} + i\omega\mathbf{C} + \mathbf{K}]\mathbf{Q}(i\omega)e^{i\omega t} = \mathbf{D}\mathbf{Q}(i\omega)e^{i\omega t} = \mathbf{F}(i\omega)e^{i\omega t}. \tag{2.19}$$

where $\mathbf{Q}(i\omega)$ and $\mathbf{F}(i\omega)$ are the Fourier transforms of $\boldsymbol{q}(t)$ and $\mathbf{F}(t)$, respectively, and $\mathbf{D}$ signifies the dynamic stiffness matrix. The time dependence $e^{i\omega t}$ will be omitted in the following. In the case of structural damping model, the stiffness matrix becomes complex, i.e. $\hat{\mathbf{K}} = \mathbf{K}(1 + i\eta)$ should be used and the EOM has the form

$$[-\omega^2\mathbf{M} + \hat{\mathbf{K}}]\mathbf{Q}(i\omega) = \mathbf{D}\mathbf{Q}(i\omega) = \mathbf{F}(i\omega). \tag{2.20}$$

Main part of this thesis is concerned with the frequency domain calculations and therefore the frequency-dependence will not be indicated in the future.

### 2.1.2 Energy flow model from FEM results

The calculations of energy (power) flow within the system can be calculated from the FEM results. A detailed description of the procedure can be found for example in [34]. First the FEM model is defined with the boundary conditions and loading. The steady state response is solved for the given excitation frequency, or number of frequencies in the range. The power flow variables: power input, power output and energy are calculated from these results.

The time-average kinetic energy of element $e$ in the steady state vibrations at frequency $\omega$ is given by [93]

$$\langle T^{(e)} \rangle_t = \frac{1}{4}\omega^2 (\mathbf{Q}^{(e)})^H \mathbf{M}^{(e)} \mathbf{Q}^{(e)} \tag{2.21}$$

where $\mathbf{Q}^{(e)}$ and $\mathbf{M}^{(e)}$ are the vector of co-ordinates belonging to element $e$ and mass matrix of that element. The symbols $\langle\ \rangle_t$ and $(\ )^H$ denote time-average and Hermitian transpose, respectively. The kinetic energy of the subsystem $s$ that includes number of elements can be calculated either by summation of energies of the elements or by the matrix product of form

$$\langle T^{(s)} \rangle_t = \sum_{e \in s} \langle T^{(e)} \rangle_t = \frac{1}{4}\omega^2 (\mathbf{Q}^{(s)})^H \mathbf{M}^{(s)} \mathbf{Q}^{(s)}. \tag{2.22}$$

It should be noted that in both cases the mass matrices ($\mathbf{M}^{(e)}$ and $\mathbf{M}^{(s)}$) of the element or subsystem should be used, i.e. before assembling in the global mass matrix. If the assembled matrices are only available then the contribution from other elements (subsystems) should be separated. In the standard FEM codes it is seldom possible to separate the mass matrices corresponding to certain elements or subsystems. Then the time-average kinetic energy of the subsystem can be approximated by

$$\langle T^{(s)} \rangle_t \approx \frac{1}{4} m^{(s)} \omega^2 \langle |(\mathbf{Q}_i^{(s)})^2| \rangle_i \tag{2.23}$$

where the averaging denoted by $\langle\ \rangle_i$ covers all translational co-ordinates in the subsystem $s$. If rotational co-ordinates are present then there will be additional contribution from these. Alternatively, the velocity amplitudes can be calculated at the number of locations from both the translational and rotational co-ordinates and the spatial average of squared velocity amplitudes used.

The time averaged power input supplied by the external force vector $\mathbf{F}^{(e)}$ to element $e$ is given by

$$\langle \Pi^{ext\,(e)} \rangle_t = \frac{1}{2} \Re \left[ (\mathbf{F}^{(e)})^T i\omega (\mathbf{Q}^{(e)})^* \right]. \tag{2.24}$$

The dissipated power depends on the model of damping used. In the case of structural damping the dissipated power can be approximated by

$$\langle \Pi^{diss\,(s)} \rangle_t = \omega \eta^{(s)} \langle T^{(s)} + W^{(s)} \rangle_t \approx 2\omega \eta^{(s)} \langle W^{(s)} \rangle_t \tag{2.25}$$

where $\langle W^{(s)} \rangle_t$ is the time-average potential energy, and the sum of potential and kinetic energy gives the total energy $E_i$ of the element (subsystem) $i$. For the light damping the time-average kinetic and potential energies are almost equal and for that reason the total energy can be approximated by twice the kinetic energy.

### 2.1.3 Limits of FEM in dynamic analysis

The dynamic analysis by FEM face an important problem with accuracy of the description. For the reliable results it is crucial that the displacement field described in terms of interpolation functions approximates well the actual displacement field.

Two methods are commonly used to assure the proper description of motions. The first one considers the wavelengths of elastic deformation present in the domain at highest frequency of interest. The 'rule of the thumb' says that for the linear interpolation functions within element one needs to include eight elements per wavelength of elastic deformation, and six elements if the second order interpolation functions are used. This rule is limited to domains where one may guess the wavelengths of motions. Also there are no rules like this concerning $h$-version of FEM. The second method consists in comparing the natural frequencies of the system under consideration. According to the inclusion principle [77, 78] the natural frequencies extracted from the multi-degree-of-freedom model of the continuous system converge to the actual values from above.

With increasing frequency of analysis the wavelengths of the deformation decrease. This requires that either the size of elements will be reduced or that the complexity of interpolation functions will be increased. In any case the size of the system matrices increases with increasing frequency of interest and the calculations become increasingly expensive. This is one of three main problems that FEM faces in the dynamic analysis.

The other two issues influencing the applicability of FEM to dynamic analysis are:

- The application of the approximate theory in high frequency analysis. The FEM equations are derived as a discretization of some approximate continuum mechanical theory such as Bernoulli-Euler beam theory or thin plate theory. It is well known that a characteristic wavelength of the considered motions should be above 5-10 times the element's width if sufficient agreement between numerical and analytical solutions are to be expected. If the wavelengths are

shorter more advanced theories have to be used which are available only in some cases.

- The deterministic description of the uncertain reality. Uncertainties in the manufacturing and material properties influence mostly the high-frequency behaviour of the structure. If the high frequency analysis are performed, the differences between the model and the structure under investigation influence the response to the extent which causes the deterministic predictions to be invalid [39,41]

- It should be noticed that FEM used to solve unbounded problems has to be combined with methods which represent the influence of the infinite medium, not considered here, see for example [105].

### 2.1.4 Methods for reduction of problem size

There is an extensive effort in extending the possibility of FEM modelling into frequencies where it is too expensive computationally at present. This can be achieved by reduction of the number of DOF. In the same time one must keep in mind the necessity to model the behaviour of the structure in the frequency range considered. Of the known methods of reduction the problem size the modal decomposition, substructure approach and hierarchical ($p$-version) of FEM will be described.

#### Modal decomposition

The modal decomposition consists in transforming the arbitrary co-ordinates of the system into orthogonal set of modal co-ordinates. The analysis is carried on in terms of this new co-ordinate system. The advantage of this method is that only the modes that have natural frequencies below the frequency of interest should be used in the analysis. The remaining modes can be omitted since their contribution to the response is insignificant.

One might consider the problem of free vibrations of an undamped system described by, (compare with (2.19))

$$[-\omega^2\mathbf{M}+\mathbf{K}]\mathbf{Q}(i\omega)=\mathbf{0} \tag{2.26}$$

from which one may determine the natural frequencies and mode shapes. The natural frequency $\tilde{\omega}_i$ is the solution of the eigenvalue problem

$$\det(\mathbf{K}-\omega_i^2\mathbf{M})=0 \tag{2.27}$$

For each natural frequency $\tilde{\omega}_i$ the mode shape $\tilde{\mathbf{\Psi}}_i$ fulfils

$$(\mathbf{K}-\tilde{\omega}_i^2\mathbf{M})\tilde{\mathbf{\Psi}}_i=\mathbf{0} \tag{2.28}$$

In terms of Rayleigh-Ritz approach [76, 77], the admissible functions are the mode shapes of structure natural vibrations. The displacement field $\mathbf{u}(\mathbf{x}, t)$ may then be expressed in terms of eigenvectors $\tilde{\mathbf{\Psi}}(\mathbf{x})$, i.e.

$$\mathbf{u}(\mathbf{x}, t) = \sum_{j=1}^{n} q_j(t)\tilde{\mathbf{\Psi}}_j(\mathbf{x}) = \tilde{\mathbf{\Psi}}(\mathbf{x})\tilde{\boldsymbol{q}}(t) \tag{2.29}$$

where the modal co-ordinates have been assembled in the modal co-ordinates vector $\tilde{\boldsymbol{q}}(t) = [\tilde{q}_1(t)\ \tilde{q}_2(t)\ \ldots\ \tilde{q}_n(t)]^T$, and the normal modes have been assembled columnwise in the modal array $\tilde{\mathbf{\Psi}} = [\tilde{\mathbf{\Psi}}_1\ \tilde{\mathbf{\Psi}}_2\ \ldots\ \tilde{\mathbf{\Psi}}_n]$. The normal modes fulfil the orthogonality conditions

$$(\tilde{\mathbf{\Psi}}_i)^T\mathbf{M}\tilde{\mathbf{\Psi}}_j = \begin{cases} 0 & , \quad i \neq j \\ \tilde{M}_i & , \quad i = j \end{cases}; \qquad (\tilde{\mathbf{\Psi}}_i)^T\mathbf{K}\tilde{\mathbf{\Psi}}_j = \begin{cases} 0 & , \quad i \neq j \\ \tilde{K}_i & , \quad i = j \end{cases} \tag{2.30}$$

where $\tilde{M}_i = (\tilde{\mathbf{\Psi}}_i)^T\mathbf{M}\tilde{\mathbf{\Psi}}_i$ signifies the modal mass of mode $i$, and $\tilde{K}_i = (\tilde{\mathbf{\Psi}}_i)^T\mathbf{K}\tilde{\mathbf{\Psi}}_i$ is the modal stiffness of mode $i$. The coupling between the modes is brought forward through the damping matrix which does not necessarily fulfil a similar orthogonality condition. The modal damping coefficient of mode $i$, $\zeta_i$ and the modal coupling coefficient $\zeta_{ij}$ are defined by, [82]

$$\zeta_i = \frac{(\tilde{\mathbf{\Psi}}_i)^T\mathbf{C}\tilde{\mathbf{\Psi}}_i}{2\tilde{\omega}_i\tilde{M}_i} \quad , \quad \zeta_{ij} = \frac{(\tilde{\mathbf{\Psi}}_i)^T\mathbf{C}\tilde{\mathbf{\Psi}}_j}{2\sqrt{\tilde{\omega}_i\tilde{M}_i\tilde{\omega}_j\tilde{M}_j}} \tag{2.31}$$

Both $\zeta_i$ and $\zeta_{ij}$ are non-dimensional and independent of the normalization of the normal modes. It is often assumed, for the sake of simplicity, that the modal damping matrix is diagonal as well. This is mainly to retain the orthogonality of the modes in order to reduce the computational costs of analysis. With the orthogonality assumption on the modal damping matrix, the natural frequency of the highest mode in the decomposition should be of the same magnitude as the frequency of interest. This implies the number of modes increase with frequency of analysis.

In terms of computational efficiency the analysis based on normal mode expansion is much more efficient than the FEM. This is because the orthogonal set of natural co-ordinates is used that can be truncated above the maximum frequency of interest. The disadvantage of the method is the necessity of solving the eigenvalue problem stated in equations (2.26)-(2.28).

The shapes of modes and natural frequencies depend upon physical properties of structure. In order to take into account the uncertainties in geometry and material properties the averaging procedures must be performed, similar to those used in original FEM, see section 2.1.5. Each change requires the new set of modal co-ordinates to be extracted. This implies that the modal analysis may become insufficient when higher frequency analysis are performed.

### Sub-structuring

The DSM can be applied in its approximate form to the FEM models. The structure is initially split in a number of sub-structures (also called elements or components), see Figure 1.2. The synthesis of the structure is performed by imposing continuity of co-ordinates in interface nodes. Different sets of component co-ordinates can be used in the synthesis [18, 65]:

- Normal modes of free vibrations of the component;
- Fixed-interface modes, i.e. normal modes of the component with fixed boundary conditions at interface nodes;
- Constraint modes, i.e. deformation field achieved when a static displacement is introduced to one of the co-ordinates in interface node when all other co-ordinates are set to zero (clamped);
- Attachment modes;
- Krylow vectors.

Craig [18] suggests that the most efficient models can be achieved using constraint modes and fixed-interface modes. Because it uses the modal expansion the method is often called the component mode synthesis (CMS). The CMS has been used in [73, 90, 92, 93] to predict the power flow. The advantages of the method over conventional FEM are the possibility to access higher frequency range by reducing the computational expenses and simplify the spatial averaging procedures i.e. there is a limited number of co-ordinates for each substructure to be averaged over. The latter two references present method for reducing calculations of power flow by introducing frequency averages and spatial averages in cases of uniformly distributed white noise excitation ('rain-on-the-roof') prior to the solution of the system of equations.

### Hierarchical FEM

Another possibility for the reduction of problem size is the use of description of the displacement field that converges better than the usual polynomials used in $h$-version of FEM (where the convergence is achieved by decreasing elements size), namely to use the hierarchical or $p$-version of FEM.

In the previous studies on hierarchical formulation of the plate problem in [2] the comparison of natural frequency convergence between hierarchical FEM, the analytical solutions and the $h$-version of FEM [64, 67] were presented. The comparison shows the computational advantages of the hierarchical formulation in terms of convergence rate. This means that less co-ordinates must be used in hierarchical FEM than in conventional FEM to model the vibrations at the given frequency with the same accuracy.

Two sources of this superior performance in comparison with $h$-version of FEM are the fact that the shape functions used in the approximations approach mode shapes and that there is a possibility to adjust the complexity of in-plane and out-of-plane interpolation. The first subject corresponds to the choice of the internal shape functions and resembles the use of fixed interface modes in CMS.

### 2.1.5 Methods for dealing with uncertainties

The uncertainties in the physical properties of the structure, the geometry or the boundary conditions are a fact. The deterministic description used in formulation of FEM does not take these uncertainties into account. In fact the data used in any deterministic model are only the nominal values. In reality this nominal values correspond, in best case, to the mean of the actual values. The response of the actual structure differs from that with nominal properties, and this difference becomes more and more important with increasing frequency of interest.

The prediction of the exact response of the real structure, due to uncertainties, is impossible. Instead by calculating the response for different realizations of the structure the distribution of the responses can be predicted. Unfortunately, to obtain reliable results the amount of calculations has to be excessive. Usually the Monte-Carlo simulations are performed and the number of calculations must be great. This method has been presented among others in [74, 93], the latter in conjunction with CMS for power flow calculations. It has been noted that the Monte-Carlo simulations have to be performed on full model. For the CMS models special combination of Monte-Carlo simulations and perturbation methods have to be used. Other methods used to incorporate the uncertainties in the MDOF models are described in [11, 31]

In some cases the uncertainties of the structure can be incorporated in the modal analysis by describing the distribution of natural frequencies [11, 61].

## 2.2 Wave Approach

Another way of analysing the power flow in the structure is by considering the propagation of wave motions through it. Time varying loading or boundary conditions or alternatively the nonzero initial conditions cause the motions of the structure, which later may propagate through the structure in the shape of elastic waves. The motions of the structure are described in mathematical form by the system of PDE. This can be transformed into wave equation. Then each wave type can be considered separately.

### 2.2.1 Wave equation

The first step of wave propagation analysis is the definition of the wave types that can propagate in the structure. This is done by the decomposition of load and response into orthogonal components. In the general case of three-dimensional (3-D) unbounded medium the Helmholz decomposition is performed.

#### Unbounded Medium

The problem of wave motion in an unbounded medium has been presented among others by Achenbach, [1] and Graff, [32]. The PDE of a homogeneous, isotropic, linearly elastic body is described in terms of the displacement vector $\mathbf{u}(\mathbf{x},t)$ as, [1]

$$\mu\nabla^2\mathbf{u}(\mathbf{x},t)+(\lambda+\mu)\nabla\nabla\mathbf{u}(\mathbf{x},t)+\rho\mathbf{f}(\mathbf{x},t)=\rho\ddot{\mathbf{u}}(\mathbf{x},t) \tag{2.32}$$

where $\lambda$ and $\mu$ are the Lamé constants. These equations represent Navier's equation. The use of Helmholtz decomposition of the displacement vector, $\mathbf{u}(\mathbf{x},t)$ and unit mass loading vector $\mathbf{f}(\mathbf{x},t)$ yields

$$\mathbf{u}(\mathbf{x},t)=\nabla\phi+\nabla\times\boldsymbol{\Phi}\quad;\quad\nabla\cdot\boldsymbol{\Phi}=0 \tag{2.33}$$

$$\mathbf{f}(\mathbf{x},t)=\nabla f+\nabla\times\boldsymbol{F}\quad;\quad\nabla\cdot\boldsymbol{F}=0. \tag{2.34}$$

Helmholtz decomposition of the vector produces scalar $(\phi,f)$ and vector $(\boldsymbol{\Phi},\boldsymbol{F})$ potentials. First consider homogeneous equation, i.e. in the absence of body forces. Then by use of Helmholtz decomposition equation (2.32) yields

$$\mu\nabla^2\mathbf{u}+(\lambda+\mu)\nabla\nabla\mathbf{u}=\rho\ddot{\mathbf{u}} \tag{2.35}$$

$$\mu\nabla^2[\nabla\phi+\nabla\times\boldsymbol{\Phi}]+(\lambda+\mu)\nabla\nabla\cdot[\nabla\phi+\nabla\times\boldsymbol{\Phi}]=\rho\frac{\partial^2}{\partial t^2}[\nabla\phi+\nabla\times\boldsymbol{\Phi}]. \tag{2.36}$$

Using $\nabla\cdot\nabla\phi=\nabla^2\phi$ and $\nabla\cdot\nabla\times\boldsymbol{\Phi}=0$ one may rearrange (2.36) into the form

$$\nabla[(\lambda+2\mu)\nabla^2\phi-\rho\ddot{\phi}]+\nabla\times[\mu\nabla^2\boldsymbol{\Phi}-\rho\ddot{\boldsymbol{\Phi}}]=0 \tag{2.37}$$

which reduces to two wave equations:

$$\nabla^2\phi=\frac{1}{c_L^2}\ddot{\phi}\quad;\quad c_L^2=\frac{\lambda+2\mu}{\rho} \tag{2.38}$$

$$\nabla^2\boldsymbol{\Phi}=\frac{1}{c_T^2}\ddot{\boldsymbol{\Phi}}\quad;\quad c_T^2=\frac{\mu}{\rho} \tag{2.39}$$

$c_L$ is the propagation velocity of longitudinal wave (2.38), also called volumetric waves or primary (P) waves. $c_T$ is the propagation velocity of shear waves (2.39),

also called rotational, equivoluminal, or secondary (S) waves. In the presence of body forces the inhomogeneous wave equations have the form

$$\nabla^2\phi - \frac{1}{c_L^2}\ddot{\phi} = -f \quad ; \quad \nabla^2\boldsymbol{\Phi} - \frac{1}{c_T^2}\ddot{\boldsymbol{\Phi}} = -\boldsymbol{F}. \tag{2.40}$$

The wave type depends on the type of excitation. The most straightforward type of excitation to analyse is the time dependent point force. In this case the solution has the polar symmetry, with the centre of the sphere being in the point of loading. This property allows for reducing the problem from three-dimensional to one-dimensional. The wavefront generated by point load propagates away from the source. The solution to line load (in-plane and out-of-plane) is also possible to obtain, but are more difficult than the one of polar symmetry.

These general consideration can be used if the medium infinite, or semiinfinite in all directions. However, similar considerations can be performed for the 1-D and 2-D structures. They are not infinite in all directions, but in one or two directions only.

### Infinite 1-D and 2-D Domains

The propagation of disturbances in one and two-dimensional media is more significant from the engineering point of view. The one-dimensional members include rods and beams, the former supporting no transverse waves. The two-dimensional members include membranes, plates and shells.

In any case the starting analysis point is the set of wave equations similar to (2.38) and (2.39), defined for each type of wave that can be supported by the member. The wave types correspond to the particular solution of homogeneous EOM. The assumptions underlying the continuum mechanics theory that is used in the analysis have impact on the wave types that should be considered. For example in the Bernoulli-Euler beam theory the bending motions in the perpendicular planes are independent. In this case two wave types, one for each plane will be considered. In addition the longitudinal and transverse waves will be present.

The consideration of wave propagation in structural members was presented among others in [21, 26]. The properties of the elastic waves that can propagate in rods, beams, plates and shells are presented and allow for better understanding of dynamic behaviour of structure and related issues including radiation and fluid-structure interaction. The transmission and reflection coefficients for different types of junctions between semiinfinite members have also been presented in these references.

#### Finite Members

In structural analysis the medium is not infinite, and the processes of reflection, refraction and transmission can appear at the boundaries and discontinuities. The wave reflected from the discontinuity interferes with the incident wave and resulting in the new wave field. Also, if two or more members are connected, the transmission of waves might appear. The multiple reflections from the boundaries give rise to the resulting standing wave patterns at certain frequencies. These standing waves are the system's natural mode shapes.

The analysis of wave propagation in finite members becomes difficult because of these multiple reflections and transmissions, and so it is seldom used. The modal decomposition is used instead, see section 2.1.4.

### 2.2.2 Limits of wave analysis

The analysis of structural motions and power flow by solving the wave equations are mainly used in the case of single members or a case of more semiinfinite members joined at one location. The assumption of members' semiinfinity is required to ensure that the wave travelling away from the junction does not return to it.

This approximation is used to calculate the coupling loss factors that relate energy transfer between subsystems in SEA. Even though the subsystem is hardly ever unbounded the assumption is equivalent to the assumption that the incident and reflected waves are uncorrelated. This is another limit of the wave approach in the case of finite members. The assumption concerning the correlation of incident and reflected wave can be justified by the fact that neither the boundary conditions nor the dimensions of the structure are not known exactly. This assumption tends to be fulfilled in high frequencies.

## 2.3 Statistical Energy Analysis

For the high frequency response of complicated structures, especially in the building acoustic the frequently used method is the SEA. The origins of SEA are grown out from the limitations of deterministic models and analysis, like FEM. One of these limitations is the use of deterministic description of uncertain reality. The second limitation is the necessity to include excessive amount of DOF in multi DOF systems to model the high frequency behaviour.

The deterministic approach results in the response of the ideal (nominal) structure. If one is concerned with the average response of the ensemble of nominally identical but slightly different structures then the additional computations are neces-

sary. The average response of the ensemble is calculated from the set of deterministic responses, each calculated for the different realization of the structure. In SEA the mean properties of the ensemble are assumed from the beginning and the variables used are the ensemble averaged quantities. The response variables are frequency averaged and it is assumed that both averaging types are equivalent. Similar problems concern the uncertain loads acting on the structure.

By the use of gross system variables, averaged over position and frequency, the amount of variables in SEA equations is reduced to few and is independent of frequency. That allows to omit the second limitation of the FEM when considering high frequency analysis.

Early works on SEA were inspired by room acoustic and statistical mechanics [41]. In room acoustic one deal with a large number of DOF and the only possible approach is through statistical considerations. Also the stochastic mechanics gives the background for considerations of uncertain systems in terms of mean values. There is, however, considerable difference between modes in room and in elastic body. In room there is a huge amount of modes present even in a narrow frequency band. Moreover, these modes, according to Boltzmann theory, have the same energy so the average value of modal energy is actually the present value of energy of mode. This does not hold for mechanical systems, and it will be presented later that the distribution of energy among modes may differ considerably from the mean. There are two approaches to present the SEA basis. In the first one the energy exchange between oscillators is presented. Then the results derived for two weakly coupled oscillators are extended to two sets of oscillators - two multi-modal subsystems, and finally to the structure consisting of several subsystems, see [21, 68].

The other way of presenting the basis of SEA is by setting up the energy balance for the set of subsystems. In this approach the general feature of SEA, namely simplicity can be seen from the very beginning, and the discussion of energy exchange among multi-modal subsystems comes later, see [19]. While the first approach follows the historical evaluation of the method, it seems more straightforward to present it using the latter one.

First the analysed structure is defined in the sense that the border is drawn between the structure and the 'rest of the world'. This is often a difficult task. Assume that the noise transmission from the equipment in the basement to the apartment on the first floor is of interest. One could build a model consisting of this equipment, surrounding room, ceiling and the room above. The radiation of noise from equipment and its attenuation by the ceiling would cause the noise level in the room. But there are other paths of transmission, like walls which could also influence the resulting noise level. Probably the vibrations generated by the equipment and transmitted by the suspension system could also be significant. This clearly shows that the decision which part of the world should be included in the analysis and which not is not straightforward.

After the structure is defined it is divided into subsystems, see Figure 1.4. Each subsystem will be described by one energy variable. The definition of subsystems is not straightforward again. More insight into the problem will be given when the SEA assumptions are discussed. Finally the basic relation of SEA, namely the power balance among subsystems is set up.

### 2.3.1 Power balance

The fundamental power balance for the subsystem states that the time averaged power influx to subsystem $i$ must balance the time averaged power flux out from this subsystem and the increase the of the subsystem energy. Most often the steady state problems are considered, so that there is no energy increase in the subsystem. This also means that for the entire system the power supplied by external sources must be dissipated within the system.

The power balance for the steady state can also be formed for each subsystem separately. The power input to the $i$th subsystem from external loading $\Pi_{i,ext}$, power exchange with other subsystems, $\Pi_{ik}$ and dissipation of energy inside the subsystem $\Pi_i^{diss}$ must add up to zero. The losses in subsystem. Then the power balance may be rewritten in the form

$$\langle \Pi_i^{ext} \rangle_t + \sum_{k=1,k\neq i}^{s} \langle \Pi_{ik} \rangle_t + \langle \Pi_i^{diss} \rangle_t = 0. \tag{2.41}$$

The relation between various elements of equation (2.41) is frequency dependent. It is argued that above first few resonant frequencies, where the resonant behaviour is high, the response of the structure can be well approximated by the frequency average. The outcomes of this assumption will be discussed later. Now it is important that the analysis is carried on with very low frequency resolution, often in octave or one/third octave bands. This is partly because of the usual resolution of acoustic analysis.

It is also assumed that the energy is equally distributed within the subsystem, so that the spatial average of the subsystem energy describes well the energy of the subsystem.

#### Power Input

The subsystem may be excited in terms of external point forces, pressures, etc. The time average power input may be evaluated as the time averaged product of the force $\mathbf{f}(\mathbf{x}, t)$ and resulting velocity $\dot{\mathbf{u}}(\mathbf{x}, t)$ at the location of applied force, i.e. [21]

$$\langle \Pi^{ext} \rangle_t = \langle \mathbf{f}(\mathbf{x}, t) \dot{\mathbf{u}}(\mathbf{x}, t) \rangle_t. \tag{2.42}$$

In the case of harmonic point load this can be calculated by the product of amplitudes of force and displacement as

$$\langle \Pi^{ext} \rangle_t = \frac{1}{2} \Re \left[ i\omega \mathbf{F}(\mathbf{x}) \mathbf{U}^*(\mathbf{x}) \right] = \frac{1}{2} |\mathbf{F}^2| \Re(Y_{point}). \tag{2.43}$$

$\Re(Y_{point})$ is the real value of the point mobility, i.e. the ratio of velocity amplitude to force amplitude (both complex quantities) at certain frequency.

If the frequency averaged value of the power input is of interest, then the mobility of infinite structure can be used [68, 96]. Care must be taken, however, when using the averaged mobility in regions of low mode number, especially for lightly damped structures. Then the modal overlap (see (2.51)) is low and the single resonance governs the response. If more than one point force acts on the structure at the same time, then the contribution from all sources should be summed. However, the loading acting in one point of the subsystem influence the response in each other point, and therefore the resulting velocity has to be considered.

When the distributed loading act on the structure then averaging procedures have to be used in order to estimate the power input. This is often done by considering modal response of the structure. By averaging over modal responses one may simplify the expressions for power input. The input power from the distributed load depends strongly on the matching between the spatial pattern of the excitation and the response.

In the case of complicated types of loading one may also estimate the power input from numerical calculations, for example by use of FEM. Only the subsystem of interest is analysed to reduce the model, and then the results of calculations are used in averaging.

### Dissipated Power

The dissipation of power occurs due to internal and external friction. The latter one may be connected with sound radiation, presence of boundaries with subsystems excluded from analysis, etc. Generally the dissipated power may be written in the form

$$\langle \Pi_i^{diss} \rangle_t = \omega \eta_i E_i \tag{2.44}$$

where $\eta_i$ denotes the loss factor due to all the energy dissipation channels and $E_i$ denotes the energy of subsystem $i$. To predict the damping loss factor $\eta_i$ one have to consider different dissipation mechanisms, like material damping , boundary damping, dissipation of energy by interaction with surrounding, etc.

### Power Transfer

Probably the strongest assumption in SEA theory is the one that relates the power transmitted through boundaries between two subsystems to the difference between their modal energy. This postulate agrees with the theory of heat transport, where the difference in temperatures governs the flow of energy. This analogy keeps also in the case of room acoustic, because of large number of modes in narrow frequency range and the smoothness of response function. Langley [53] has shown that it can also be used in the case of structural coupling if the appropriate definition of modal energy, weak coupling and coupling loss factors are used.

From the modal point of view the exchange of energy between subsystems is governed by the mode to mode coupling. This analogy is drawn from the energy exchange between two conservatively coupled oscillators, i.e. there is no dissipation of energy within coupling. In the early works on SEA the problems of conservatively coupled oscillators have been studied in, for example [69, 87]. Conclusion from those analysis was that providing the coupling between oscillators is 'weak', and the broadband stochastic excitation acts on the oscillators then the power flow will be proportional to the energies of 'uncoupled' oscillators, $\varepsilon_1$ and $\varepsilon_2$ , i.e.

$$\langle \Pi_{12} \rangle_t = \gamma(\varepsilon_1 - \varepsilon_2) \tag{2.45}$$

where $\gamma$ is the frequency dependent proportionality factor. The energy of single oscillator has been denoted by $\varepsilon_i$ which in the case of single DOF equals to $E_i$. This different symbol has been used in order to underline that equation (2.45) is valid for the single DOF systems, or for MDOF systems if the average modal energy is considered, i.e. the energy of single mode, not the energy of subsystem.

By analogy the exchange of power between subsystems consisting of several modes can be driven. First one considers only one mode from one subsystem. It exchanges energy with all modes from the other subsystem according to two oscillator models. Then contribution from all the modes is calculated by summing all the modes in this subsystem. To simplify the further calculations the general assumptions are made as follows.

- Each subsystem is drawn from the assembly of nominally identical subsystems with uncertainties. Therefore, the natural frequency of the mode, providing it is within frequency band of interest, is uniformly probable within this frequency band. In other words the modal density is constant and equals $n(\omega) = dN/d\omega$ where $N$ is the number of modes.
- Each mode is equally energetic, and therefore the averaged modal energy can be used instead of exact value. Modes are incoherent with other modes of the same subsystem. These assumptions require that the subsystems are properly defined, for example the longitudinal and bending modes should not be included in the same subsystem.

- For convenience one also assumes the modal damping factors to be equal for each mode. This assumption is not necessary, but it simplifies the notation considerably.

Using the fact that each mode has equal energy and that there are $N_i$ modes in frequency band ($N_i = n_i\Omega$) one may express the energy flow from $m$th mode of subsystem $i$ to $n$th mode in subsystem $j$ at certain frequency as $(\Pi_{ij})_{mn} = \gamma\omega(E_i/n_i - E_j/n_j)$. Taking the combination of all possible interchanges between modes the power flow between subsystems $i$ and $j$ is then expressed by

$$\langle \Pi_{12} \rangle_t = \omega \left[ \eta_{ij} E_i - \eta_{ji} E_j \right] \tag{2.46}$$

where the total energy of subsystem is denoted by $E_i$ and the coupling loss factor $\eta_{ij}$ have been introduced. The coupling loss factor is defined in the similar way to the coupling loss factor, so it acts on the product of energy and frequency. Equation (2.46) holds if the assumptions of SEA are fulfilled. Those include the so-called weak coupling between subsystems.

The reciprocal relation for coupling loss factors is stated as [68]

$$\eta_{ij} N_j = \eta_{ji} N_i \quad ; \quad \eta_{ij} n_j = \eta_{ji} n_i \tag{2.47}$$

in terms of number of modes and modal density respectively. The modal approach is not widely used for the development of coupling loss factors. It is rather used as a justification for the assumption of energy flow being proportional to the average energy difference.

Another way of calculating the coupling loss factor is more often used [19,21,68], i.e. by considering the transmission and reflection of travelling waves that reach the discontinuity in the material properties, like the junction. Each type of wave carries certain amount of energy that is either reflected from the junction or transmitted through it. The main assumption in using the wave approach to calculate the coupling loss factors is that the members are semiinfinite, i.e. the wave that leaves the vicinity of the junction does not return after reflection from another boundaries.

### System of Equations

Once the terms in power balance, (2.41), are determined the system of equations can be set up. This may be written in the matrix form as

$$\begin{bmatrix} \eta_1 + \sum_{k\neq 1} \eta_{1k} & -\eta_{21} & \cdots & -\eta_{s1} \\ -\eta_{12} & \eta_2 + \sum_{k\neq 2} \eta_{2k} & \cdots & -\eta_{s2} \\ \vdots & \vdots & \ddots & \vdots \\ -\eta_{1s} & -\eta_{2s} & \cdots & \eta_s + \sum_{k\neq s} \eta_{sk} \end{bmatrix} \begin{bmatrix} \omega E_1 \\ \omega E_2 \\ \vdots \\ \omega E_s \end{bmatrix} = \begin{bmatrix} -\langle \Pi_1^{ext} \rangle_t \\ -\langle \Pi_2^{ext} \rangle_t \\ \vdots \\ -\langle \Pi_s^{ext} \rangle \end{bmatrix} \tag{2.48}$$

In the presented form the coupling matrix is not symmetric. One may change this property by use of modal energy $\varepsilon_i = E_i/n_i$ of subsystems instead of total energy $E_i$. By dividing each row of energy vector by the proper modal density and multiplying the coupling matrix in order to fulfil the equality one obtains

$$\boldsymbol{\eta}\omega\boldsymbol{\varepsilon} + \langle \boldsymbol{\Pi}^{ext} \rangle_t = \mathbf{0} \tag{2.49}$$

where the coupling matrix $\boldsymbol{\eta}$ is defined as

$$\boldsymbol{\eta} = \begin{bmatrix} (\eta_1 + \sum_{k\neq 1} \eta_{1k})n_1 & -\eta_{21}n_2 & \cdots & -\eta_{s1}n_s \\ -\eta_{12}n_1 & (\eta_2 + \sum_{k\neq 2} \eta_{2k})n_2 & \cdots & -\eta_{s2}n_s \\ \vdots & \vdots & \ddots & \vdots \\ -\eta_{1s}n_1 & -\eta_{2s}n_2 & \cdots & (\eta_s + \sum_{k\neq s} \eta_{sk})n_s \end{bmatrix}. \tag{2.50}$$

The modal energies and the input power have been grouped in the vector of modal energies $\boldsymbol{\varepsilon} = [\varepsilon_1, \ \ldots, \ \varepsilon_s]^T$ and vector of power input $\boldsymbol{\Pi}^{ext} = [\Pi_1^{ext}, \ \ldots, \ \Pi_s^{ext}]^T$. When the coupling and damping loss factors are calculated, the coupling matrix can be found and (2.49) can be solved for energy levels.

### 2.3.2 Limits of SEA

The limits of SEA follow the assumptions used to derive the power balance. A comprehensive discussion of SEA limits can be found for example in [23].

#### Low modal overlap

The shape of the frequency response function of multi-modal system depends on the properties of its modes, namely the modal density and bandwidth of the resonance curve. Modal density is an average number of modes per frequency band. Bandwidth is a width between points which are 3 [dB] lower than the resonant peak at the resonance curve. The bandwidth of the resonance curve is given by $b_r = \eta\omega_r$ (in radians) where $\omega_r$ is the resonant angular frequency .

The response at given frequency is controlled by modes which resonance lies close to this frequency. If the number of modes is low and the bandwidth of each resonance curve is small, then the overall response is highly frequency dependent. It is controlled by single resonance, and the deviation from the frequency averaged value is high [25]. On the other hand, if the modal density is high and/or the bandwidth wide then the resonant peaks overlap. The response is smooth, close to its frequency averaged value.

> If the damping is relatively high (...), then the frequency response of a subsystem is fairly smooth compared to the case where the damping is

low. A more useful parameter is the modal overlap factor , defined as the ratio of the modal bandwidth (either the half-power bandwidth or the effective bandwidth which is $\pi/2$ times higher)to the average frequency spacing between modes [19].

The modal overlap $\mathcal{M}^{(s)}$ of the subsystem $s$ is therefore given as

$$\mathcal{M}^{(s)} = \begin{cases} \frac{\eta^{(s)} f}{\delta f_s} = \eta^{(s)} f n_s(f) = \eta^{(s)} \omega n_s(\omega) & \text{(half-power bandwidth)} \\ \frac{\pi}{2} \frac{\eta^{(s)} f}{\delta f_s} & \text{(effective bandwidth)} \end{cases} \tag{2.51}$$

where $\delta f_s = 1/n(f) = 1/2\pi n(\omega)$ is the average frequency spacing (in [Hz]). If modal overlap is below unity then the single responses will be visible in the response function.

### Strong coupling

The term 'weak coupling' is used when the power flow between coupled multi-modal systems is considered. But the term itself is not clear, and there exist no definition of weak coupling, or maybe too many different definitions [24, 28, 48, 50, 51, 55] to be able to judge if the subsystems of interest are or are not weakly coupled. The proposed criteria of strength of the coupling consider:

- Ratio between coupling forces and internal forces. The coupling forces should be small in comparison to the internal forces, or in other words the internal forces with and without presence of coupling should be similar. However, there is no quantitative measure of this difference that would be appropriate in order for the coupling to be weak.
- The influence of the coupling on the subsystem's response functions or the Green's functions. If the Green's functions of the subsystem are not affected by the presence of coupling than the coupling is weak. This definition is again only a quantitative one, and there are no indications on how the strength of coupling influences the quality of SEA predictions.
- Ratio between coupling loss factors and internal loss factors. The bigger the internal dissipation is the stronger the coupling could be. However, the strong damping is in opposition to energy equipartition within subsystems which in SEA are assumed to have uniform energy distribution. This requires that the wave field can propagate freely within the subsystem to excite the entire subsystem equally. In the conditions of strong damping the wave amplitude reduces faster and there will be an energy gradient within the subsystem.

The criteria of weak coupling is required for the energy transmission approximation to hold. If the coupling is weak then only resonant coupling will be present.

The second definition of the strength of coupling can be in the easiest way incorporated in the considerations of application SEA in low frequency region. It is well known that the lowest modes of the system are most affected by the boundary conditions. The response function or Green's function can be presented in terms of modal expansion. This means also that the Green's functions of the system are most affected by the boundary conditions in low frequencies. The presence or absence of coupling changes the boundary conditions of the subsystem. The main differences will be visible in the low frequencies. Therefore, even though the coupling can be assumed weak in high frequency, it will still be strong in low frequencies.

### Indirect coupling

Another limitation of SEA is the assumption of resonant power exchange (resonant coupling) that leads to the problems with treating the indirect coupling. The SEA coupling loss factor is zero between subsystems that have no common junction.

The issue of indirect coupling and non-resonant coupling have been discussed among others in [28, 39]. The indirect coupling can occur at the low modal overlap conditions, where the non-resonant coupling becomes important. Then the energy can be transmitted from one subsystem to another through the middle subsystem that does not accumulate energy but acts more as a junction. This property, i.e. the ability of the subsystem to transmit energy without dissipating it is sometimes called 'tunneling'. The fairly standard example of 'tunneling' appears in the case of three plates assembly where the two external plates are parallel to each other and perpendicular to the middle one. The bending modes of the two parallel plates are coupled to the in-plane modes of the middle plate. The resonant coupling between either of external plates to the middle plate is poor, but the energy can be transmitted to the bending of the remaining plate and excite it fairly strong.

These considerations are most important in the case of experimental extracting of coupling loss factors. It is because in the measurements the in-plane energy is difficult to consider and therefore is excluded from analysis, even though it can take part in energy transfer. Other conditions where the 'tunneling' can occur include strongly coupled set of structures and periodic structures.

## 2.4 Deriving CLF from FEM results

Several authors have proposed the use of FEM modelling to asses the coupling loss factors (CLF) [68, 89, 95]. The aim of this approach was to incorporate the non-resonant energy distribution, and to extend the applicability of SEA models in lower frequencies. It is also meant for junctions that cannot be analysed by the classic wave approach due to the complexity. The approach uses some sort of 'numerical

experiment' similar to the real test by power injection method. Usually only one junction is considered at a time. The power is injected by means of loading, either 'rain on the roof' (spatially distributed uncorrelated white noise), or other load type and the distribution of energy is studied. From the distribution of energy the CLF can be estimated.

The reason for modelling one junction at a time is to reduce the computational costs of the method. Unfortunately, in the low frequency region other assumptions of SEA are not met. The behaviour of subsystems extracted to approximate the CLF is, in low frequencies, dependent of boundary conditions. By analysis of the part of the structure only the information about boundary conditions in original configuration is lost. One possibility of making the method general could be by averaging the CLF obtained in calculations with various boundary conditions. Simmons [95] discusses difficulties encountered when introducing additional constraints in the analysis.

Unfortunately, the assumptions of SEA apply not only to coupling loss factors. In low frequency range the assumption of weak coupling breaks down power flow through one junction can be affected by the presence of other junctions. This issue was discussed in [28]. Therefore for the derivation of CLFs in low frequency region the global FEM model should be used instead of modelling separate junctions.

One of the approaches that reduce the computational costs of FEM power flow calculations is the substructure approach. The structure should be divided into parts which are only connected at specific points. If the line connection is considered then only finite number of points at the junction is considered. The substructures are analysed separately and the Green's functions that relate the forces and co-ordinates at the junction points are derived either in terms of infinite or finite number of normal modes. Finally the assembly of the substructures can be considered and solved for energy distributions or energy flow coefficients (deterministic CLF) or coupling loss factors if the ensemble averages are introduced. This approach has been successfully used in [73, 92].

## 2.5 Hybrid FEM-SEA

The first step of hybrid formulation is the partition of co-ordinates into global and local set [63]. This partition is performed because of the differences in dynamic properties of different members and at different frequencies. The global co-ordinates are to be modelled by deterministic methods, like the FEM. The local modes should be modelled only in statistical sense for example by the use of SEA power balance. This kind of partition has also been proposed in the fuzzy structure theory [83], where partition in the 'master' structure and the 'fuzzy' structure is performed. The partition of structural response into short wavelength and long wavelength components has been proposed in [6].

The rationale for the partitioning of the co-ordinates is common for the two previously mentioned methods and hybrid FEM-SEA. That is to distinguish between the part of the response that should be modelled in a deterministic way to account for resonant and non-resonant behaviour and the part of response that is highly uncertain, and only the statistical measures can give insight in this problem.

If the partition of the shape functions is performed, the displacement field $\mathbf{u}(\mathbf{x}, t)$ within the structure will have the form (compare to (2.3), where single co-ordinate set was used)

$$\mathbf{u}(\mathbf{x}, t) = \sum_{i=1}^{N_{glob}} q_{g_i}(t)\boldsymbol{\Psi}_i^g(\mathbf{x}) + \sum_{i=1}^{N_{loc}} q_{l_i}(t)\boldsymbol{\Psi}_i^l(\mathbf{x}). \tag{2.52}$$

$N_{glob}$ is a number of global co-ordinates, i.e. $\boldsymbol{q}_g = [q_{g_1},\ q_{g_2}, \ldots, q_{g_{N_{glob}}}]^T$. $N_{loc}$ is the number of local co-ordinates, i.e. $\boldsymbol{q}_l = [q_{l_1},\ q_{l_2}, \ldots, q_{l_{N_{loc}}}]^T$. The Fourier transforms of $\boldsymbol{q}_g$ and $\boldsymbol{q}_l$ are denoted by $\mathbf{Q}_g$ and $\mathbf{Q}_l$, respectively.

The performed partition may be seen to some extent as a application of substructure method [92].The main difference comes from the criteria used for the partition of the co-ordinates and from the fact that the local modes are modelled statistically. The partition performed in (2.52) allows to write equation (2.19) in the form

$$\begin{bmatrix} \mathbf{D}_{gg} & \mathbf{D}_{gl} \\ \mathbf{D}_{gl}^T & \mathbf{D}_{ll} \end{bmatrix} \begin{bmatrix} \mathbf{Q}_g \\ \mathbf{Q}_l \end{bmatrix} = \begin{bmatrix} \mathbf{F}_g \\ \mathbf{F}_l \end{bmatrix}. \tag{2.53}$$

Reduction of local co-ordinates $\mathbf{Q}_l$ from the first row yields the global EOM in form:

$$[\mathbf{D}_{gg} - \mathbf{D}_{gl}\mathbf{D}_{ll}^{-1}\mathbf{D}_{gl}^T]\ \mathbf{Q}_g = \mathbf{F}_g - \mathbf{D}_{gl}\mathbf{D}_{ll}^{-1}\mathbf{F}_l \Rightarrow [\mathbf{D}_{gg} - \Delta\mathbf{D}]\ \mathbf{Q}_g = \mathbf{F}_g - \Delta\mathbf{F}. \tag{2.54}$$

The size of this set of equations is equal to the number of co-ordinates in the global set. However, the solution of (2.54) is only possible after the additional terms $\Delta\mathbf{D}$ and $\Delta\mathbf{F}$ are known. The additional dynamic stiffness $\Delta\mathbf{D}$ can be evaluated by assuming that the local dynamic stiffness matrix is diagonal. The local dynamic stiffness matrix consists of a set of dynamic stiffness matrices of single subsystems. Each of the dynamic stiffness matrices for subsystems can be diagonal if the natural co-ordinate system (natural modes) is used for the description. The assumption that the coupled matrix is still diagonal requires that the coupling among local modes from different subsystems is weak. This is an assumption of the SEA which have to be fulfilled in order to apply SEA for local calculations, and therefore must be fulfilled. Certain choices of local co-ordinates may cause this assumption to be exactly fulfilled, as in the case of rod elements. This issue will be further considered in Section 5 because it is one of the crucial points in the approach. With the diagonal local dynamic stiffness matrix the entries of $\Delta\mathbf{D}$ can be written as, see [63]

$$(\mathbf{D}_{gl}\mathbf{D}_{ll}^{-1}\mathbf{D}_{gl}^T)_{mn} = \sum_{s=1}^{N_{sub}} \sum_{j=1}^{N_{loc}^{(s)}} (\mathbf{D}_{gl})_{mr(j,s)} (\mathbf{D}_{gl})_{nr(j,s)} \left[(\omega_j^s)^2(1 + i\eta_s) - \omega^2\right]^{-1} \tag{2.55}$$

where the summation covers all subsystems (from 1 to $N_{sub}$) and all local modes within each of subsystems, i.e. up to $N_{loc}^{(s)}$ which is the number of local modes in subsystem $s$. In addition the term $r(j,s)$ denotes the co-ordinate of the $j^{\text{th}}$ local mode in subsystem $s$, $\eta_s$ is the damping loss factor in subsystem $s$ and $\omega_j^s$ is the $j^{\text{th}}$ natural frequency of subsystem $s$.

One possibility of calculating the additional terms in the global equation has been presented in [63] in the case of rod elements. The partition is performed in the local co-ordinates (modes) depending on the relation between the natural frequencies and the analysed frequency. The contribution from resonant modes, and from inertia dominated modes is considered, and the contribution from stiffness dominated modes is omitted. Detailed description of the method presented in [63] to calculate the additional stiffness matrix and the additional loading vector in the case of rod assembly will be presented in the example, see Section 2.6.4. The additional loading vector is calculated using similar approximations as in the case of additional stiffness matrix.

It should be noted that the additional terms are only calculated in terms of their mean value as the local modes are supposed to be uncertain. In similar way the influence from the 'fuzzy structure' on the master structure' is presented, [83].

The remaining local EOM:

$$\mathbf{D}_{gl}^T \mathbf{Q}_g + \mathbf{D}_{ll} \mathbf{Q}_l = \mathbf{F}_l \tag{2.56}$$

is solved after the equation (2.54) has been solved. The term $\mathbf{D}_{gl}^T \mathbf{Q}_g$ is then known and can be regarded as the known distributed load on the local structure. A set of SEA equation similar to (2.41) should be set up for subsystems. Subsystems are defined as a set of local modes. For that reason the local modes should fulfil SEA assumptions concerning modal overlap, equipartition of modal energy etc. (see Section 2.3).

The coupling between local modes across subsystems depends on the definition of local shape functions. For the case of 1-D structure the number of coupling points is finite. All the coupling variables can be included in the global set of co-ordinates. Then, there are at least two possibilities for the choice of local co-ordinates. If the local co-ordinates are taken to be the clamped modes of each of elements then the contribution from these vanishes at the coupling points. In this case there is no direct coupling between local modes across the coupling point and the subsystems in SEA sense are uncoupled. Then the energy balance for each of the elements should be set up separately. However, the local modes could also be defined as modes of an element with free boundary conditions. Than the local modes influence the coupling points and therefore the coupling between SEA subsystems should be considered. In that case the normal CLF should be used in the same way as in standard SEA. If the 2-D or 3-D cases are considered, the clamped modes can no longer be used because the number of coupling variables is infinite. Therefore, the energy can be

exchanged directly among subsystems and it is governed by equation 2.46.

Two sources of power input to the subsystems have to be considered. The direct power input from external sources can be dealt with in the same manner as in the standard SEA. The remaining power input comes from the coupling with the global modes. Since the global EOM is solved prior to the local EOM the coupling forces from the global motions that act on the local motions are known, and the power input can be approximated. Generally, the cross-terms of the power input between the two sources should be considered.

### 2.5.1 Requirements for the basis of hybrid approach

The partition of co-ordinates into the global and local set is performed based on the wavelengths of the structural motions that can be described by either set. the global co-ordinates correspond to long wavelengths, the local co-ordinates to short wavelengths. There is a difference between the behaviour of either set. With the same material properties the long wavelengths correspond to stiff members and the short wavelengths to the soft members. The stiff members dominate the stiffness of the entire structure and the soft members do this in limited amount.

The long waves can also be seen as the low order natural modes of the same member and the short waves correspond to the high order natural modes. The low order modes are very sensitive to the definition of boundary conditions. The high order modes are almost independent on the boundary conditions. This is another reason for including the former ones in global equations and the latter ones in the local equations.

The modal overlap (see (2.51)) is proportional to the frequency and so the high modal overlap condition, which is assumed in SEA, will be met at high frequencies, where the description is dominated by short wavelengths. This is another reason for separating the short and long wave components.

Finally, the low order modes are less sensitive to structural uncertainties than the high order (apart from the uncertainties in boundary conditions considered before). Therefore, the deterministic description can be used for the global formulation and the statistical description is necessary for the local description.

The term global co-ordinate is used as a synonym to the term global mode and wave component with long wavelength. In similar way the local co-ordinate corresponds to local (high order) mode or wave component with short wavelength. Therefore, the correspondence between the co-ordinates and the wavelengths have to be assured, so that the partition into global and local co-ordinates is equivalent with the partition into short and long wavelength motions.

The use of natural modes of the whole structure would be a straightforward choice as a basic set of co-ordinates. The low order modes would be included in the

global set of co-ordinates and the high order modes - in the local set. Unfortunately, the knowledge of mode shapes and the natural frequencies can only be obtained for limited cases, especially if high order modes are required.

To overcome the problem of calculating the exact modes of the whole structure the component mode synthesis could be used. The modes of separate substructures (or subsystems in SEA terminology) could be used, but with greater care, as an approximate modal set. In much the same way the hierarchical formulation of FEM can be used. This has an additional advantage that the modal analysis is not necessary even for substructures. Again an approximation of the modal co-ordinate set is achieved, in similar manner as by use of component mode synthesis. Care must be taken in the general formulation that the partition of the co-ordinates is performed according to the wavelength criteria.

## 2.6 Example of Power Flow Calculations

The analysis of two coupled rods vibrating longitudinally may serve as the example of FEM, SEA and hybrid FEM-SEA applied to power flow calculations. The availability of the analytical solution is an advantage in this case because the exact solution can be used for comparison. The aim of the example is to introduce the terms and algorithms used in power flow calculations as well as discuss the issues of convergence, quality of results etc.

The rods can only support the longitudinal waves propagating along the rod's axis so that the problem becomes one-dimensional and the co-ordinate system $\mathbf{x}$ can be reduced to single co-ordinate $x$. The length of rod $i$ is denoted by $L^{(i)}$, and the position of point $i$ in global co-ordinate system is denoted by $x_{(i)}$, see Figure 2.1.

The material properties include the cross-section area $A^{(i)}$, mass density $\rho^{(i)}$ and elasticity module $E^{(i)}$ as well as damping loss factor $\eta^{(i)}$. The possibility of modifying the properties of the structure in order to reduce or modify the energy flow is crucial for applying the method. For that reason several cases with different sets of data are used (see Table 2.1) and the necessary steps involved in updating the model are

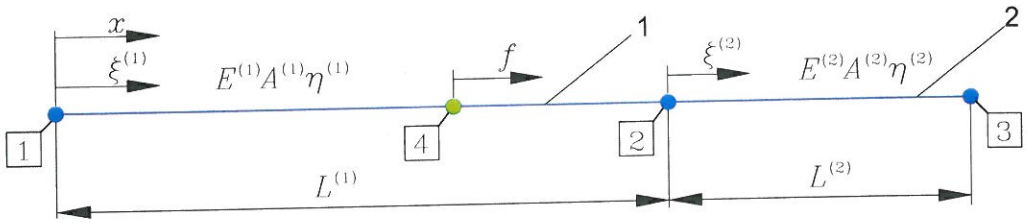


**Figure 2.1**: Two coupled rods

**Table 2.1**: Geometry, material properties and minimum number of elements necessary for convergence below 20 [kHz] of coupled rods.

| | Element | $L$ [m] | $A$ [m$^2$] | $E$ [MPa] | $\rho$ [kg/m$^3$] | $\eta$ | $L/l^{(el)}$ |
|---|---|---|---|---|---|---|---|
| Case I | rod 1 | 1 | 0.0025 | 210 | 7800 | 0.003 | 31 |
| | rod 2 | 1.3 | 0.0001 | 210 | 7800 | 0.001 | 41 |
| Case II | rod 1 | 1 | 0.0025 | 210 | 7800 | 0.003 | 31 |
| | rod 2 | 1.3 | 0.0001 | 60 | 8500 | 0.001 | 79 |
| Case III | rod 1 | 1 | 0.0025 | 210 | 7800 | 0.003 | 31 |
| | rod 2 | 1.3 | 0.0036 | 60 | 8500 | 0.001 | 79 |

presented.

The axial displacement of a rod $i$ denoted by $u^{(i)}(x,t)$ can be derived from the differential EOM [76]. The EOM of longitudinally vibrating rod has the form:

$$\frac{\partial}{\partial x}\left[A^{(i)}(x)E^{(i)}(x)\frac{\partial u^{(i)}(x,t)}{\partial x}\right] - \rho^{(i)}(x)A^{(i)}(x)\frac{\partial^2 u^{(i)}(x,t)}{\partial t^2} = 0 \tag{2.57}$$

in time domain and transformed to frequency domain reads:

$$\frac{\partial}{\partial x}\left[A^{(i)}(x)E^{(i)}(x)\frac{\partial U^{(i)}}{\partial x}\right] + \omega^2\rho^{(i)}(x)A^{(i)}(x)U^{(i)} = 0 \tag{2.58}$$

for natural undamped vibrations. In the case of constant parameters $A^{(i)}$, $E^{(i)}$ and $\rho^{(i)}$ along the rod the equation (2.58) simplifies to the form of wave equation:

$$\frac{\partial^2 U^{(i)}}{\partial x^2} + (k^{(i)})^2 U^{(i)} = 0 \tag{2.59}$$

where the wave number $(k^{(i)})^2 = \omega^2\rho^{(i)}/E^{(i)}$. The solution of the homogeneous wave equation has the form:

$$U^{(i)} = c_1 \sin(k^{(i)}x) + c_2 \cos(k^{(i)}x). \tag{2.60}$$

Damping may be introduced in the system by including the complex elasticity $\hat{E} = E(1+i\eta)$. Then the wave number becomes complex, too. For the small values of $\eta$ the complex wave number is well approximated by $\hat{k} = k(1 - i\eta/2)$ [21].

In the case of two coupled rods set of two equations should be set up for each homogeneous rod separately. Additional continuity and boundary conditions have to be applied in the points 1, 2 and 3. A harmonic point force $f(x,t) = Fe^{i\omega t}\delta(x - x^{(4)})$ is applied at point 4 on rod 1.

### 2.6.1 FEM

In the FEM model each rod is divided into the number of elements. The first order interpolation functions are used for the element, resulting in two DOF per element. The standard FEM requires that the displacement field of discrete model can well approximate the actual displacement field. The spatial distribution of the displacement field is given by (2.60). The wavelength of the displacement field is given by $\lambda = 2\pi/k$. For the linear interpolation functions used approximately eight elements must be used to model the wavelength of the deformation. If the maximum frequency of interest is defined as $\omega_{max}$ then the required length of elements for rod $i$, $l^{(i)}$ can be calculated as

$$l^{(i)} \leq \frac{\lambda^{(i)}}{8} = \frac{\pi}{4\,\omega_{max}}\sqrt{\frac{E^{(i)}}{\rho^{(i)}}} \tag{2.61}$$

The number of elements is given by the ratio $L^{(i)}/l^{(i)}$.

The time average kinetic energy $E^{kin}_{(i)}$ of a rod $i$ at frequency $\omega$ is defined as (see equation (2.21)), i.e.

$$\langle T^{(i)} \rangle = \frac{1}{4}\omega^2 (\mathbf{Q}^{(i)})^H \mathbf{M}^{(i)} \mathbf{Q}^{(i)} \tag{2.62}$$

where $\mathbf{Q}^{(i)}$ is a vector of co-ordinates that belong to rod $i$ (complex amplitudes of displacement) and $\mathbf{M}^{(i)}$ is a mass matrix of the rod $i$ prior to assembly procedure with rod 2.

#### FEM results

In the first two cases (I and II) rod 1 dominates the response because of the much bigger cross section. This can be observed for example by considering the natural modes and natural frequencies.

Figure 2.2 presents first 6 natural modes of single rod 1 together with their natural frequencies. The longitudinal displacement $u$ is presented in direction normal to the rod's axis. Figure 2.3 presents the natural modes and frequencies of coupled system for case I. The properties of rod 1 are unchanged. In addition the material properties are the same, which follows with the same wavelengths of deformation.

Some features of the coupled system are visible from the natural modes. First, the modes of rod 1 are almost the same as for the single rod. Modes 1, 3, 6, 8 and 10 of a coupled system correspond to modes 1-5 in the case of single rod. The differences between natural frequencies of these modes are generally below 2%. It can also be seen that the displacement in these modes of a coupled structure is of similar magnitude in both rods. On the contrary, when the modes dominated by

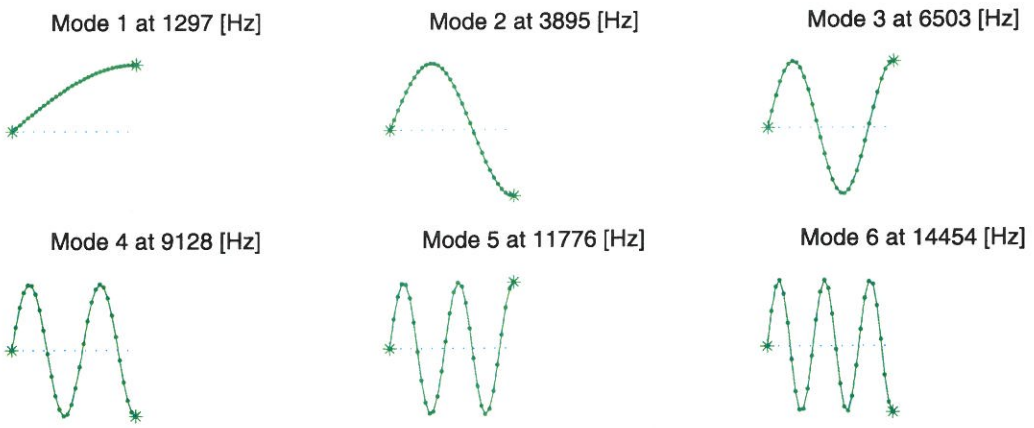


**Figure 2.2**: Natural frequencies and modes of single rod 1. Longitudinal displacement plotted in direction normal to the axis.

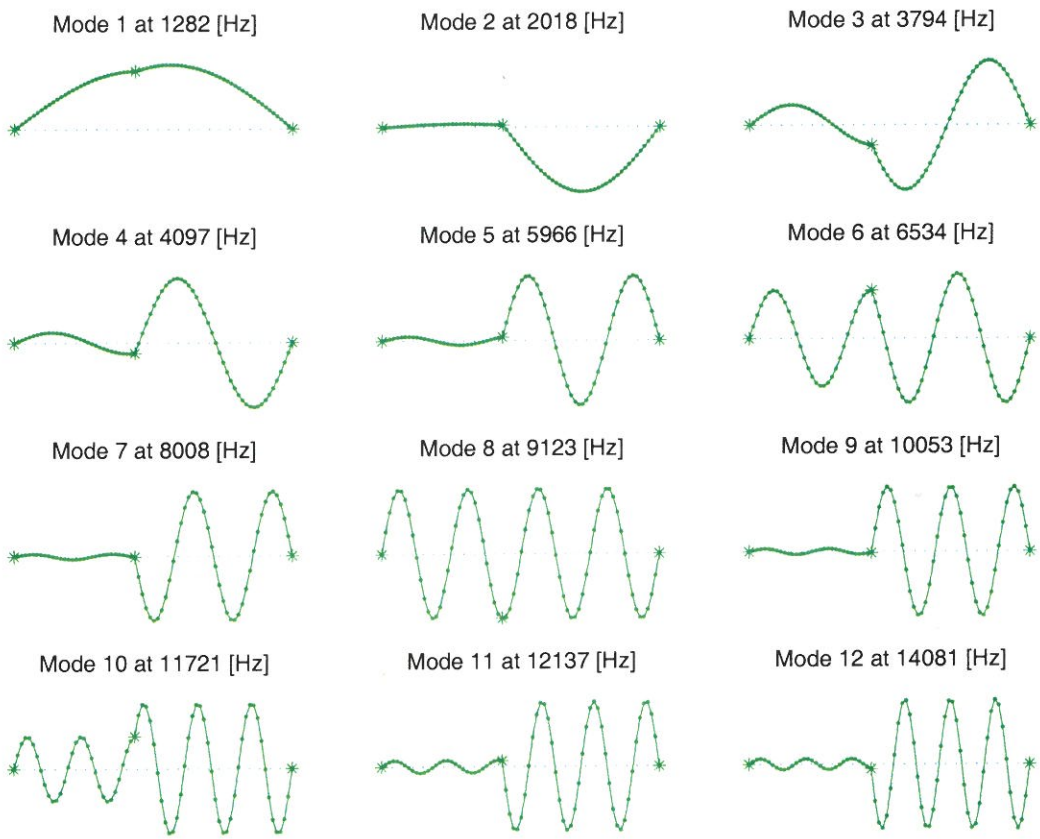


**Figure 2.3**: Natural frequencies and modes of two rods in case I. Longitudinal displacement plotted in direction normal to the axis.

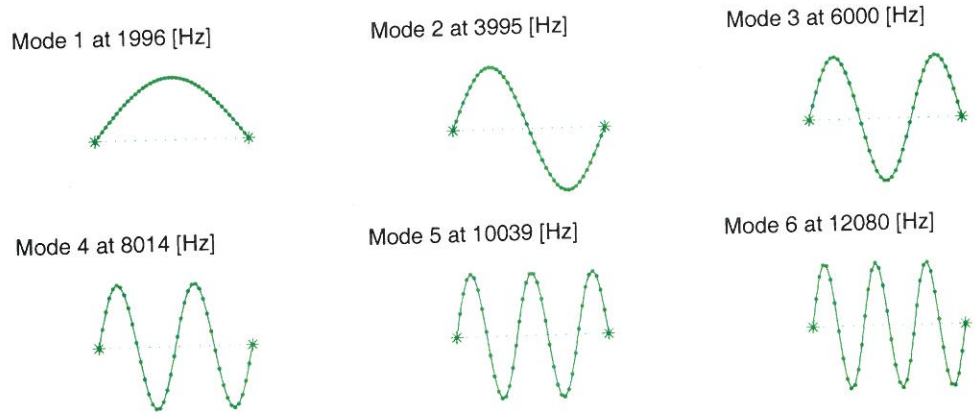


**Figure 2.4**: Natural frequencies and modes of single rod 2 with both ends clamped. Longitudinal displacement plotted in direction normal to the axis.

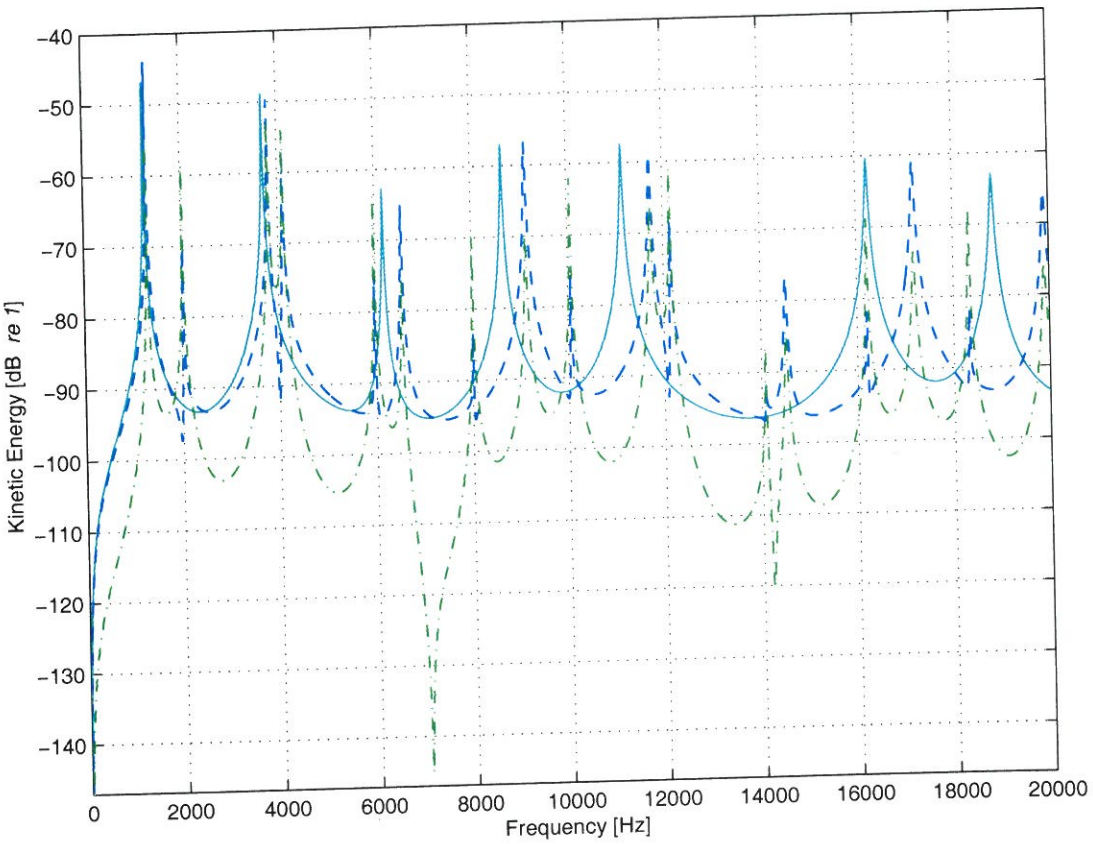


**Figure 2.5**: Energy of the rods for case I, load applied at rod 1.- - - energy in rod 1 (driven); -·-·- energy in rod 2; — reference energy in single rod 1.

rod 2 are considered, i.e. modes 2, 5, 7, 9, 11 or 12 then there is a remarkable difference between amplitudes of displacement between the two rods. That means that rod 2 acts on rod 1 as a free boundary conditions, whereas rod 1 acts on rod 2 as almost clamped boundary conditions. This can be verified by comparing modes dominated by rod 2 in Figure 2.3 with clamped modes of rod 2 separately presented in Figure 2.4. By calculating the response in the steady state condition and adding energy of elements belonging to each of the rods the energies of the two rods can be calculated. The energy of rod 1 without rod 2 is calculated for reference. Figure 2.5 presents the kinetic energy of the rods due to the point force acting at rod 1. Comparison of energy of rod 1 with and without rod 2 agrees with the previous considerations concerning mode shapes. The energy of rod 1 is hardly affected by the presence of rod 2. In this case the rod 1 can be considered weakly coupled to rod 2 in SEA terminology, because it does not 'recognize' whether rod 2 is present or not.

In the second case considered rod 2 has different material properties (it is made of brass) and therefore the wavelengths differ. It might be seen first in Table 2.1 as nearly twice as many elements is necessary to model rod 2 as it was in the previous case. The differences in wavelengths are also visible on the shape functions of the coupled system, see Figure 2.6. Again modes 1 to 4 of single rod 1 can be recognized in the modes 2, 5, 9 and 12 of a coupled system as dominant.

In the third and final configuration rods have similar cross section, see Table 2.1. The mode shapes of the coupled structure are equally present at both rods, see Figure 2.7 and the differences between natural frequencies of rods before and after coupling are highly modified. The energy of rods is compared to energy of single rod 1 in Figure 2.8.

### 2.6.2 Hierarchical FEM

The development of hierarchical rod element consists of definition of shape functions, calculation of the mass and stiffness matrices and definition of assembly procedure that allows for coupling elements. The material properties and cross-section are constant within each element. There is no restriction on the length of the element.

Two types of shape functions used are constraint/static modes and clamped modes [17]. The static modes are defined by the shape of static displacement when one and only one of the constraint variables has been displaced. The clamped modes are the mode shapes of the clamped rod (normalized to unit mass matrix).

The natural co-ordinate system can be introduced for each of the rods. The natural co-ordinate $\xi^{(i)}$ is placed in the left end of the rod $i$ and is normalized with respect to the length, i.e. $\xi^{(i)} \in (0, 1)$. The transformation from global co-ordinate

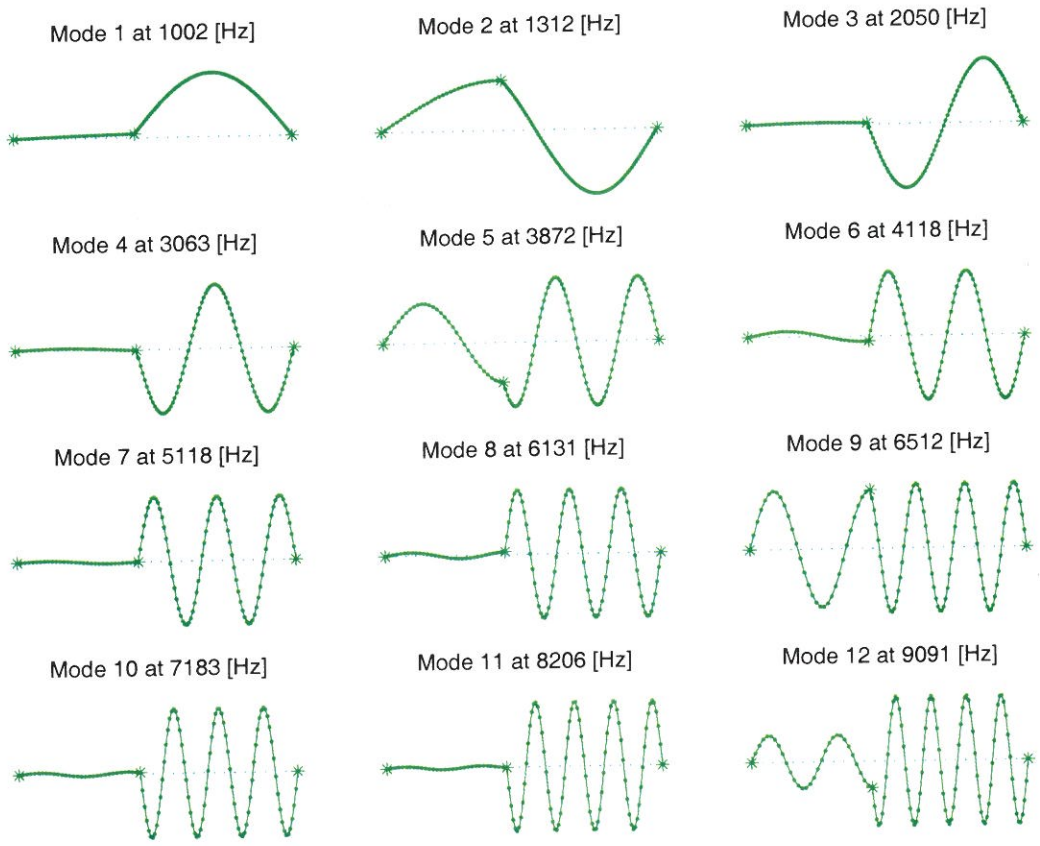


**Figure 2.6**: Natural frequencies and modes of two rods in case II. Longitudinal displacement plotted in direction normal to the axis.

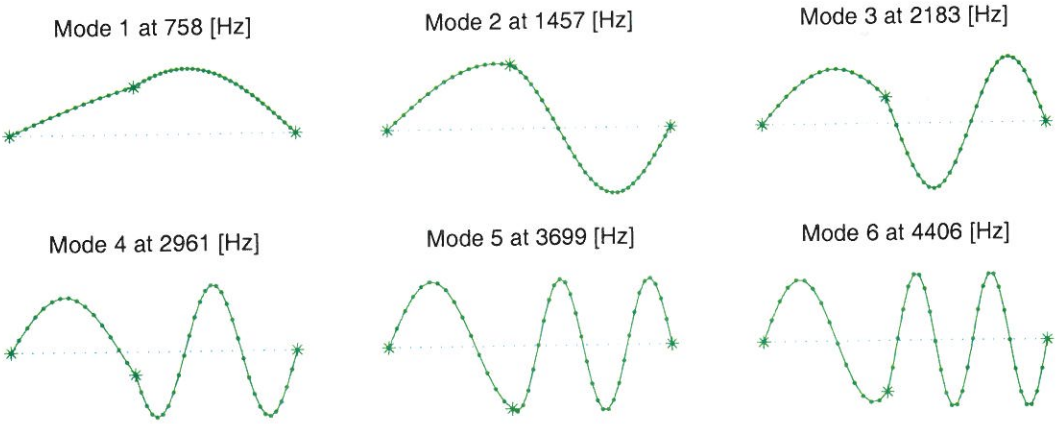


**Figure 2.7**: Natural frequencies and modes of two rods in case III. Longitudinal displacement plotted in direction normal to the axis.

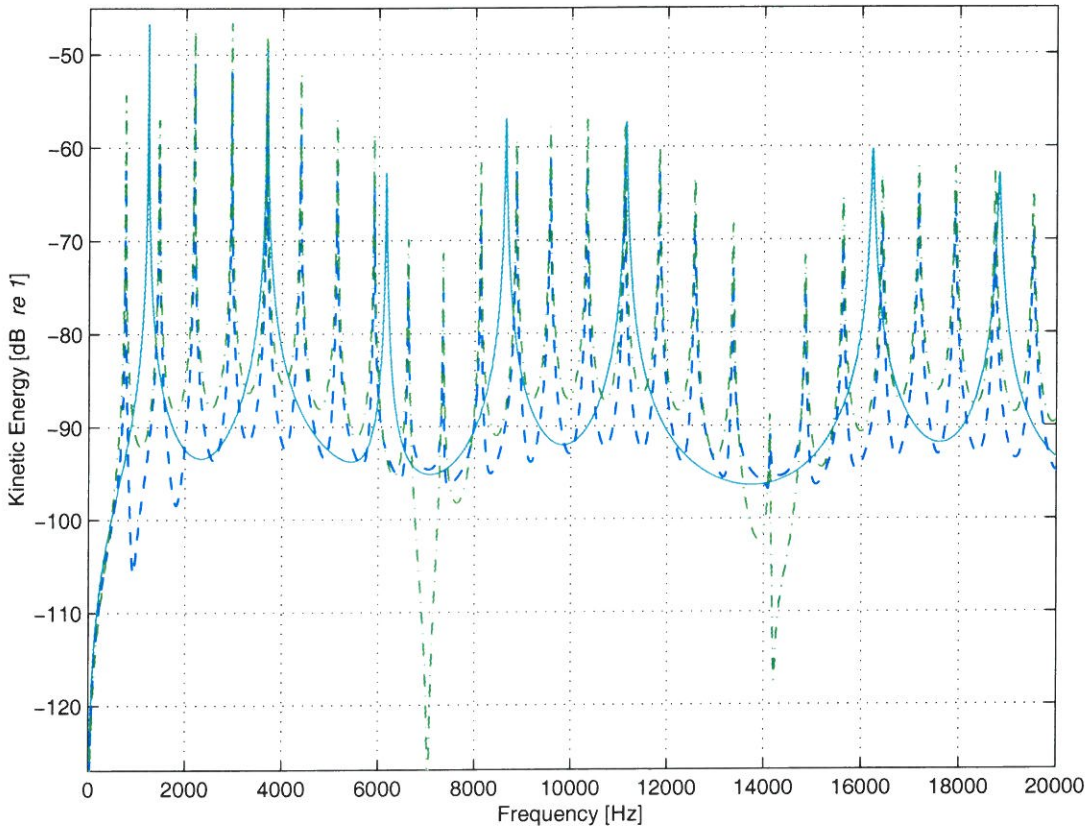


**Figure 2.8**: Energy of the rods for case III, load applied at rod 1.- - - energy in rod 1 (driven); -·-·- energy in rod 2; — reference energy in single rod 1.

system to local co-ordinate system is given by

$$\xi^{(1)} = \frac{x - x_{(1)}}{L^{(1)}} \quad ; \quad \xi^{(2)} = \frac{x - x_{(2)}}{L^{(2)}}. \tag{2.63}$$

The longitudinal displacement within an element $v(\xi^{(e)}, t)$ is given by the product of co-ordinates and shape functions, see equation (2.3), i.e.

$$v(\xi^{(e)}, t) = \mathbf{\Psi}(\xi^{(e)})\boldsymbol{q}(t). \tag{2.64}$$

The shapes of the two constraint modes can be defined as

$$\Psi_1(\xi^{(e)}) = 1 - \xi^{(e)} \quad ; \quad \Psi_2(\xi^{(e)}x) = \xi^{(e)} \tag{2.65}$$

and infinite number of clamped modes of the form

$$\Psi_{n+2} = \sqrt{\frac{2}{\rho^{(e)} A^{(e)} L_2^{(e)}}} \sin(n\pi\xi^{(e)}). \tag{2.66}$$

The infinite set of co-ordinates cannot be used in the direct analysis and the high order clamped modes have to be truncated. In $h$-version of FEM the convergence criteria required the length of the (first order) element corresponding to one-eighth of the wavelength of deformation. The convergence criteria in $p$-version can also be defined based on the correspondence of wavelength of deformation and wavelength of shape functions. Generally, all shape functions with wavelengths shorter than the wavelength of elastic deformation should be included in the set of internal co-ordinates. The number of internal co-ordinates in the element $e$ is denoted by $n_{int}^{(e)}$. The displacement field follows as

$$\begin{aligned} \upsilon(\xi^{(e)},t) =& (1-\xi^{(e)})\, q_1(t) + \xi^{(e)}\, q_2(t) \\ &+ \sqrt{\frac{2}{\rho^{(e)} A^{(e)} L_2^{(e)}}} \sum_{n=1}^{n_{int}^{(e)}} \sin(n\pi\xi^{(e)})\, q_{n+2}(t) = \boldsymbol{\Psi}(\xi^{(e)})\boldsymbol{q}(t) \end{aligned} \tag{2.67}$$

and $\boldsymbol{\Psi}(\xi^{(e)})$ and $\boldsymbol{q}(t)$ have the size $(2+n_{int}^{(e)}) \times 1$ and $1 \times (2+n_{int}^{(e)})$, respectively.

### Calculation of stiffness and mass matrices

From the definition of the element mass matrix (2.16), the orthogonality of clamped modes and the normalization used the evaluation of element mass matrix yields

$$\mathbf{M}^{(e)} = \begin{bmatrix} \frac{1}{3}\rho AL & \frac{1}{6}\rho AL & \frac{\sqrt{2\rho AL}}{\pi} & \frac{\sqrt{2\rho AL}}{2\pi} & \dots & \frac{\sqrt{2\rho AL}}{n_{int}\pi} \\ \frac{1}{6}\rho AL & \frac{1}{3}\rho AL & \frac{\sqrt{2\rho AL}}{\pi} & -\frac{\sqrt{2\rho AL}}{2\pi} & \dots & -(-1)^{n_{int}}\frac{\sqrt{2\rho AL}}{n_{int}\pi} \\ \frac{\sqrt{2\rho AL}}{\pi} & \frac{\sqrt{2\rho AL}}{\pi} & 1 & 0 & \dots & 0 \\ \frac{\sqrt{2\rho AL}}{2\pi} & -\frac{\sqrt{2\rho AL}}{2\pi} & 0 & 1 & \dots & 0 \\ \vdots & \vdots & \vdots & \vdots & \ddots & \vdots \\ \frac{\sqrt{2\rho AL}}{n_{int}\pi} & -(-1)^{n_{int}}\frac{\sqrt{2\rho AL}}{n_{int}\pi} & 0 & 0 & \vdots & 1 \end{bmatrix} \tag{2.68}$$

In a similar way the stiffness matrix is evaluated from (2.9) as

$$\mathbf{K}^{(e)} = \begin{bmatrix} \frac{EA}{L} & \frac{-EA}{L} & 0 & \dots & 0 \\ \frac{-EA}{L} & \frac{EA}{L} & 0 & \dots & 0 \\ 0 & 0 & \omega_1^2 & \dots & 0 \\ \vdots & \vdots & & \ddots & 0 \\ 0 & 0 & 0 & \dots & \omega_{n_{int}}^2 \end{bmatrix}, \quad \omega_n = \frac{n\pi}{L}\sqrt{\frac{E}{\rho}} \tag{2.69}$$

where $\omega_n$ is the $n$th natural frequency of clamped rod. All quantities ($\rho$, $\omega$, $A$, $E$, and $n_{int}$) in (2.68) and (2.69) correspond to element $e$ quantities, i.e. ($\rho^{(e)}$, $\omega^{(e)}$, $A^{(e)}$, $E^{(e)}$ and $n_{int}^{(e)}$).

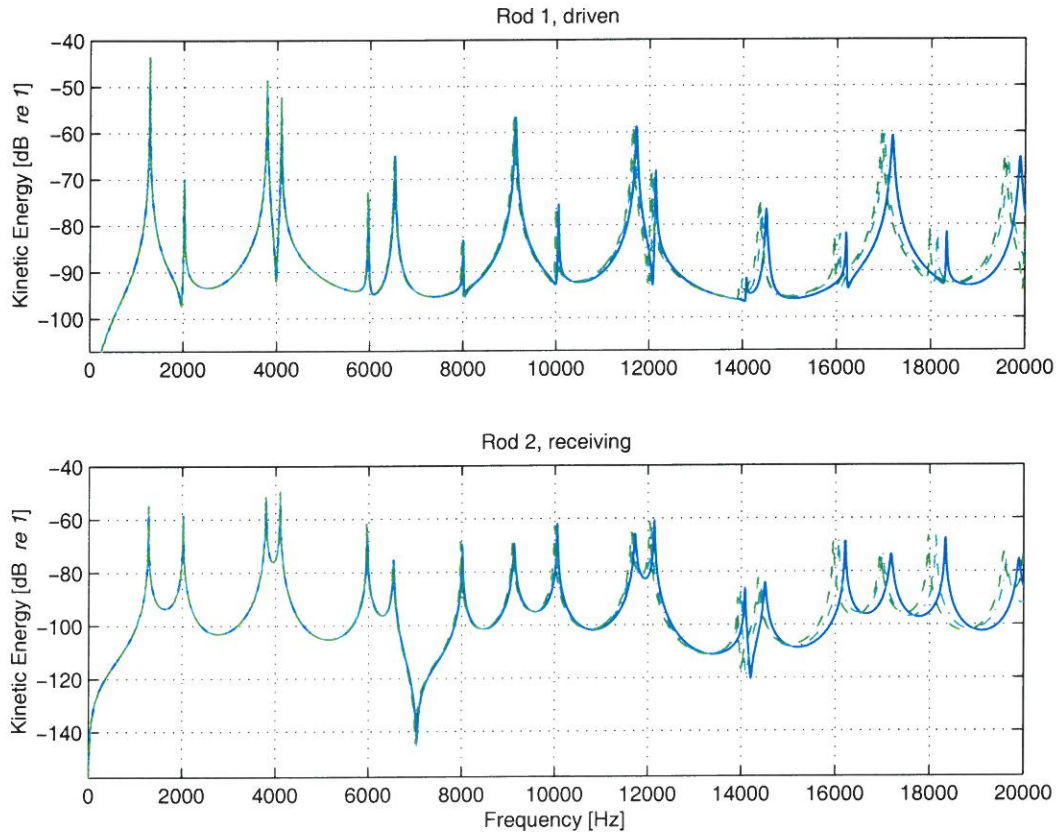


**Figure 2.9**: Comparison of hierarchical and standard FEM results for energy of the rods in case I, load applied at rod 1. Energy in rod 1 (top) and rod 2 (bottom). — standard FEM with 8 elements per wavelength; -·-·- standard FEM with 12 elements per wavelength; - - - hierarchical FEM.

The elements are assembled into the global description in the same way as in the standard FEM. The kinetic energy is defined in the same way as in the standard FEM, too (see Equation (2.21)).

### Hierarchical FEM results

The results of hierarchical FEM are compared to the classic FEM in terms of energy in rod 1 and rod 2. The results for case I are presented in Figure 2.9. First only the results for standard FEM with 8 elements per wavelength should be compared to the results of hierarchical FEM. The energy contents agree very well among the two approaches, but there is a difference between the natural frequencies. It can be seen that the use of 12 elements per wavelength (at 20 kHz) gives better estimation

of natural frequencies in standard FEM. However, even in this case hierarchical FEM gives lower and therefore better estimations of natural frequencies, according to the inclusion principle [77]. For the sake of comparison the standard FEM with 8 elements per wavelength has 73 DOF (see Table 2.1), with 12 elements 109 DOF and the hierarchical FEM has only 24 DOF.

Similar agreement can be seen in the remaining two cases, see figures 2.10 and 2.11. The models used in both case II and case III have 111 DOF for course FEM mesh (8 el.) and 166 DOF for finer mesh (12 el.) and 34 DOF for the hierarchical FEM. This superior performance of hierarchical FEM in the case of coupled rods comes from two sources. First, the elements are coupled at discrete points so that there is no approximation involved in the definition of continuity. Secondly, the set of shape functions can be built from the constraint modes and clamped modes. This means that the hierarchical formulation in this case is a case of substructuring. By the use of normal modes for the set of internal shape functions it can also be seen as an example of CMS, see section 2.1.4.

### 2.6.3 SEA

The first step of the SEA calculations is the identification of subsystems. Two subsystems model can be used in this example, since there are only two components each supporting one wave type only. Subsystem 1 represents rod 1, subsystem 2 represents rod 2. The point force acting on rod 1 is the only external power source. The time average power input from harmonic point load can be calculated as

$$\langle \Pi^{ext} \rangle_t = \frac{1}{2} |F^2| \Re(Y_{inp}) \tag{2.70}$$

The amplitude of point force $F$ is one in this example. The input point mobility $Y_{inp}$ can be either calculated exactly or approximately. The usual approximation for input mobility in SEA calculations is the use of input mobility of an infinite structure with properties similar to the ones of the actual element. According to the mean value method (MVM) by Skudrzyk [96] the infinite structure input mobility approaches the mean value of the input mobility of finite structure. In the example the two input mobilities used are the infinite input mobility of axially vibrating rod, given by $Y_{inp}^{\infty} = 1/2\rho A c_L$ and the input mobility calculated in hierarchical FEM.

#### SEA results

Figure 2.12 presents the results from the SEA calculations. The results of hierarchical FEM are used as comparison. It can be seen that the SEA results with input mobility of infinite rod predict quite well the mean value energy. However, due to low damping in the system and low modal overlap ($\mathcal{M} \ll 1$) the peaks of subsequent resonances are well separated, the actual peaks and throughs extend above

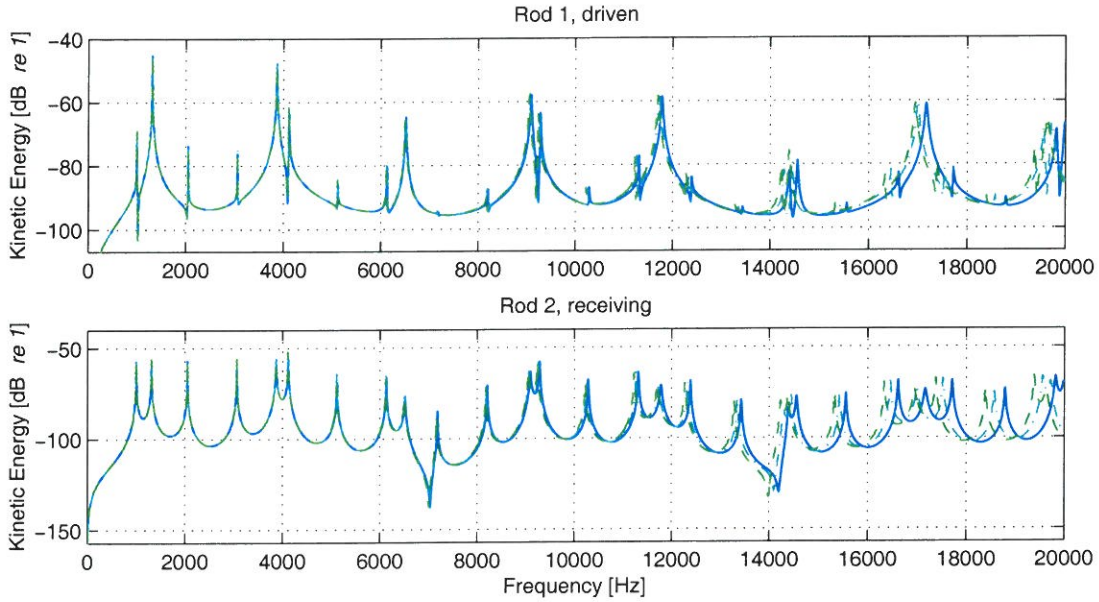


**Figure 2.10**: Comparison of hierarchical and standard FEM, case II. Energy in rod 1 (top) and rod 2 (bottom). — standard FEM with 8 elements per wavelength; -·-·- standard FEM with 12 elements per wavelength; - - - hierarchical FEM.

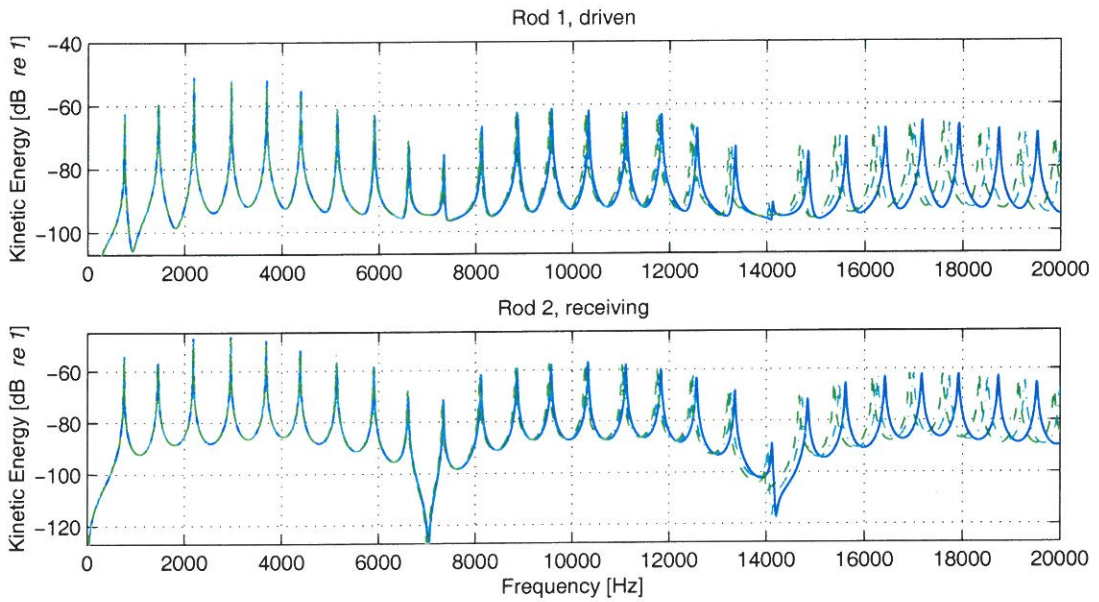


**Figure 2.11**: Comparison of hierarchical and standard FEM, case III. Energy in rod 1 (top) and rod 2 (bottom).— standard FEM with 8 elements per wavelength; -·-·- standard FEM with 12 elements per wavelength; - - - hierarchical FEM.

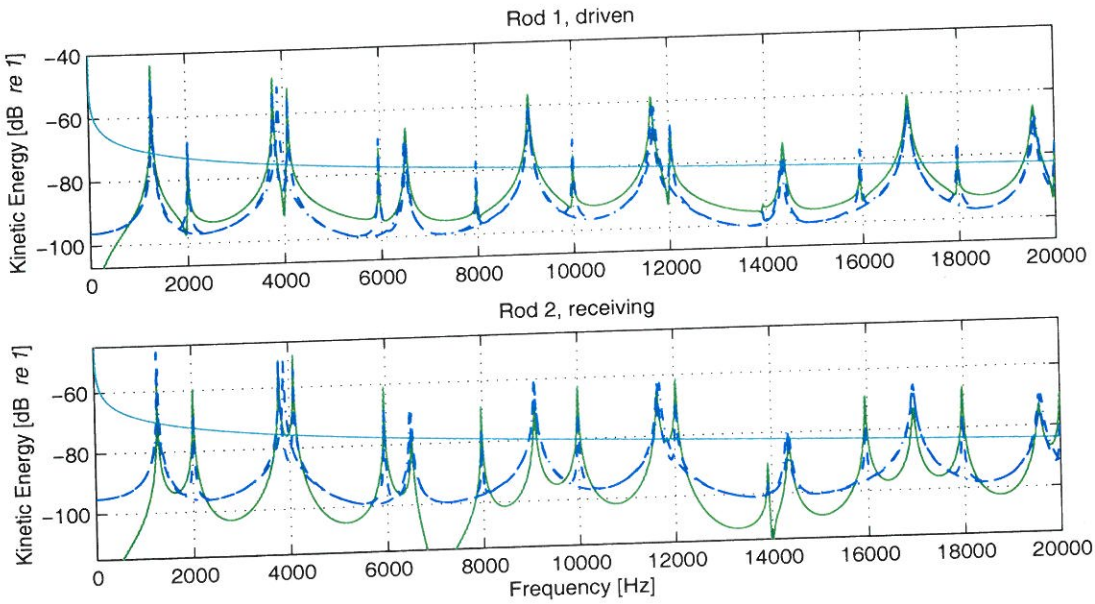


**Figure 2.12**: Comparison of results from SEA and hierarchical FEM for energy of the rods in case I, load applied at rod 1. Energy in rod 1 (top) and rod 2 (bottom). — hierarchical FEM; — SEA with input mobility of infinite rod; — · — SEA with input mobility of single rod 1; - - - SEA with actual input mobility.

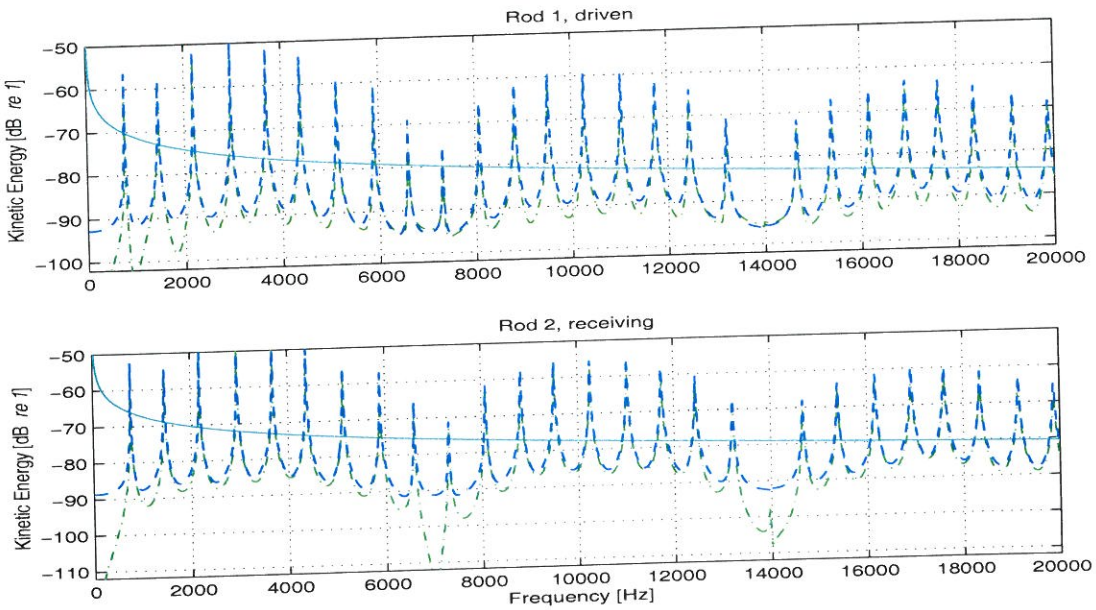


**Figure 2.13**: Comparison of results from SEA and hierarchical FEM for energy of the rods in case III, load applied at rod 1. Energy in rod 1 (top) and rod 2 (bottom). — · — hierarchical FEM; — SEA with input mobility of infinite rod; — · — SEA with input mobility of single rod 1; - - - SEA with actual input mobility.

and below the mean as much as 25 dB. This makes the prediction of mean value quite useless.

Quite substantial improvement can be achieved by the use of input mobility of finite rod. Two results are presented for the numerically calculated input mobility. First, the input mobility of single rod 1 clamped at one end and free at the other end was calculated. Quite often it is possible to either calculate the input mobility of a single subsystem (either analytically or numerically) or to measure it. It can be seen in Figure 2.12 that the results obtained by the use of input mobility of a single rod 1 are in much better agreement with the FEM results.

The second possibility is to use the input mobility of the entire structure, which is perhaps more possible in the case of measurements than in the case of calculating it. That is because it is seldom possible to model entire structure, and if in fact it would be possible, then the energy flow can also be calculated that way. Nevertheless, the SEA results in case I obtained by using single subsystem input mobility and mobility of entire structure do not differ considerably. That is because rod 2 in this case has only limited influence on rod 1.

Figure 2.13 presents similar set of results for the case III. It can be seen that again the SEA with $Y_{inp}^{\infty}$ predicts the mean value of the response. The main difference between cases one and three (compare figures 2.12 and 2.13) lies in the differences between responses calculated using numerical values of input mobilities. In case III rod 2 changes the behaviour of rod 1 in much bigger extent and so the use of single rod input mobility is a much worse approximation than the use of actual input mobility of coupled structures.

The approximation involved in the calculation of power input by the use of input mobilities of either infinite or uncoupled substructure is only one of the approximations that influence the results of SEA. It can be seen in case I (Figure 2.12) that even with the appropriate definition of input power, the energies calculated by SEA differ from those of hierarchical FEM. The energy of rod 1 is underestimated by SEA results between resonances, and the energy of rod 2 is overestimated.

The limits of SEA, as discussed in Section 2.3.2 of this Thesis are clearly seen from the examples presented. First, the SEA results are very sensitive to the definition of input power and the actual amount of power injected should be carefully examined. Secondly, even if the power input is calculated correctly, the power flow approximation does not hold in the case of low damping and low modal overlap.

To verify this statement the additional calculations have been performed. In cases I and III the amount of damping was increased ten times as compared to previous results and Table 2.1. The results derived from these calculations are presented in Figure 2.14 for case I and in Figure 2.15 for case III.

It can be seen that the amplitude of resonances is reduced by 20 dB in comparison with the previous results and the reduction in amplitudes with frequency

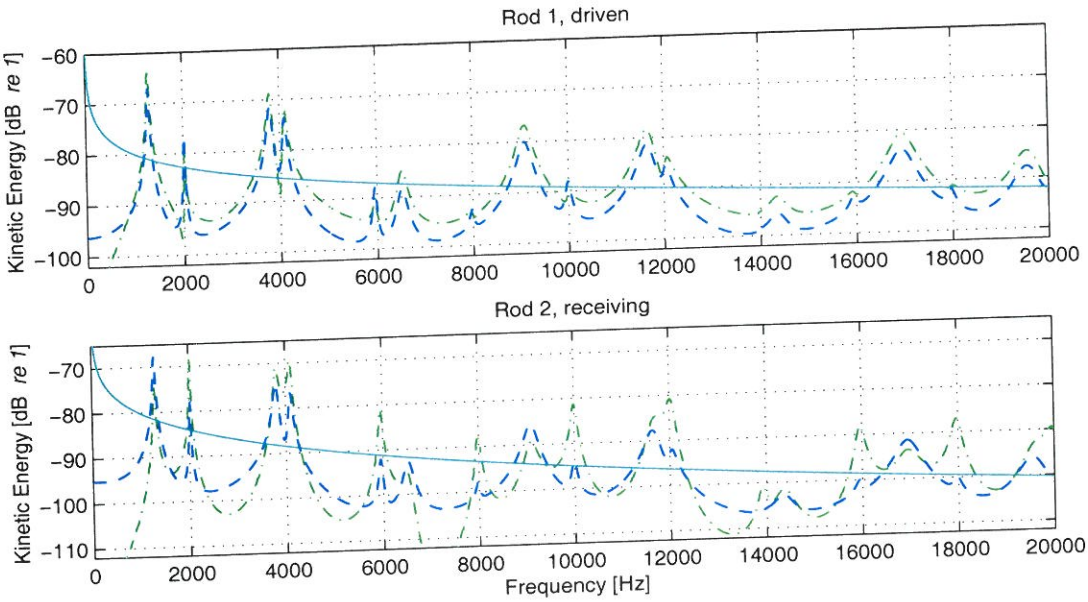


**Figure 2.14**: Comparison of results from SEA and hierarchical FEM for energy of the rods in case I with damping increased ten times. Energy in rod 1 (top) and rod 2 (bottom). — · — hierarchical FEM; — SEA with input mobility of infinite rod; - - - SEA with actual input mobility.

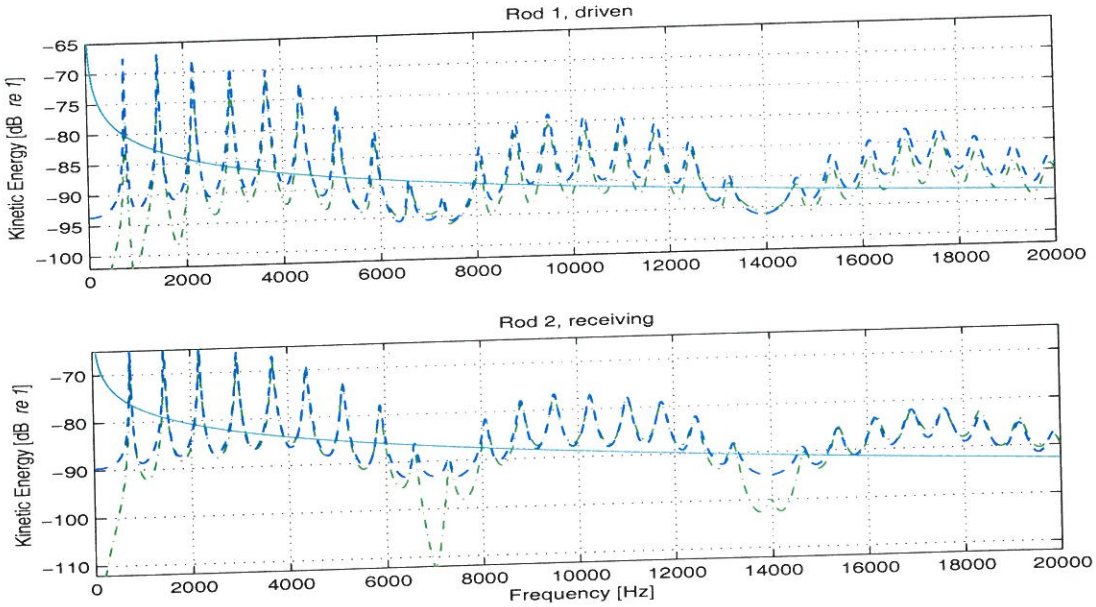


**Figure 2.15**: Comparison of results from SEA and hierarchical FEM for energy of the rods in case III with damping increased ten times. Energy in rod 1 (top) and rod 2 (bottom). — · — hierarchical FEM; — SEA with input mobility of infinite rod; - - - SEA with actual input mobility.

In the first case the SEA with infinite input mobility is still close to the mean value of the hierarchical FEM results.

### 2.6.4 Hybrid FEM-SEA

The basics of hybrid FEM-SEA has been presented in Section 2.5 where the partition of co-ordinates has been introduced. The global EOM and set of local EOM are derived in (2.54) and (2.56). It has also been proposed that the hierarchical FEM formulation can be used as a base to apply the hybrid FEM-SEA. In this case the global co-ordinates include all nodal co-ordinates of hierarchical FEM. In addition lower order internal co-ordinates (up to co-ordinate $n_{intg}$) can be added to the global set if necessary. The local sets constitute of all remaining internal co-ordinates in each of subsystems, i.e. from $n_{intg}$ to infinity. Each subsystem can be built up from several finite elements. The local set of co-ordinates for each subsystem forms an infinite set.

Evaluation of the additional stiffness matrix and the additional loading vector will be presented as these terms are crucial for the application of hybrid approach.

#### Additional stiffness matrix

The $mn$ entry of additional stiffness matrix for subsystem $s$ is given by, (see (2.55))

$$\Delta\mathbf{D}^{(s)} = (\mathbf{D}_{gl^s}\mathbf{D}_{l^sl^s}^{-1}\mathbf{D}_{gl^s}^{T})_{mn} = \sum_{j=n_{intg}+1}^{N_{loc}^s}\sum_{k=n_{intg}+1}^{N_{loc}^s}(\mathbf{D}_{gl^s})_{mj}(\mathbf{D}_{l^sl^s}^{-1})_{jk}(\mathbf{D}_{gl^s}^{T})_{kn} \quad (2.71)$$

$n_{intg}$ is the number of internal modes in the global description; $N_{loc}^s$ is the total number of local modes in subsystem $s$, and the aim of the approach is to allow for infinite number of those. Hence, the summation should be evaluated analytically. The local co-ordinates are a subset of internal co-ordinates of hierarchical rod element. Internal shape functions have been defined as a clamped modes of the rod. That means that the internal shape functions, and therefore local shape functions are orthogonal. It can be seen from equations (2.68), (2.69) and (2.19) that the local dynamic stiffness matrix is orthogonal, and the additional stiffness matrix can be written in the form

$$(\Delta\mathbf{D}^{(s)})_{mn} = \sum_{j=n_{intg}+1}^{\infty}(\mathbf{D}_{gl^s})_{mj}(\mathbf{D}_{gl^s}^{T})_{jn}\left[\omega_j^2(1+i\eta_s)-\omega^2\right]^{-1} \quad (2.72)$$

In addition, assumption of the stiffness proportional damping causes that the only contribution to the $\mathbf{D}_{gl^s}$ comes from the mass matrix, i.e. from the inertial coupling

$$\mathbf{D}_{gl^s} = -\omega^2\mathbf{M}_{gl^s} \quad (2.73)$$

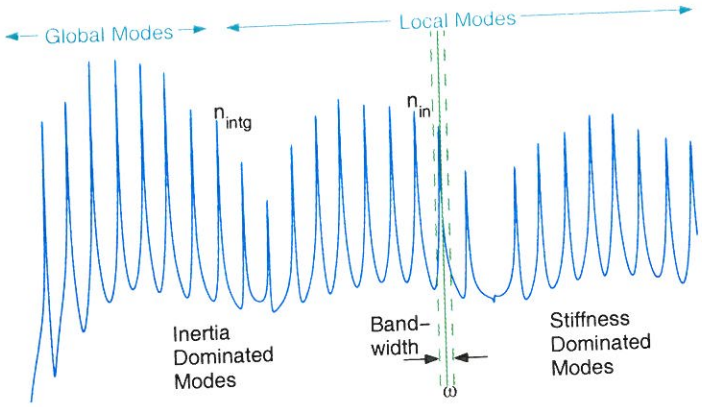


**Figure 2.16**: Partition of local modes to resonant, inertia and stiffness dominated modes.

and only the first two rows of the matrix do not vanish. This means that the product $\mathbf{D}_{gl^s}(\mathbf{D}_{gl^s})^T$ is of the size $2 \times 2$ corresponding to constraint (nodal) co-ordinates. There is no contribution from cross products between clamped modes included in global description and those in local one. Therefore the entries to be calculated are: $(\mathbf{D}_{gl^s}\mathbf{D}_{l^sl^s}^{-1}\mathbf{D}_{gl^s}^T)_{11} = (\mathbf{D}_{gl^s}\mathbf{D}_{l^sl^s}^{-1}\mathbf{D}_{gl^s}^T)_{22}$ and$(\mathbf{D}_{gl^s}\mathbf{D}_{l^sl^s}^{-1}\mathbf{D}_{gl^s}^T)_{12} = (\mathbf{D}_{gl^s}\mathbf{D}_{l^sl^s}^{-1}\mathbf{D}_{gl^s}^T)_{21}$. The entries of the mass matrix, (2.68) has already been evaluated, and the summation yields:

$$(\mathbf{D}_{gl^s}\mathbf{D}_{gl^s}^T)_{mn} = \sum_{j=n_{intg}+1}^{\infty} (\mathbf{D}_{gl^s})_{mj}(\mathbf{D}_{gl^s})_{nj} = \omega^4 \sum_{j=n_{intg}+1}^{\infty} (\mathbf{M}_{gl^s})_{mj}(\mathbf{M}_{gl^s})_{nj} \quad (2.74)$$

and the components are:

$$(\mathbf{D}_{gl^s}\mathbf{D}_{gl^s}^T)_{11} = (\mathbf{D}_{gl^s}\mathbf{D}_{gl^s}^T)_{22} = \omega^4 \sum_{j=n_{intg}+1}^{\infty} \frac{2\rho A^{(s)} L^{(s)}}{\pi^2 j^2} \quad (2.75)$$

$$(\mathbf{D}_{gl^s}\mathbf{D}_{gl^s}^T)_{12} = (\mathbf{D}_{gl^s}\mathbf{D}_{gl^s}^T)_{21} = -\omega^4 \sum_{j=n_{intg}+1}^{\infty} (-1)^j \frac{2\rho A^{(s)} L^{(s)}}{\pi^2 j^2} \quad (2.76)$$

Further considerations require that the local co-ordinates are divided into three groups, i.e. inertia dominated, resonant and stiffness dominated modes, see Figure 2.16.

For inertia dominated modes ($\omega \gg \omega_j$) the term $\omega_j^2(1+i\eta_j) - \omega^2$ can be approximated by $-\omega^2$. This will give contribution to $\Delta\mathbf{D}^{(s)}$ for $j \in [n_{intg}+1,\ n_{in}]$. Here $n_{in}$ denotes the highest order of local co-ordinates with natural frequency below $\omega$, see Figure 2.16.

For resonant modes ($\omega \approx \omega_j$) the wavelength of local modes is approximately equal to the wavelength of elastic deformation at frequency $\omega$ denoted by $k_0 = \omega\sqrt{\rho/E}$. Then the product $j\pi = k_0 L$ becomes constant and can be taken out from the summation. At low frequencies the modes do not overlap (modal overlap factor is less than 1, see (2.51)) and the resonant modes will be present only at certain frequencies. As the modal overlap increases above unity there are always some modes that resonate. The number of modes that resonate at frequency $\omega$ is given by the modal density of the subsystem. The local modes should be used to describe the motions in the case of high modal overlap in the same conditions as plain SEA. One may approximate the term $\sum_k [\omega_k^2(1+i\eta_k)-\omega^2]^{-1}$ with the summation covering the resonant modes as [58]

$$\sum_k \frac{1}{\omega_k^2(1+i\eta_k)-\omega^2} \approx -i\frac{\pi n(\omega)}{2\omega} \quad for\ \omega_k \approx \omega \tag{2.77}$$

Finally, for $\omega_k$ above $\omega$ the influence would be controlled by stiffness. This contribution will be omitted in the analysis based on the assumption of inertia dominated coupling.

$$(\Delta\mathbf{D}^{(s)})_{11} = -iA^{(s)}k_0^{(s)}E^{(s)}H(\omega-\omega_{l_1^{(s)}}) + 2\omega^2\rho A^{(s)}L^{(s)}\frac{1}{\pi^2}\sum_{j=n_{intg}^{(s)}+1}^{n_{in}^{(s)}}\frac{1}{j^2} \tag{2.78}$$

$$(\Delta\mathbf{D}^{(s)})_{12} = -2\omega^2\rho A^{(s)}L^{(s)}\frac{1}{\pi^2}\sum_{j=n_{intg}^{(s)}+1}^{n_{in}^{(s)}}\frac{(-1)^j}{j^2} \tag{2.79}$$

where the Heaviside function $H(\omega-\omega_{l_1^{(s)}})$ is used to signify the frequency at which first local mode of subsystem $s$ ($l_1^{(s)}$) resonate.

### Additional loading vector

It has been shown in [63] that the additional loading vector may be evaluated as:

$$(\mathbf{D}_{gl}\mathbf{D}_{ll}^{-1}\mathbf{F}^l)_m = \sum_{j=n_{intg}+1}^{\infty}(\mathbf{D}_{gl})_{mj}(\mathbf{D}_{ll}^{-1}\mathbf{F}^l)_j = \sum_{j=n_{intg}+1}^{\infty}(\mathbf{D}_{gl})_{mj}\,Q_j^{lB} \tag{2.80}$$

where summation covers all local modes, and the term $Q_j^{lB}$ denotes the blocked response of the local mode $j$. Using $\mathbf{D}_{gl} = -\omega^2\mathbf{M}_{gl}$ w and making use of (2.16) one

obtains:

$$(\mathbf{D}_{gl}\mathbf{D}_{ll}^{-1}\mathbf{F}^{l})_m = \sum_{j=n_{intg}+1}^{\infty} -\omega^2 \int_L \rho\, \Psi_m^{gT}\, \Psi_j^l\, dx\, Q_j^{lB}$$
$$= -\omega^2 \int_L \rho\, \Psi_m^{gT} \sum_{j=n_{intg}+1}^{\infty} Q_j^{lB}\, \Psi_j^l\, dx = -\omega^2 \int_L \rho\, \Psi_m^{gT} U^B \quad (2.81)$$

where $\sum_{j=1}^{\infty} Q_j^{lB}\, \Psi_j^l$ gives the total displacement of the clamped rod due to applied load. However, the summation covers only modes from $n_{intg}+1$. This is the response of the clamped modes included in local description. Therefore, to asses $U^B$ one has to calculate the response of clamped rod and then subtract the response of all $n_{intg}$ clamped modes which are included in the global description. Alternatively, the displacement of the rod can be calculated as a result of force acting only on local co-ordinates, i.e. the original force minus the modal force corresponding to global co-ordinates. This means that the additional loading vector can first be calculated for all internal modes but the force vector should then be modified.

From the properties of the mass matrix, see (2.16), it follows that the only contribution to the additional loading vector will come from first two rows, i.e. for $m = 1, 2$. These can be evaluated for the case of point load applied at $x_0$ as

$$(\mathbf{D}_{gl}\mathbf{D}_{ll}^{-1}\mathbf{F}^{l})_1 = \frac{F_{red}}{A(1-i\eta/2)} \left[ \frac{\sin(\hat{k}(L-x_0))}{\sin(\hat{k}L)} - \left(1 - \frac{x_0}{L}\right) \right] \quad (2.82)$$

$$(\mathbf{D}_{gl}\mathbf{D}_{ll}^{-1}\mathbf{F}^{l})_1 = \frac{F_{red}}{A(1-i\eta/2)} \left[ \frac{\sin(\hat{k}x_0)}{\sin(\hat{k}L)} - \frac{x_0}{L} \right] \quad (2.83)$$

where $F_{red}$ signifies the reduced force amplitude.

### Power input to local modes

The point force acting on the system inputs power to local modes in two ways:

- by acting directly on local co-ordinates
- by acting through coupling of global co-ordinates with local co-ordinates

The direct power input may be calculated by subtracting the power supply to the clamped modes in global description from the analytical solution for power input to clamped rod. According to SEA assumptions the time average power input to the longitudinally vibrating rod equals

$$\Pi_{in} = \frac{1}{2}|F^2|\Re(Y_{inp}) \quad (2.84)$$

where the input mobility of infinite rod can be used. Part of that power is already included in global description. This is given by

$$\begin{aligned}\Pi_{in}^{g} &= \sum_{s=1}^{n_{intg}} F_s(x_0)\Re\left(\frac{dU(x)}{dt}\right)_{x=x_0} \\ &= \sum_{s=1}^{n_{intg}} F\sqrt{\frac{2}{\rho AL}}\sin(\frac{s\pi x_0}{L})\Re(i\omega Q_{s+2})\sqrt{\frac{2}{\rho AL}}\sin(\frac{s\pi x_0}{L}) \\ &= F\omega\frac{2}{\rho AL}\sum_{s=1}^{n_{intg}}\sin^2(\frac{s\pi x_0}{L})\Im(Q_{s+2}) \end{aligned} \tag{2.85}$$

and consequently the power input to local modes will be given as the difference of the two.

The power input from the global modes, given by $\langle i\omega \mathbf{Q}_{li}^T \mathbf{D}_{gl^i}^T \mathbf{Q}_g \rangle$, see (5.9) can be evaluated using again the SEA approach. The forces acting on the structure result in vibrations of the nodal points. This velocity is a prescribed condition for the vibrations of the internal modes of the rod. That means that the nodal velocity acts as a loading with prescribed amplitude. The power input from this kind of loading can be evaluated using the inverse of input mobility, i.e. impedance of an semiinfinite rod. Power will be injected mainly to resonant modes because these respond strongest to the load and therefore this source of power should be included above the "switch" frequency.

### Hybrid FEM-SEA results

The results of the hybrid method are presented in the way similar to the previous results. Each Figure consists of two plots, for rods 1 and 2, respectively and the energy of the rod is plotted as a result of unit harmonic point load. Each plot contains four curves:

- the results of hierarchical FEM as the benchmark for other methods (···);
- the results of classic SEA with input mobility of infinite rod (- · -);
- the results of hybrid FEM-SEA ( ) and;
- the results of hierarchical FEM with the same number of co-ordinates as used for global description in hybrid FEM-SEA to indicate the contribution of local modes in the results (- - -);

In the case I both rods have the same modal density and similarly low damping. Therefore, it is difficult to present the results of hybrid calculations, because in the frequency considered, i.e. below 20 kHz both rods have low mode count and low modal overlap. The modal spacing of rod 2 is approximately 1700 Hz whereas the

half-power bandwidth of rod 2 at maximum frequency is approximately 130 Hz. In order to fulfil the assumptions of hybrid approach local modes should overlap with the modal overlap factor close to 2 or bigger. This means that the half-power bandwidth should be double the modal spacing. The damping in rod 2 to increased to $\eta^{(2)} = 0.05$ creates the modal overlap conditions in rod 2 at approximately 10 kHz.

Figure 2.17 presents results of different calculations for the case I with increased damping of rod 2. 9 and 12 internal co-ordinates have been used for hierarchical results in rods 1 and 2, respectively. Comparison with Figure 2.12 shows the influence of the increase in damping loss factor for the energies in the rods. Nodal co-ordinates and 9 and 4 internal co-ordinates have been included in hybrid formulation in the global set for rods 1 and 2, respectively. Also a hierarchical FEM model with the same number of co-ordinates as taken in global set was used. The comparison of the full hierarchical calculations and the reduced hierarchical calculations indicate that minor differences can be expected in results for rod 1, and major in results for rod 2. It can also be seen that the additional terms in hybrid take over the 'missing' description and the energies in both cases are almost indistinguishable from the full hierarchical formulation. The only visible difference appears in vicinity of 'switch' frequency (approximately 10 kHz), i.e. in frequencies just before the first local modes resonate.

In the remaining two cases the same problem, as in case I occurs, i.e. the modal overlap does not exist in the system at the frequencies of interest. Again, instead of increasing the frequency level, the increase of damping loss factor causes the modes to overlap, and creates the proper conditions for the hybrid approach. Only the results for case II are presented here, see Figure 2.18.

Further examples of application of hybrid formulation to coupled rods problem can be found in [63]. It should be pointed here that the hybrid FEM-SEA can reduce the size of the MDOF system substantially because it aims in subsystems with high modal density, which in deterministic description would require high number of co-ordinates. The second conclusion is that the hybrid FEM forms, as expected, good base for application of hybrid FEM-SEA.

## 2.7 Summary of Chapter 2

Methods used for power flow analysis in structures have been presented in this chapter. The techniques suitable for low and high frequency analysis have been presented. The presence of the medium frequency range has also been discussed. Methods that address the medium frequency range have been introduced with the main focus on the hybrid FEM-SEA formulation. The advantage of this approach namely its generality has been found to be a distinct feature. For that reason it has

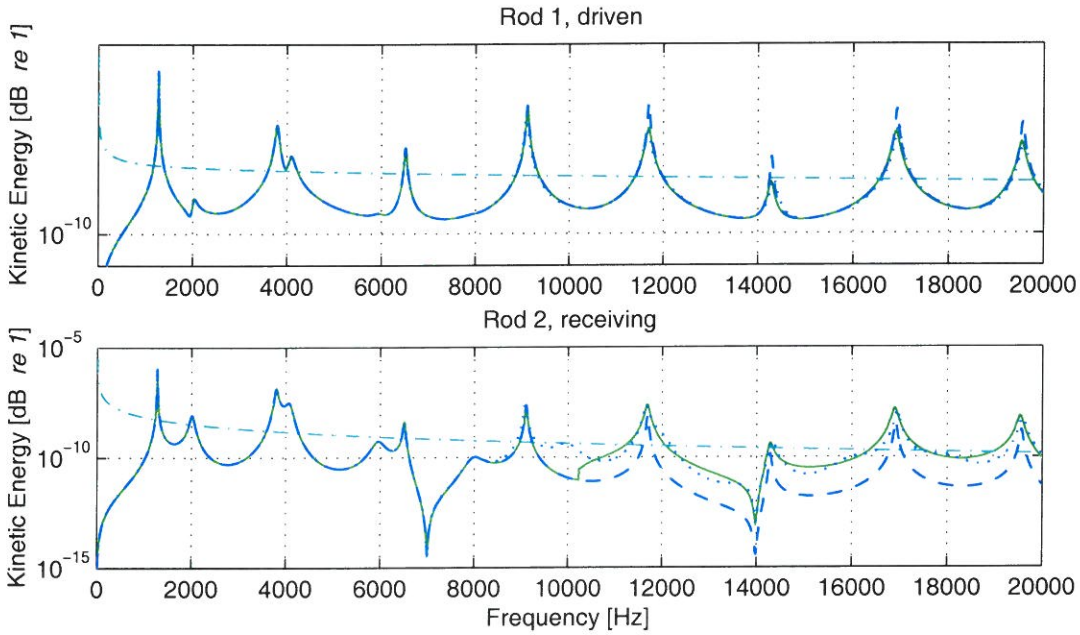


**Figure 2.17**: Results in case I with damping of rod 2 increased to $\eta^{(2)} = 0.05$. Energy in rod 1 (top) and rod 2 (bottom).

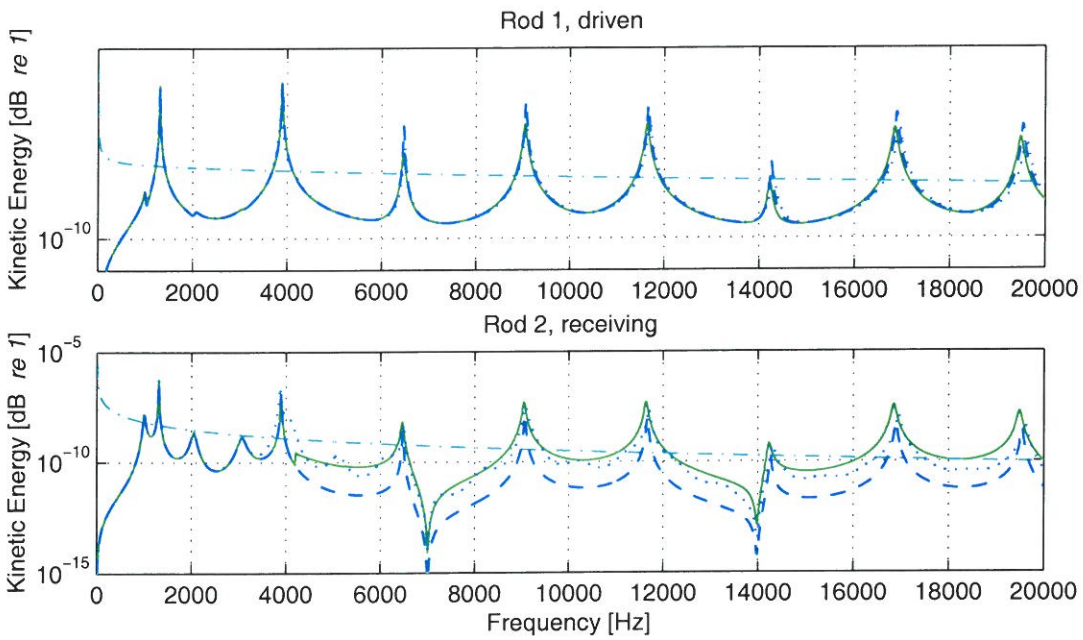


**Figure 2.18**: Results in case II with damping of rod 2 increased to $\eta^{(2)} = 0.05$. Energy in rod 1 (top) and rod 2 (bottom).

been decided that the research in this project should be focused on the extension of the hybrid formulation to the problems concerning coupled plates.

The requirements of the hybrid FEM-SEA have been presented in section 2.5.1 where it has been found that the hierarchical FEM forms a good base for further development of hybrid FEM-SEA. Therefore, a hierarchical FEM program should be developed first and hybrid FEM-SEA afterwards.

# Chapter 3

# Hierarchical FEM for Thin Plates

In section 2.5.1 it has been concluded that the hierarchical FEM forms a good basis for application of the hybrid FEM-SEA. In order to apply the proposed hybrid FEM-SEA formulation to the plate assemblies the hierarchical formulation of FEM has to be developed first. Later, on the basis of hierarchical formulation the coupling terms for the energy exchange between global and local description can be calculated. The development of the hierarchical formulation is presented in this chapter. First, the formulation of a hierarchical element is presented. The definition of continuity conditions follows. In the latter part the properties of the formulation are compared with the requirements of the hybrid approach with the main focus on the correspondence between co-ordinates and normal modes at different frequencies.

## 3.1 Definition of the Plate Element

In the previous studies on hierarchical formulation of the plate problem in [2] the polynomial set of interpolation functions was introduced. Apart from polynomial set of shape functions other sets were presented in the literature, namely the set of products of trigonometric functions [2, 10], the combination of trigonometric functions and polynomials [43,66]. In the current studies the combination of polynomials and products of trigonometric functions are used.

In previous works only the out-of-plane motions were considered. However, the present application requires that both the in-plane and the out-of-plane motions can be modelled. One of the reasons for considering only the out-of-plane motions in the previous studies on the hierarchical formulation is that the wavelengths of the bending waves are much shorter than the wavelengths of in plane longitudinal and shear waves. This is generally true for the thin plate structures. The use of a element mesh with e.g. 10 nodes per wavelength of bending wave in standard FEM might result in ten times as much per wavelength of shear wave for certain frequency

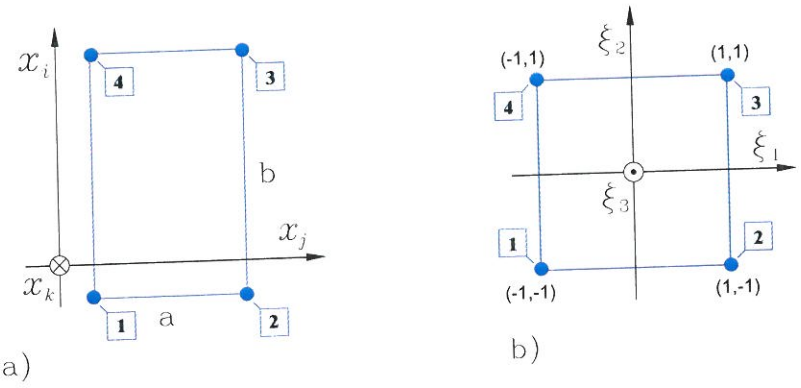


**Figure 3.1**: Element in a) global co-ordinate system; b) natural co-ordinate system

range and plate thickness. This is because in one element there is equal amount of co-ordinates in each direction, both in plane and out of plane. The use of hierarchical formulation gives the possibility of varying the amount of co-ordinates in each of the directions. In order to keep the formulation simpler the in-plane formulation may be chosen with no internal co-ordinates. Then the order of out-of-plane interpolation can be adjust so that the convergence conditions are met in both cases.

### Definition of element co-ordinate systems and co-ordinates

Natural co-ordinate system is defined for each element with the co-ordinates $\xi_1$ and $\xi_2$ being in the plane of element and $\xi_3$ normal to the element's plane. The origin is placed in the centre of the element, and the in-plane co-ordinates $\xi_1$ and $\xi_2$ are normalized with respect to element geometry (see Figure 3.1) , i.e.

$$\boldsymbol{\xi}^{(e)} = [\xi_1^{(e)}, \xi_2^{(e)}, \xi_3^{(e)}]; \qquad \xi_1 \in (-1,1),\ \xi_2 \in (-1,1). \tag{3.1}$$

The displacement field $\boldsymbol{v}^{(e)}(\boldsymbol{\xi}^{(e)}, t)$ within each element (denoted by superscript $e$) is interpolated in terms of the shape functions $\boldsymbol{\Psi}^{(e)}(\boldsymbol{\xi}^{(e)})$, defined in local co-ordinate system $\boldsymbol{\xi}^{(e)}$ and corresponding time dependent variables $q(t)$, i.e.

$$\boldsymbol{v}^{(e)}(\boldsymbol{\xi}^{(e)}, t) = \sum_{n=1}^{N} q_n^{(e)}(t) \boldsymbol{\Psi}_n^{(e)}(\boldsymbol{\xi}^{(e)}) \tag{3.2}$$

where the summation covers number of shape functions ($N$) which is required to approximate the displacement field sufficiently. The displacement field of the entire structure is given by the displacement fields of elements transformed into global co-ordinate system, i.e.

$$\mathbf{u}(\mathbf{x}, t) = \sum_{e=1}^{max\ el} \boldsymbol{T}^{(e)} \boldsymbol{v}^{(e)}(\boldsymbol{\xi}^{(e)}, t) \tag{3.3}$$

where $\boldsymbol{T}^{(e)}$ denotes transformation matrix between the local and global co-ordinate systems.

The shape functions $\boldsymbol{\Psi}^{(e)}(\xi_1^{(e)}, \xi_2^{(e)})$ are two-dimensional and are defined as a product of one-dimensional shape function in $\psi_i(\xi_1^{(e)})$ direction and one-dimensional shape function in $\psi_j(\xi_2^{(e)})$ direction

$$\boldsymbol{\Psi}_m^{(e)}(\boldsymbol{\xi}^{(e)}) = \psi_i(\xi_1^{(e)})\,\psi_j(\xi_2^{(e)}); \quad m = m(i,j). \tag{3.4}$$

$m = m(i,j)$ is a co-ordinate number corresponding to the combination of two indices $i$ and $j$.

Two groups of co-ordinates are generally used in hierarchical formulation of FEM. The first group contains the so-called nodal co-ordinates, i.e. the co-ordinates that correspond to nodal variables (displacements and rotations). The second group contains the so-called internal co-ordinates, i.e. co-ordinates that have no influence on the displacement field in nodes. This is because the requirement for the shape functions of the internal co-ordinates is that they vanish with derivatives at the nodal points. However, in the 2-D formulation, the internal co-ordinates influence the displacement at the boundaries of the element. This issue will be discussed latter in more details.

The element displacement field $\boldsymbol{v}^{(e)}(\boldsymbol{\xi}^{(e)}, t)$ can be divided into the in-plane displacement field: $v_1(\xi_1, \xi_2, t)$ in direction $\xi_1$ and $v_2(\xi_1, \xi_2, t)$ in direction $\xi_2$; and the out-of-plane displacement field: $v_3(\xi_1, \xi_2, t)$ in direction $\xi_3$. According to the thin plate theory, the motions in plane (membrane forces) and out of plane (plate forces) of the element can be analysed independently for one element. In the assembly the in-plane motions of one element can be coupled to the out-of-plane motions of the other and then the two formulations must be coupled. The partition between in-plane and out-of-plane motions will be kept in the definition of finite elements. Then the two contributions will be added to yield full description.

The continuity conditions between elements will be considered in more details later, but at the present time one point should be underlined. The continuity between elements should be fulfilled along the edge and not only in nodal point. It is because the length of the element can be longer than the wavelength of deformation and if only the continuity in nodes would be fulfilled then these short waves could not propagate within the structure. This requirement can only be met if the shape functions of adjusting elements have the same shape along the common edge. This should also work for elements that are perpendicular to each other. For this reason the shape functions of the in-plane formulation have to be the same as for the out-of-plane formulation.

The convergence criteria for the FEM can be defined from the correspondence between displacement field in the structure and complexity of shape functions used in the analysis. If the linear approximation is used then as a 'rule of thumb' 10 nodes

is required for each wavelength of the elastic deformation. In $h$-version of FEM the convergence is achieved by increasing the number of nodes (reducing the size of elements). In $p$-version of FEM (hierarchical FEM is a special type of $p$-version) the convergence is achieved by increasing the order of shape functions within the element.

### 3.1.1 In-plane motions - membrane element

Since the formulation of hierarchical FEM should allow for coupling the plates in different planes, the shape functions used in plane and out of plane should allow for fulfilling the continuity conditions. Also, the co-ordinates that are in plane of one element can be out of plane of the other element. For that reason the third order interpolation is used in the in-plane formulation of membrane element. A standard 4-node finite element would have first order (linear) interpolation functions. The first order interpolation functions cannot be used for the bending problem because bending energy corresponds to the curvature of element, and with linear interpolation the curvature cannot be modelled, and higher order interpolation has to be used. Using different order of interpolation functions for in-plane and out-of-plane motions causes lack of inter-element compatibility. In the standard FEM this fact is often insignificant since the elements are small in comparison with the wavelength of bending deformation. In the hierarchical FEM this fact might have significant contribution because the dimensions of the element can be comparable or bigger than the wavelength of bending deformation. To overcome this problem the in-plane shape functions are defined based on the third order polynomials, the same as used for the out-of-plane interpolation.

#### Co-ordinates and Shape Functions

In each node the following nodal co-ordinates will be present:

1. displacement in $\xi_1$ direction, $v_1$;
2. displacement in $\xi_2$ direction, $v_2$;
3. rotation around $\xi_3$ axis, $\frac{\delta v_1}{\delta \xi_2} - \frac{\delta v_2}{\delta \xi_1}$.

The numbering of in-plane co-ordinates in an element is presented in Figure 3.2.

The in-plane displacement field is given as:

$$\begin{bmatrix} v_1^{(e)} \\ v_2^{(e)} \end{bmatrix} = \boldsymbol{\Psi}^{(e)} \boldsymbol{q}^{(e)} \tag{3.5}$$

where the shape function matrix $\boldsymbol{\Psi}^{(e)}$ has the dimension of $12 \times 2$ and the co-ordinate vector has the dimension $1 \times 12$. The natural co-ordinate system is used, see Figure 3.1.

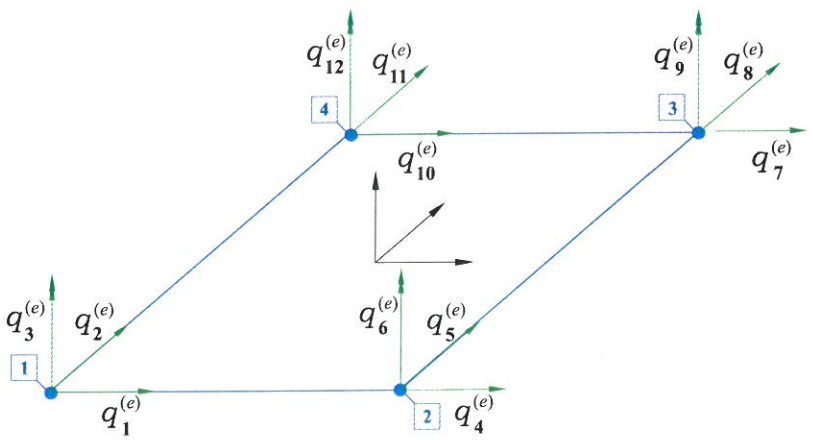


**Figure 3.2**: Co-ordinate numbering convention for in-plane element formulation. Single arrowheads symbolize displacement co-ordinates, double arrowheads symbolize rotational co-ordinates.

Two sets of 1-D shape functions are used to construct the 2-D shape functions. In one direction the linear variation is assumed. This is equivalent with the use of:

$$\psi_1(\xi) = \frac{1-\xi}{2}; \qquad \psi_2(\xi) = \frac{1+\xi}{2} \tag{3.6}$$

for one direction. The signs have to be adjusted so that the unit displacement is achieved in the chosen node. In the second direction the third order polynomials are used, defined as:

$$\begin{aligned} \psi_1(\xi) &= \frac{1}{2} - \frac{3}{4}\xi + \frac{1}{4}\xi^3; \qquad \psi_2(\xi) = \frac{l}{2}(\frac{1}{8} - \frac{1}{8}\xi - \frac{1}{8}\xi^2 + \frac{1}{8}\xi^3) \\ \psi_3(\xi) &= \frac{1}{2} + \frac{3}{4}\xi - \frac{1}{4}\xi^3; \qquad \psi_4(\xi) = -\frac{l}{2}(\frac{1}{8} - \frac{1}{8}\xi + \frac{1}{8}\xi^2 + \frac{1}{8}\xi^3) \end{aligned} \tag{3.7}$$

where $l$ is the length of the element in the global co-ordinates (corresponding to either $a$ or $b$, see Figure 3.1a). This scaling assures that the rotational DOF is scaled with the element size as the displacements are. The 1-D shape functions presented in Figure 3.3 correspond to the 1-D nodal shape functions of a beam element. Therefore, from now on they will be referred to as 1-D nodal shape functions.

The resulting displacement field interpolation can be presented in the form:

$$\begin{bmatrix} v_1^{(e)} \\ v_2^{(e)} \end{bmatrix} = \begin{bmatrix} \Psi_1^{(e)} & 0 & \Psi_3^{(e)} & \Psi_5^{(e)} & 0 & \Psi_7^{(e)} & \Psi_9^{(e)} & 0 & \Psi_{11}^{(e)} & \Psi_{13}^{(e)} & 0 & \Psi_{15}^{(e)} \\ 0 & \Psi_2^{(e)} & \Psi_4^{(e)} & 0 & \Psi_6^{(e)} & \Psi_8^{(e)} & 0 & \Psi_{10}^{(e)} & \Psi_{12}^{(e)} & 0 & \Psi_{14}^{(e)} & \Psi_{16}^{(e)} \end{bmatrix} \begin{bmatrix} q_1^{(e)} \\ q_2^{(e)} \\ \vdots \\ q_{12}^{(e)} \end{bmatrix} \tag{3.8}$$

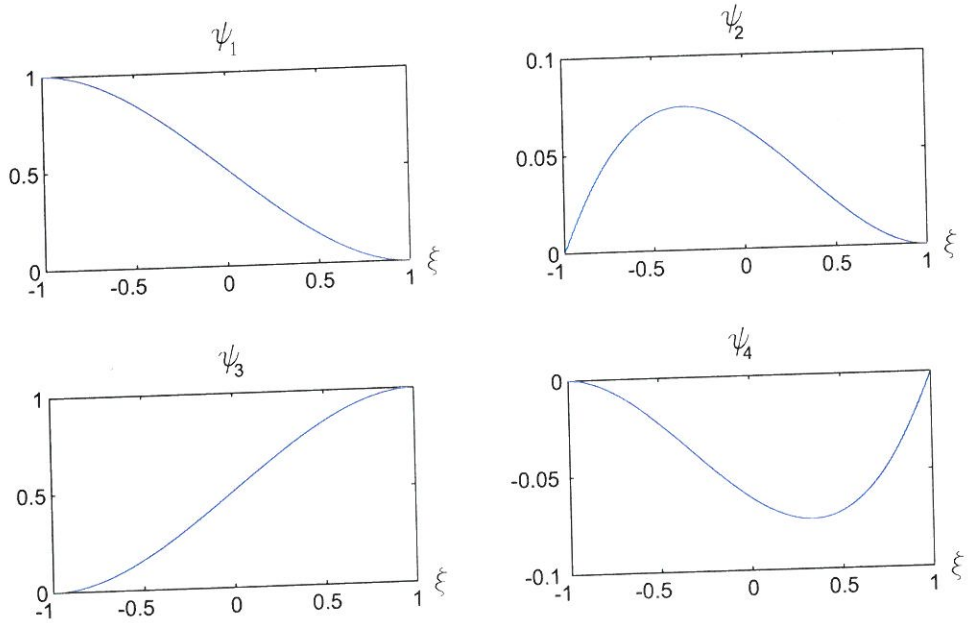


**Figure 3.3**: One-dimensional nodal shape functions, ($\psi_1$, $\psi_2$, $\psi_3$, $\psi_4$)

The entries of the shape function matrix are listed below.

$$\Psi_1^{(e)} = \tfrac{1}{8}(2-3\xi_1+\xi_1^3)(1-\xi_2); \qquad \Psi_2^{(e)} = \tfrac{1}{8}(2-3\xi_2+\xi_2^3)(1-\xi_1)$$
$$\Psi_3^{(e)} = \tfrac{-b}{32}(1-\xi_1-\xi_1^2+\xi_1^3)(1-\xi_2); \qquad \Psi_4^{(e)} = \tfrac{a}{32}(1-\xi_2-\xi_2^2+\xi_2^3)(1-\xi_1)$$
$$\Psi_5^{(e)} = \tfrac{1}{8}(2-3\xi_1+\xi_1^3)(1+\xi_2); \qquad \Psi_6^{(e)} = \tfrac{1}{8}(2+3\xi_2-\xi_2^3)(1-\xi_1)$$
$$\Psi_7^{(e)} = \tfrac{-b}{32}(1-\xi_1-\xi_1^2+\xi_1^3)(1+\xi_2); \qquad \Psi_8^{(e)} = \tfrac{-a}{32}(1+\xi_2-\xi_2^2-\xi_2^3)(1-\xi_1)$$
$$\Psi_9^{(e)} = \tfrac{1}{8}(2+3\xi_1-\xi_1^3)(1+\xi_2); \qquad \Psi_{10}^{(e)} = \tfrac{1}{8}(2+3\xi_2-\xi_2^3)(1+\xi_1)$$
$$\Psi_{11}^{(e)} = \tfrac{b}{32}(1+\xi_1-\xi_1^2-\xi_1^3)(1+\xi_2); \qquad \Psi_{12}^{(e)} = \tfrac{-a}{32}(1+\xi_2-\xi_2^2-\xi_2^3)(1+\xi_1)$$
$$\Psi_{13}^{(e)} = \tfrac{1}{8}(2+3\xi_1-\xi_1^3)(1-\xi_2); \qquad \Psi_{14}^{(e)} = \tfrac{1}{8}(2-3\xi_2+\xi_2^3)(1+\xi_1)$$
$$\Psi_{15}^{(e)} = \tfrac{b}{32}(1+\xi_1-\xi_1^2-\xi_1^3)(1-\xi_2); \qquad \Psi_{16}^{(e)} = \tfrac{a}{32}(1-\xi_2-\xi_2^2+\xi_2^3)(1+\xi_1)$$

The first four 2-D shape functions of an in-plane formulation corresponding to the node **1** are plotted in Figure 3.4.

### Element Stiffness and Mass Matrices

The stiffness and mass matrices of the element can be evaluated according to the general FEM formulation presented in section 2.1.1. Based on (2.9) and (2.16) the matrices of the element can be calculated.

The strain-displacement matrix **B** and the stress-strain matrix **E** for the plane

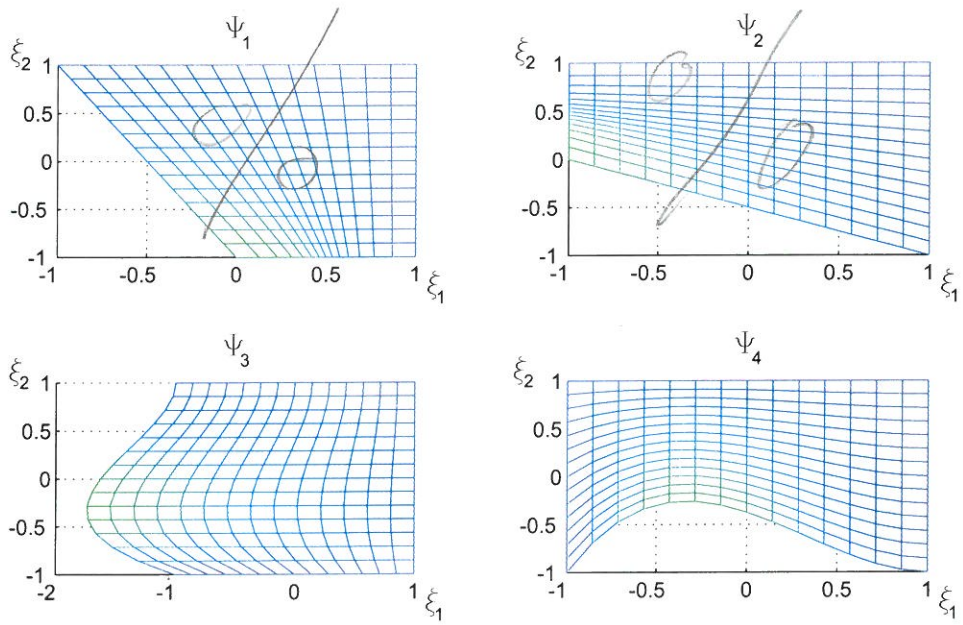


**Figure 3.4**: 2-D shape functions for in-plane formulation at node **1**.

stress (or plain strain) element are defined as, see for example [4, 16]:

$$\mathbf{B} = \begin{bmatrix} \frac{\partial}{\partial \xi_1} & 0 \\ 0 & \frac{\partial}{\partial \xi_2} \\ \frac{\partial}{\partial \xi_2} & \frac{\partial}{\partial \xi_1} \end{bmatrix} \mathbf{\Psi}; \quad \mathbf{E} = \frac{E}{1-\nu^2} \begin{bmatrix} 1 & \nu & 0 \\ \nu & 1 & 0 \\ 0 & 0 & \frac{1-\nu}{2} \end{bmatrix} \tag{3.9}$$

The size of the $\mathbf{B}$ matrix is $12 \times 3$, and the resulting stiffness and mass matrices are of the size $12 \times 12$. The integration involved in calculating the entries of matrices are performed analytically.

### 3.1.2 Out-of-plane motions

The definition of the out-of-plane contribution is quite similar to that for the in-plane contribution. In each node the following nodal co-ordinates are present

1. displacement in $\xi_3$ direction, $v_3$;
2. rotation around $\xi_1$ axis, $\frac{\partial v_3}{\partial \xi_2}$ ;
3. rotation around $\xi_2$ axis, $\frac{\partial v_3}{\partial \xi_1}$ ;
4. second derivative of displacement, $\frac{\partial^2 v_3}{\partial \xi_1 \partial \xi_2}$.

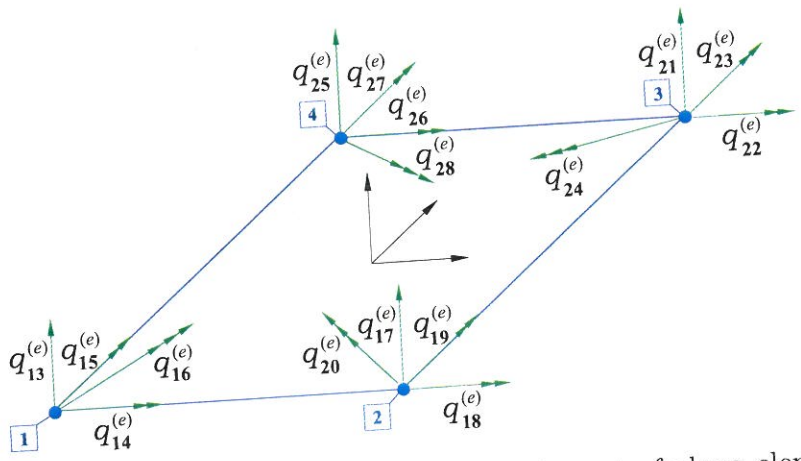


**Figure 3.5**: Co-ordinate numbering convention for out-of-plane element formulation. Single arrowheads symbolize displacement co-ordinates, double arrowheads symbolize rotational co-ordinates and triple arrowheads symbolize the second derivative of displacement.

The numbering of co-ordinates in element is presented in Figure 3.5.

The two-dimensional (2-D) shape functions used to approximate the out-of-plane displacement field are defined as a product of two one-dimensional (1-D) shape functions [2], i.e.

$$\Psi^{(e)}_m(\boldsymbol{\xi}^{(e)}) = \psi_k(\xi^{(e)}_1)\,\psi_l(\xi^{(e)}_2); m = m(k,l);\ k = 1 \ldots K^{(e)}_1;\ l = 1 \ldots K^{(e)}_2 \quad (3.10)$$

where $K^{(e)}_1$, $K^{(e)}_2$ signify the highest interpolation function in element $e$ in directions $\xi_1$ and $\xi_2$, respectively. $K^{(e)}_1$ and $K^{(e)}_2$ can be chosen from the convergence criteria independently from each other. Since the quantity on the left-hand side of equation (3.10) should only have one index the transformation $(k,l) \rightarrow m$ of double indices $k$ and $l$ is introduced. The transformation for the nodal 2-D shape functions is performed by inspection. For the internal 2-D shape functions the transformation is defined as

$$m = 13 + max(k,l)^2 - max(k,l) + l - k. \quad (3.11)$$

The inverse transformation is sometimes necessary. That allows to extract double index from the single index. It can be applied to the internal 2-D shape functions as well as to the corresponding co-ordinates.

### 1-D shape functions

The nodal 1-D shape functions defined in (3.7) are used also for the out-of-plane formulation. The additional shape functions are defined as a product of trigonometric

functions as follows:

$$\psi_{n+4}(\xi) = \sin\left(\frac{n\pi}{2}(\xi+1)\right)\sin\left(\frac{\pi}{2}(\xi+1)\right). \tag{3.12}$$

This definition assures that both the displacement and the slope of the shape function will vanish at the end points, so that the functions could be used as internal shape functions for a beam element. In Figure 3.6 some of the one-dimensional shape functions of higher order are presented.

### 2-D shape functions-nodal

According to (3.10) the 2-D shape functions are defined as a product of two 1-D shape functions. Clearly, the product of two nodal 1-D functions will give the nodal 2-D shape function. The adequate 2-D shape functions for each of the co-ordinates in certain node consist of the product of appropriate 1-D shape functions. The nodal 2-D shape functions for interpolation of the out-of-plane displacement field are listed below. The numbering of shape functions corresponds to the numbering of element's co-ordinates, see Figure 3.5

$$\begin{aligned}
\Psi_{13}^{(e)} &= \tfrac{1}{16}(4-3\xi_1+2\xi_1^3)(4-3\xi_2+\xi_2^3)\\
\Psi_{14}^{(e)} &= \tfrac{-a}{64}(2-3\xi_1+\xi_1^3)(1-\xi_2-\xi_2^2+\xi_2^3)\\
\Psi_{15}^{(e)} &= \tfrac{b}{64}(1-\xi_1-\xi_1^2+\xi_1^3)(2-3\xi_2+\xi_2^3)\\
\Psi_{16}^{(e)} &= \tfrac{-ab}{256}(1-\xi_1-\xi_1^2+\xi_1^3)(1-\xi_2-\xi_2^2+\xi_2^3)\\
\Psi_{17}^{(e)} &= \tfrac{1}{16}(2-3\xi_1+\xi_1^3)(2+3\xi_2-\xi_2^3)\\
\Psi_{18}^{(e)} &= \tfrac{a}{64}(2-3\xi_1+\xi_1^3)(1+\xi_2-\xi_2^2-\xi_2^3)\\
\Psi_{19}^{(e)} &= \tfrac{b}{64}(1-\xi_1-\xi_1^2+\xi_1^3)(2+3\xi_2-\xi_2^3)\\
\Psi_{20}^{(e)} &= \tfrac{ab}{256}(1-\xi_1-\xi_1^2+\xi_1^3)(-1-\xi_2+\xi_2^2+\xi_2^3)\\
\Psi_{21}^{(e)} &= \tfrac{1}{16}(2+3\xi_1-\xi_1^3)(2+3\xi_2-\xi_2^3)\\
\Psi_{22}^{(e)} &= \tfrac{-a}{64}(2+3\xi_1-\xi_1^3)(-1-\xi_2+\xi_2^2+\xi_2^3)\\
\Psi_{23}^{(e)} &= \tfrac{-b}{64}(1+\xi_1-\xi_1^2-\xi_1^3)(2+3\xi_2-\xi_2^3)\\
\Psi_{24}^{(e)} &= \tfrac{-ab}{256}(1+\xi_1-\xi_1^2-\xi_1^3)(1+\xi_2-\xi_2^2-\xi_2^3)\\
\Psi_{25}^{(e)} &= \tfrac{1}{16}(2+3\xi_1-\xi_1^3)(2-3\xi_2+\xi_2^3)\\
\Psi_{26}^{(e)} &= \tfrac{-a}{64}(2+3\xi_1-\xi_1^3)(1-\xi_2-\xi_2^2+\xi_2^3)\\
\Psi_{27}^{(e)} &= \tfrac{-b}{64}(1+\xi_1-\xi_1^2-\xi_1^3)(2-3\xi_2+\xi_2^3)\\
\Psi_{28}^{(e)} &= \tfrac{ab}{256}(1+\xi_1-\xi_1^2-\xi_1^3)(1-\xi_2-\xi_2^2+\xi_2^3)
\end{aligned}$$

The 2-D shape functions corresponding to element node **1** (see Figure 3.1b) at the position $(\xi_1, \xi_1) = (-1, -1)$ are presented in Figure 3.7.

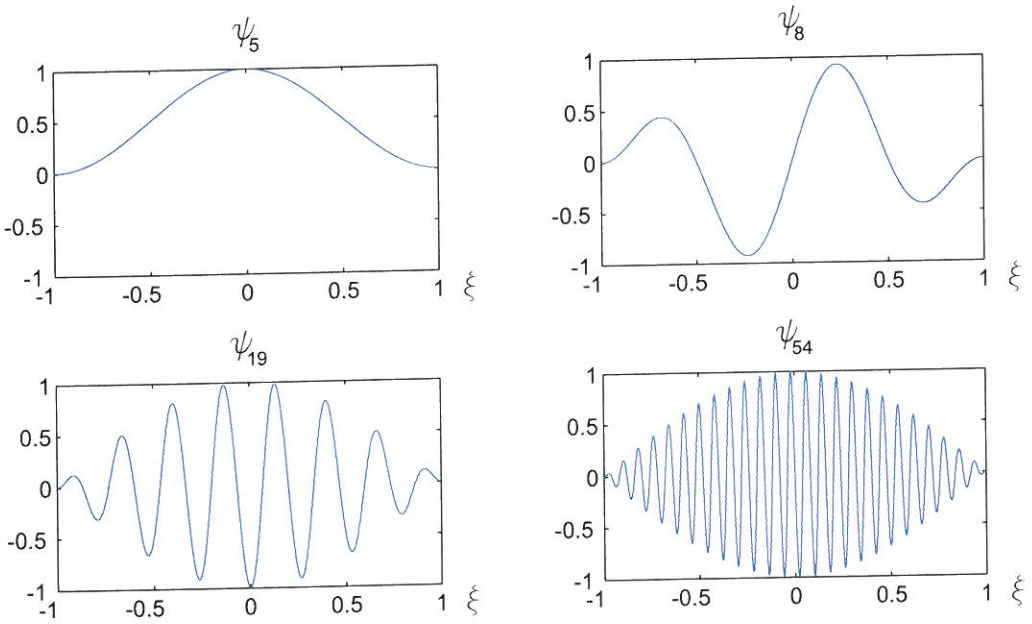


**Figure 3.6**: One-dimensional shape functions, higher order shape functions ($\psi_5$, $\psi_8$, $\psi_{19}$, $\psi_{54}$)

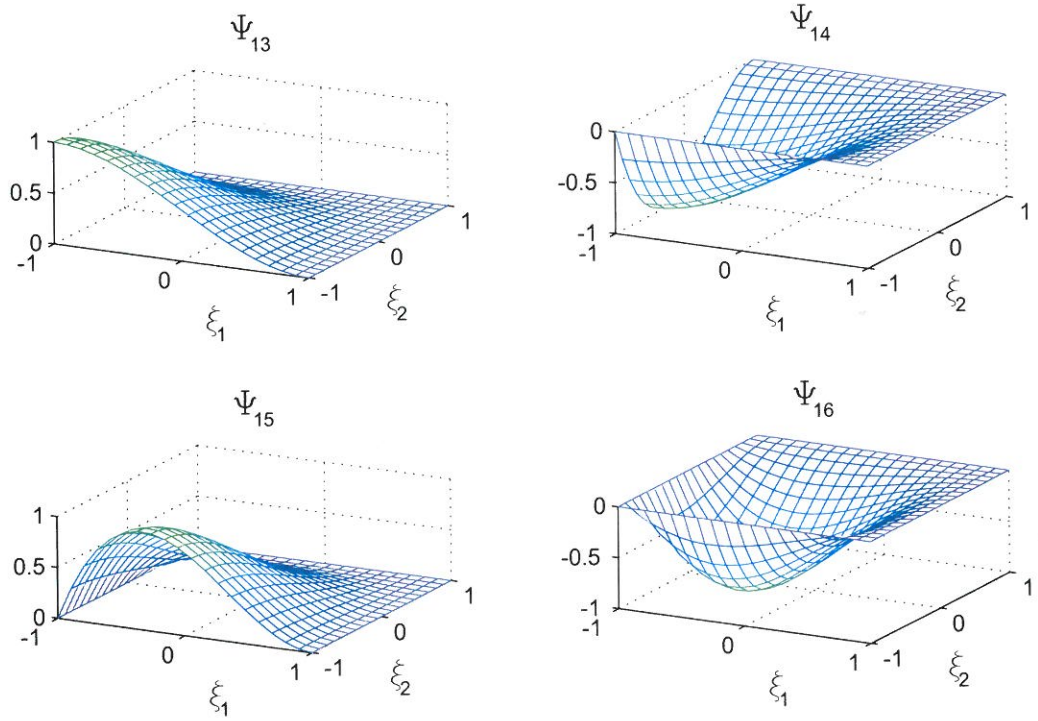


**Figure 3.7**: Two-dimensional nodal shape functions at node 1

### 2-D shape functions-internal

The product of two internal 1-D functions produces the internal 2-D function that vanishes not only at the nodal point but also along the edges of the elements. The third group of 2-D shape functions contains product of nodal 1-D shape function in one direction and internal 1-D shape function in the second direction. These shape functions also vanish at the nodal positions, but they have a nonzero value at one of the element's edges. This third group of shape functions is characteristic for 2-D formulation (and 3-D of course). Disregarding this group would simplify the formulation of hierarchical FEM, but it leads to degenerated set of shape functions. Therefore, the shape functions from the third group are included in the formulation. The continuity of displacements along edges of connected elements has to be considered not only in terms of nodal co-ordinates but also in terms of co-ordinates corresponding to this third group of shape functions.

Examples of internal 2-D shape functions from the second and the third group (products of two internal 1-D shape functions and internal and nodal 1-D shape functions) are presented in Figure 3.8 a and b, respectively. It can be seen that the internal shape functions in Figure 3.8 give no contribution either to the displacement or to the slope at the edges of the element. In contrast the shape functions from the third group give contribution to either slope (Figure 3.8 b, upper) or to displacement (Figure 3.8 b, lower) along the edge of the element.

### Element Stiffness and Mass Matrices

According to the Kirchhoff plate theory the potential energy $W$ and kinetic energy $T$ of the out-of-plane motions of the plate assuming small displacements may be written as [2]

$$W = \frac{1}{2}\frac{4Bb}{a^3}\int_{-1}^{1}\int_{-1}^{1}\left[\left(\frac{\partial^2 \upsilon_3}{\partial \xi_1^2}\right)^2 + \frac{1}{(b/a)^4}\left(\frac{\partial^2 \upsilon_3}{\partial \xi_2^2}\right)^2 + \frac{2\nu}{(b/a)^2}\left(\frac{\partial^2 \upsilon_3}{\partial \xi_1^2}\right)\left(\frac{\partial^2 \upsilon_3}{\partial \xi_2^2}\right) + \frac{2(1-\nu)}{(b/a)^2}\left(\frac{\partial^2 \upsilon_3}{\partial \xi_1 \partial \xi_2}\right)^2\right] d\xi_1 d\xi_2 \tag{3.13}$$

and:

$$T = \frac{1}{2}\frac{\rho h a b}{4}\int_{-1}^{1}\int_{-1}^{1}\left(\frac{\partial \upsilon_3}{\partial t}\right)^2 d\xi_1 d\xi_2 \tag{3.14}$$

where $B$ is the plate bending stiffness, $B = Eh^3/12(1-\nu^2)$, $\rho$ is the mass density of plate material, $\upsilon_3$ is the out-of-plane displacement; $a$ and $b$ are the dimensions of

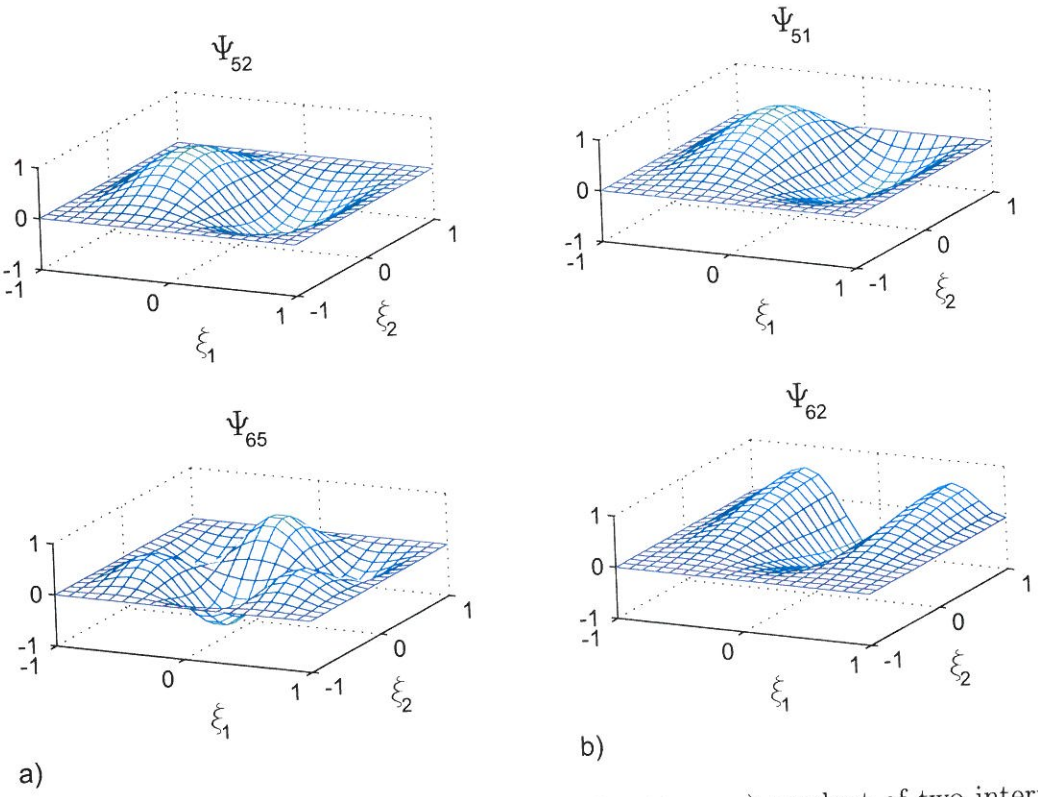


**Figure 3.8**: Two-dimensional internal shape functions; a) product of two internal 1-D shape functions; b) product of internal and nodal 1-D shape functions.

the plate. Using 3.2 and 3.10 in expressions for potential and kinetic energy yields

$$W = \frac{1}{2}\frac{4Bb}{a^3}\sum_{r=1}^{p}\sum_{s=1}^{p} q_r q_s \int_{-1}^{1}\int_{-1}^{1}\left[\left(\frac{\partial^2\Psi_r}{\partial\xi_1^2}\frac{\partial^2\Psi_s}{\partial\xi_1^2}\right) + \frac{1}{(b/a)^4}\left(\frac{\partial^2\Psi_r}{\partial\xi_2^2}\frac{\partial^2\Psi_s}{\partial\xi_2^2}\right)\right.$$
$$\left. + \frac{\nu}{(b/a)^2}\left(\frac{\partial^2\Psi_r}{\partial\xi_1^2}\frac{\partial^2\Psi_s}{\partial\xi_2^2} + \frac{\partial^2\Psi_s}{\partial\xi_1^2}\frac{\partial^2\Psi_r}{\partial\xi_2^2}\right) + \frac{2(1-\nu)}{(b/a)^2}\left(\frac{\partial^2\Psi_r}{\partial\xi_1\partial\xi_2}\frac{\partial^2\Psi_s}{\partial\xi_1\partial\xi_2}\right)\right] d\xi_1 d\xi_2$$
$$= \frac{1}{2}(\boldsymbol{q}^{(e)})^T\mathbf{K}^{(e)}\boldsymbol{q}^{(e)} \tag{3.15}$$

$$T = \frac{1}{2}\frac{\rho hab}{4}\sum_{r=1}^{p}\sum_{s=1}^{p}\dot{q}_r\dot{q}_s\int_{-1}^{1}\int_{-1}^{1}\Psi_r\Psi_s d\xi_1 d\xi_2 = \frac{1}{2}(\dot{\boldsymbol{q}}^{(e)})^T\mathbf{M}^{(e)}\dot{\boldsymbol{q}}^{(e)} \tag{3.16}$$

The $(r, s)$ component of the stiffness matrix is defined as:

$$(K^{(e)})_{r,s} = \frac{4Bb}{a^3}\int_{-1}^{1}\int_{-1}^{1}\left[\left(\frac{\partial^2\Psi_r}{\partial\xi_1^2}\frac{\partial^2\Psi_s}{\partial\xi_1^2}\right) + \frac{1}{(b/a)^4}\left(\frac{\partial^2\Psi_r}{\partial\xi_2^2}\frac{\partial^2\Psi_s}{\partial\xi_2^2}\right) + \frac{\nu}{(b/a)^2}\left(\frac{\partial^2\Psi_r}{\partial\xi_1^2}\frac{\partial^2\Psi_s}{\partial\xi_2^2} + \frac{\partial^2\Psi_s}{\partial\xi_1^2}\frac{\partial^2\Psi_r}{\partial\xi_2^2}\right) + \frac{2(1-\nu)}{(b/a)^2}\left(\frac{\partial^2\Psi_r}{\partial\xi_1\partial\xi_2}\frac{\partial^2\Psi_s}{\partial\xi_1\partial\xi_2}\right)\right] d\xi_1 d\xi_2 \tag{3.17}$$

The $r, s$ entry of the element's mass matrix is defined as

$$(M^{(e)})_{r,s} = \frac{\rho hab}{4}\int_{-1}^{1}\int_{-1}^{1}\Psi_r\Psi_s d\xi_1 d\xi_2 \tag{3.18}$$

Equations (3.17) and (3.18) are implemented in Maple [47] and the solution for the elements matrices are calculated. The geometry and the material properties are left in symbolic manner rather than given a value, so that the integration is performed only once at the program development stage. Later the matrices are adjusted for a given element's properties ($a$, $b$, $b/a$, $E$, $\rho$, $\nu$, $B$) . This reduces the computational costs of the method and prevents the necessity of numerical integration of complicated shape functions.

## 3.2 Continuity and Boundary Conditions

In this section two important subjects are considered, namely how the continuity and boundary conditions should be defined in the assembly procedure.

The definition of continuity conditions can be divided into two parts, namely the continuity between nodal co-ordinates and between internal co-ordinates.

### 3.2.1 Continuity of nodal co-ordinates

The continuity of nodal co-ordinates is assured by the use of one set of nodal co-ordinate set. The nodal co-ordinates belong to the nodes, and the co-ordinates of the element are defined in terms of nodal co-ordinates. Since the nodal shape functions have a unit value in the node, the continuity between displacements is ensured. In Figure 3.9 three elements lying in different planes are coupled. The displacement field of the assembly due to setting one of the nodal co-ordinates to unity is presented. The only additional continuity conditions for nodal co-ordinates require that co-ordinates corresponding to shape functions defined as the second derivative of displacement with respect to both directions in plane of element must be excluded from calculations if more than one element is present at the node. This corresponds to $\Psi_{16}^{(e)}$; $\Psi_{20}^{(e)}$; $\Psi_{24}^{(e)}$; $\Psi_{28}^{(e)}$, see Figure 3.7.

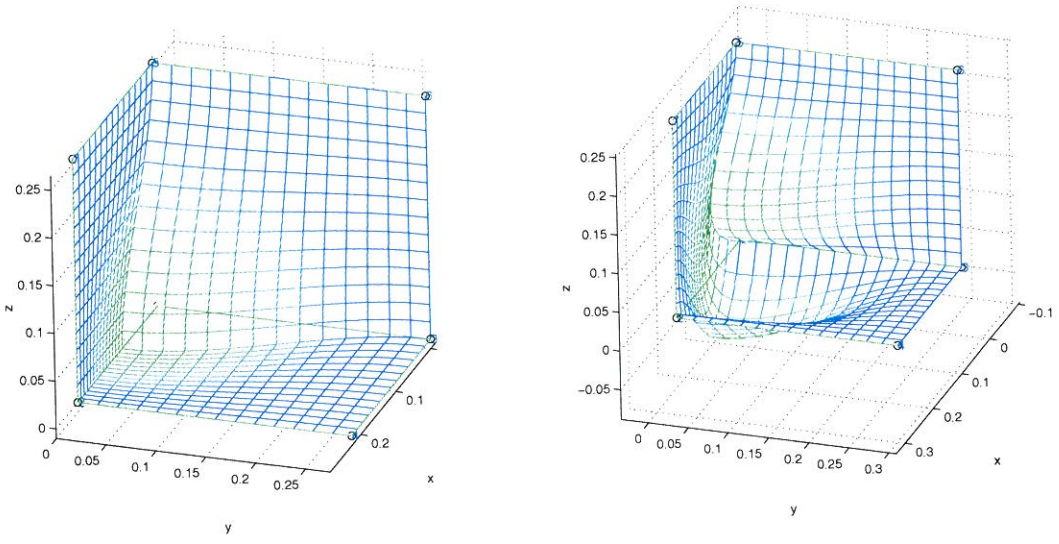


a) b)

**Figure 3.9**: Continuity of displacement in different elements due to nodal co-ordinates; examples of a) translational nodal co-ordinate; b) rotational nodal co-ordinate.

### 3.2.2 Continuity of internal co-ordinates

The continuity between internal co-ordinates cannot be treated in the same way. This is because the amount of internal co-ordinates may vary among elements in the mesh. Coupling will take place if two conditions are met:

- the 1-D shape functions along the axis parallel to the junction are the same in both elements, because only this condition assures continuity along the edge;
- the 1-D shape function in the perpendicular direction does not vanish at the junction, which means that this functions have to belong to the nodal 1-D shape functions.

Since the product of two nodal 1-D shape functions forms a nodal 2-D shape function and the continuity is applied by the use of the same co-ordinate, then the only group to be considered is the group of internal 2-D shape functions that are built out of one internal and one nodal 1-D function. Clearly, it is necessary to consider the 1-D components of the 2-D shape function. Therefore, a new description of the 2-D shape functions $\Psi_i^{(e)}$ will be used. The single subscript $i$ will temporary be exchanged by the double subscript $(r, s)$ signifying the 1-D component in $\xi_1$ and $\xi_2$

direction, respectively. Also, the subscript of a corresponding element's co-ordinate $q_i^{(e)}$ is exchanged in a similar way. This is an inverse operation to the one performed in (3.10) where the two indices were transformed into one. First, the continuity of the displacements between elements that lie in the same plane are considered. The perpendicular junctions are considered later.

### Elements in one plane

In the case of elements that lie in the same plane and have a common edge, the conditions stated above are quite easy to apply. The local co-ordinate systems of two elements are parallel to each other and one is translated with respect to the other along either $\xi_1$ or $\xi_2$. For the sake of clearness it can be assumed that the subsequent elements $n$ and $m$ have common edge along $\xi_2$ direction, see Figure 3.10. If the position of the common edge in element's $n$ co-ordinate system is $\xi_1^{(n)} = 1$ then in the element's $m$ co-ordinate system it is $\xi_1^{(m)} = -1$.

The continuity of displacements in this case will require that:

$$q_{3,s}^{(n)} = q_{1,s}^{(m)}; \quad \text{for } s = 5 \ldots min(K_2^{(n)}, K_2^{(m)}) \tag{3.19}$$

$$q_{4,s}^{(n)} = q_{2,s}^{(m)}; \quad \text{for } s = 5 \ldots min(K_2^{(n)}, K_2^{(m)}). \tag{3.20}$$

The $min(K_2^{(n)}, K_2^{(m)})$ is used to indicate that the order of interpolation functions may differ among elements. The double indices of internal co-ordinates $q_{r,s}^{(n)}$ can be transformed into one index form using (3.11).

Clearly additional condition is required for the element that has higher order of interpolation functions, namely the corresponding co-ordinates must be removed from the set. In the case when $K_2^{(n)} > K_2^{(m)}$ these conditions will read

$$q_{3,s}^{(n)} = q_{4,s}^{(n)} \equiv 0; \quad \text{for } s = K_2^{(m)} \ldots K_2^{(n)} \tag{3.21}$$

From now on this condition will not be repeated, but it should be understand that this condition should always be applied.

In the case when the two elements have the common edge in the $\xi_1$ direction, as elements $t$ and $u$ in Figure 3.10. Then the continuity of displacements will require the following

$$q_{r,3}^{(n)} = q_{r,1}^{(m)}; \quad \text{for } s = 5 \ldots min(K_1^{(n)}, K_1^{(m)}) \tag{3.22}$$

$$q_{r,4}^{(n)} = q_{r,2}^{(m)}; \quad \text{for } s = 5 \ldots min(K_1^{(n)}, K_1^{(m)}). \tag{3.23}$$

### Elements in perpendicular planes

The continuity of displacements across the junction of elements that lie in different planes requires additional attention. At this type of junction the in-plane and out-

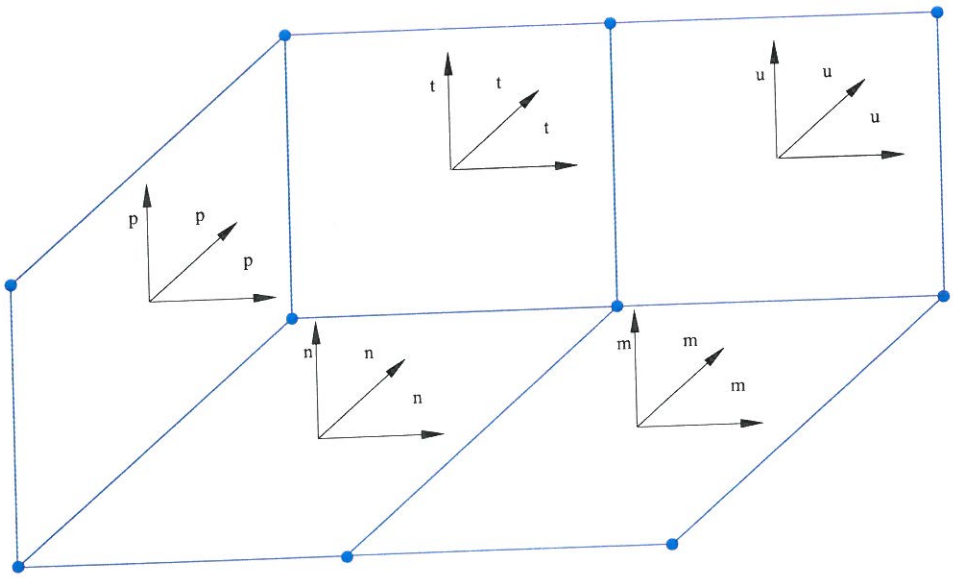


**Figure 3.10**: Coupled elements.

of-plane motions couple. The stiffness of the junction is dominated by the stiffness of the in-plane component. Therefore, the displacement field will be similar to the displacement field of the in-plane component. For this reason the displacement at the junction will only have nodal components.

The rotational co-ordinates in the plane normal to both elements couples the out-of-plane components in the coupled elements. This type of motion is not affected by the presence of the junction and can propagate freely. Therefore, for the type of junction considered the continuity conditions will include:

- cancellation of internal co-ordinates corresponding to the internal shape functions with nonzero displacement along the common edge;
- coupling of internal co-ordinates corresponding to the internal shape functions with nonzero rotation around the common edge.

As an example the junction between elements $p$ and $n$ can be considered, see Figure 3.10. The continuity conditions for this case will have the form

$$q_{r,1}^{(p)} \equiv 0; \qquad \text{for } r = 5 \ldots K_1^{(p)} \tag{3.24}$$

$$q_{1,s}^{(n)} \equiv 0; \qquad \text{for } s = 5 \ldots K_2^{(n)} \tag{3.25}$$

$$q_{r,2}^{(p)} = q_{2,s}^{(n)}; \qquad \text{for } r = s = 5 \ldots min(K_1^{(p)}, K_2^{(n)}) \tag{3.26}$$

Conditions for other types of junction between elements have the similar form.

### 3.2.3 Boundary conditions

In the similar way as with the continuity conditions, the boundary conditions should be considered for both nodal and internal co-ordinates. The boundary conditions for the nodal co-ordinates are defined by defining the set of nodal DOF that should be clamped, i.e. the zero displacement should be imposed to the co-ordinate. In the case of imposed boundary conditions along edges of elements there will be an additional group of internal co-ordinates that should be included in the set of boundary conditions, i.e. set to zero.

### 3.2.4 Imposing of continuity and boundary conditions

The continuity conditions for the structure, as defined in equations (3.19) to (3.26) and the boundary conditions have to be imposed to the structure.

Imposing the continuity between dependent and independent co-ordinates requires condensation of the system matrices. This can be explained by considering a pair of co-ordinates $q_i$ and $q_j$ that are bounded by the continuity equation $q_i = \alpha_{ij} q_j$ and $\alpha_{ij}$ is a constant. If $q_i$ is taken as a dependent co-ordinate and $q_j$ as an independent co-ordinate (the choice is arbitrary) then the dependent co-ordinate have to be removed from the vector of co-ordinates i.e. the original co-ordinate vector in the form $\boldsymbol{q} = [q_1, \ldots, q_i, \ldots, q_j, \ldots]^T$ should be reduced to $\bar{\boldsymbol{q}} = [q_1, \ldots, 0, \ldots, q_j, \ldots]^T$ where the $\bar{\boldsymbol{q}}$ denotes the reduced vector of co-ordinates. Since the product $\boldsymbol{q}^T \mathbf{M} \boldsymbol{q}$ should not change by the condensation process, i.e.

$$\boldsymbol{q}^T \mathbf{M} \boldsymbol{q} = \bar{\boldsymbol{q}}^T \bar{\mathbf{M}} \bar{\boldsymbol{q}}; \qquad \boldsymbol{q}^T \mathbf{K} \boldsymbol{q} = \bar{\boldsymbol{q}}^T \bar{\mathbf{K}} \bar{\boldsymbol{q}} \tag{3.27}$$

The condensed mass matrix $\bar{\mathbf{M}}$ should obey:

$$\begin{aligned} \bar{q}_j \bar{M}_{jn} \bar{q}_n &= q_i M_{in} q_n + q_j M_{jn} q_n = \alpha_{ij} q_j M_{in} q_n + q_j M_{jn} q_n \\ &= q_j (\alpha_{ij} M_{in} + M_{jn}) q_n; \qquad \text{for } n \neq i,\ n \neq j \end{aligned} \tag{3.28}$$

$$\begin{aligned} \bar{q}_n \bar{M}_{nj} \bar{q}_j &= q_n M_{ni} q_i + q_n M_{nj} q_j = q_n M_{ni} \alpha_{ij} q_j + q_n M_{nj} q_j \\ &= q_n (\alpha_{ij} M_{ni} + M_{nj}) q_j; \qquad \text{for } n \neq i,\ n \neq j \end{aligned} \tag{3.29}$$

$$\begin{aligned} \bar{q}_j \bar{M}_{jj} \bar{q}_j &= q_i M_{ii} q_i + q_i M_{ij} q_j + q_j M_{jj} q_j + + q_j M_{ji} q_i = \\ &= q_j (\alpha_{ij}^2 M_{ii} + \alpha_{ij} M_{ij} + M_{jj} + \alpha_{ij} M_{ji}) q_j \end{aligned} \tag{3.30}$$

The same conditions apply to the stiffness matrix. The relations between the condensed and original matrices can therefore be written as:

$$\bar{M}_{jn} = \alpha_{ij} M_{in} + M_{jn};\ n \neq i,\ n \neq j \tag{3.31}$$

$$\bar{M}_{nj} = \alpha_{ij} M_{ni} + M_{nj};\ n \neq i,\ n \neq j \tag{3.32}$$

$$\bar{M}_{jj} = \alpha_{ij}^2 M_{ii} + 2\alpha_{ij} M_{ij} + M_{jj} \tag{3.33}$$

for the mass matrix and as:

$$\bar{K}_{jn} = \alpha_{ij} K_{in} + K_{jn};\ n \neq i,\ n \neq j \tag{3.34}$$
$$\bar{K}_{nj} = \alpha_{ij} K_{ni} + K_{nj};\ n \neq i,\ n \neq j \tag{3.35}$$
$$\bar{K}_{jj} = \alpha_{ij}^2 K_{ii} + 2\alpha_{ij} K_{ij} + K_{jj} \tag{3.36}$$

for the stiffness matrix. This operation should be performed for each pair of co-ordinates. Care should be taken for the co-ordinates that take part in more than one continuity equation. Then the independent variable in one equation might become a dependent variable in the other equation. In the case where $q_i = \alpha ij q_j$ and $q_j = \alpha jk q_k$ the $q_i$ should first be reduced, and the $q_j$ afterwards. In the case where the continuity conditions are defined as $q_i = \alpha ij q_j$ and $q_i = \alpha in q_n$ first one of the equations should be inverted, so that $q_i$ is not a dependent variable in both of them.

After solving the set of equations either in static or dynamic analysis the dependent variables can be calculated from equations (3.19) to (3.26) if necessary. This is often necessary in the energy calculations in the case when the two variables belong to different subsystems. The contribution is summed into the condensed equations and therefore the separate contribution cannot be found. The original matrices have to be used instead.

The continuity conditions require also that some of the co-ordinates are set to zero. This type of continuity conditions can therefore be applied in the same way as the boundary conditions.

## 3.3 Co-ordinate-Frequency Correspondence

The main requirement for the co-ordinate partition in the hybrid FEM-SEA is that the groups of co-ordinates corresponding to different wave components can be identified. If the modal co-ordinates are used then this is straightforward because the modes have distinct natural frequencies and are orthogonal.

The internal co-ordinates of the hierarchical FEM should posses at least the first of these properties, i.e. to be associated with certain frequency as the characteristic frequency. It has been the case when the coupled rods have been considered in Section 2.6. It can also be easily shown that the same applies to the beam element with the internal shape functions defined as the 1-D shape functions, see (3.7) and

(3.12). The mass matrix of a hierarchical beam element has the form:

$$\mathbf{M}^{(e)} = \frac{\rho^{(e)} A^{(e)} L^{(e)}}{2} \begin{bmatrix} \mathbf{M}_{nn} & & & \mathbf{M}_{ni} & & \\ & \frac{3}{4} & 0 & \frac{1}{4} & 0 & \cdots & 0 \\ & 0 & \frac{1}{2} & 0 & \frac{-1}{4} & \ddots & \vdots \\ \mathbf{M}_{ni}^T & \frac{-1}{4} & 0 & \frac{1}{2} & 0 & \ddots & 0 \\ & 0 & \frac{-1}{4} & 0 & \frac{1}{2} & \ddots & \frac{-1}{4} \\ & \vdots & \ddots & \ddots & \ddots & \ddots & 0 \\ & 0 & \cdots & 0 & \frac{-1}{4} & 0 & \frac{1}{2} \end{bmatrix} \tag{3.37}$$

This can be verified by inserting the 1-D internal shape functions defined in (3.12) in the definition of mass matrix (2.16).

The kinetic energy has been defined in (2.21). Since the entries of the mass matrix are of the same order of magnitude the contribution of the co-ordinate to the kinetic energy will depend on its amplitude (for the diagonal entries the energy is proportional to the amplitude squared). Therefore, by considering the amplitudes of the co-ordinates in the solution its contribution to the energy can be estimated.

The amplitude $Q_r$ of the co-ordinate $r$ results from the interpolation of the actual displacement field by the set of shape functions. Figure 3.11 presents the comparison of amplitudes of co-ordinates in different cases of displacement field, corresponding to different wavelengths of deformation in the element (different frequencies). The displacement varies sinusoidally along the element. The wavelength of this motion depends on the frequency (with material and geometrical properties remaining constant), so that the subsequent plots of displacement on Figure 3.11 symbolize the displacement field at different frequencies. On the right-hand side the ratio between amplitudes of internal co-ordinates to the amplitude of internal co-ordinate with maximum amplitude is presented. The ratio is shown in logarithmic scale. The internal co-ordinate set includes co-ordinates $q_5$ to $q_{45}$.

The co-ordinates with maximum amplitudes carry most of the energy. It can be seen from Figure 3.11 that as the wavelength of deformation (indicated above the displacement plots) shortens the more co-ordinates is involved in the interpolation. This means that the relationship between co-ordinates and frequencies can be found.

In a similar way the 2-D problem can be analysed. Each of the 2-D shape function represents the displacement field for which the characteristic wavelength can be found. If the characteristic wavelength of the 2-D shape function is shorter than the actual wavelength of deformation of the structure, then this shape function will not contribute to the interpolation of the deformation. The co-ordinate corresponding to this shape function will not be excited, and therefore will not contribute to the energy of the element. This property makes the internal set of co-ordinates of the hierarchical FEM suitable for partition required in the hybrid FEM-SEA.

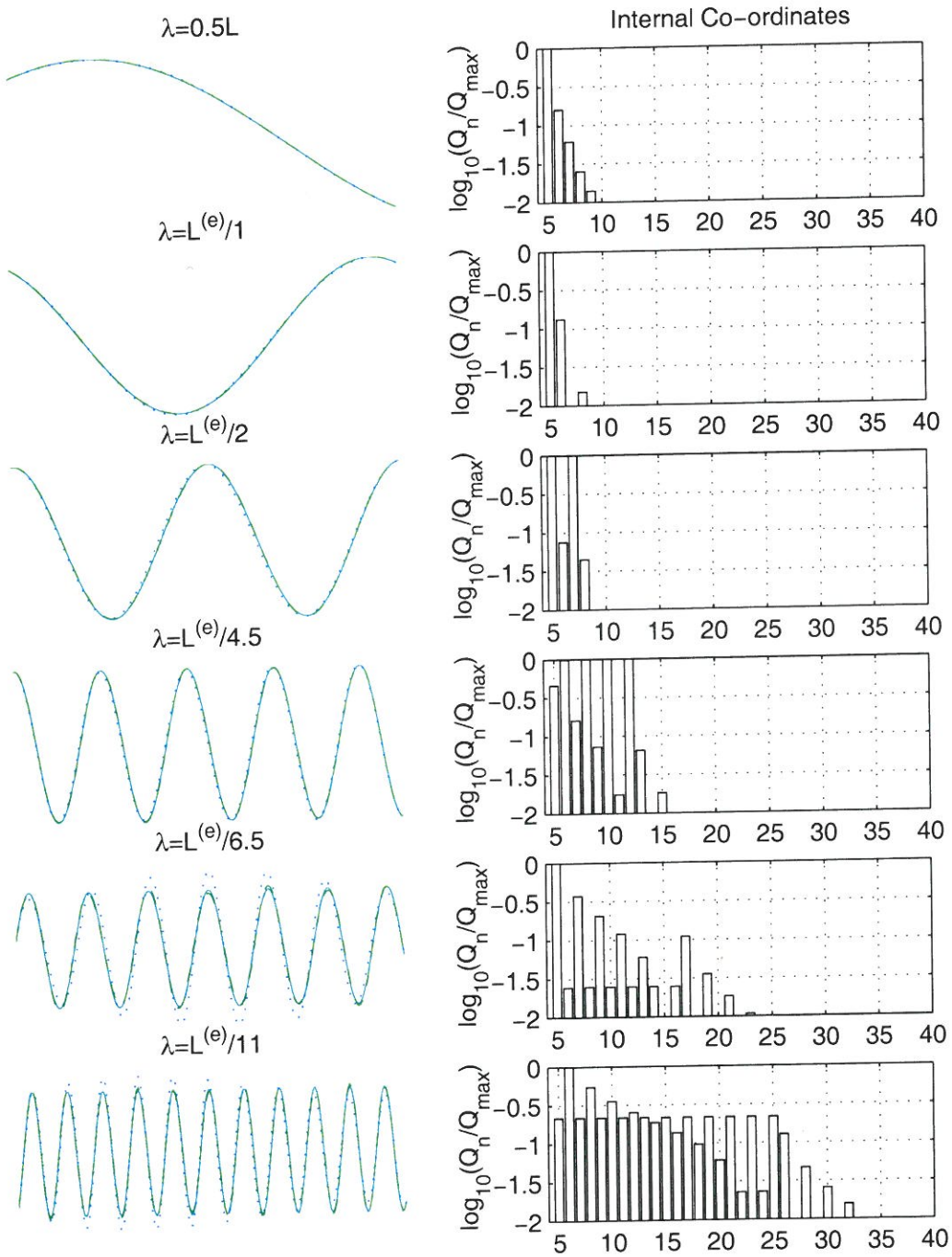


**Figure 3.11**: Displacement field of the element (on the left). — displacement field, ··· approximation with 10% filter, - - - approximation with 1% filter. Participation of internal co-ordinates in interpolation of different displacement fields (on the right). The bars indicate the ratio between amplitude of given co-ordinate and the amplitude of dominate co-ordinate (in logarithmic scale).

## 3.4 Summary of Chapter 3

The formulation of the hierarchical plate element has been presented in this chapter. The in-plane and out-of-plane motions have been considered. The approximation functions that allow for coupling plates in different planes have been chosen, and the appropriate definition of continuity conditions has been developed.

Finally the suitability of the hierarchical FEM for the development of hybrid FEM-SEA has been demonstrated.

# Chapter 4

# Implementation and Validation of Hierarchical FEM

The implementation of the hierarchical FEM described in the previous chapter and developed in the course of the current project is presented in this chapter. First the issues concerned with assembly of the hierarchical plate elements into the final geometry are discussed. The algorithm developed in Matlab [106] is explained in a simple example. In the latter part of the chapter the validation of the method is presented by comparison with analytical and numerical results of eigenvalue extraction and power flow calculations.

## 4.1 Implementation of the Assembly Procedure

In the $h$-version of FEM (the standard FEM) the convergence is achieved by increasing the number of elements (reducing the size of elements). Every time this operation is performed a new mesh is defined and the elements matrices (mass, stiffness and possibly also the damping matrix, depending on the damping model) have to be recalculated. Because of that the new system matrices have to be assembled, too, every time the elements' mesh is updated. On the contrary, in the hierarchical version of FEM the convergence is achieved by increasing the order of interpolation within an element that remains otherwise unchanged. Adding the co-ordinate of the order $p+1$ to the element of order $p$ requires that the $p+1^{\text{st}}$ row and column of the element matrices are added to the matrices of order $p$. Symbol $\mathbf{R}^{(n)}$ can be used to denote any of the $n^{\text{th}}$ matrices of the element, i.e. either mass, stiffness or damping matrix. The indices $i, j$ in superscript are used to denote the entry of the matrix in $i^{\text{th}}$ row and $j^{\text{th}}$ column of the matrix. The size of the matrix is marked by superscript in brackets [ ]. The matrix of the element of the order $p+1$ can

therefore be written as:

$$\mathbf{R}^{(n)}_{[p+1\times p+1]} = \begin{bmatrix} \mathbf{R}^{(n)}_{1,1} & \cdots & \mathbf{R}^{(n)}_{1,p} & \mathbf{R}^{(n)}_{1,p+1} \\ \vdots & \ddots & \vdots & \vdots \\ \mathbf{R}^{(n)}_{p,1} & \cdots & \mathbf{R}^{(n)}_{p,p} & \mathbf{R}^{(n)}_{p,p+1} \\ \mathbf{R}^{(n)}_{p+1,1} & \cdots & \mathbf{R}^{(n)}_{p+1,p} & \mathbf{R}^{(n)}_{p+1,p+1} \end{bmatrix} = \begin{bmatrix} & & \mathbf{R}^{(n)}_{1,p+1} \\ \mathbf{R}^{(n)}_{[p\times p]} & & \vdots \\ & & \mathbf{R}^{(n)}_{p,p+1} \\ \mathbf{R}^{(n)}_{p+1,1} & \cdots & \mathbf{R}^{(n)}_{p+1,p+1} \end{bmatrix} \tag{4.1}$$

In a similar way the system matrix of the hierarchical FEM is affected in a limited way when the co-ordinates are added, and the original matrices can be used to create the additional ones.

The assembly procedure should be designed in the way that would allow for and simplify the definition of additional co-ordinates. In the assembly procedure developed in this project the assembly is performed in few steps. First the nodal co-ordinates of the elements are assembled for the whole structure. This 'nodal' part of the matrices is unaffected by the change in the order of interpolation used for internal co-ordinates and therefore should be kept separately. It is also responsible for the description of coupling between plates that lie in different planes. Secondly, the internal co-ordinates are added in groups corresponding to each of the elements. Finally, the continuity and boundary conditions are applied as introduced in Section 3.2.

An example of assembly of the matrices for the simple structure will be used to present the method. Only two elements are considered in this presentation for the sake of clearness.

### 4.1.1 Nodal co-ordinates

The nodal co-ordinates of elements are considered in the first step. The geometry of the structure is defined in terms of nodes and elements. Figure 4.1 presents the nodes and elements definition. The position and the orientation of natural elements co-ordinate systems with respect to the global co-ordinate system is also shown.

Nine co-ordinates are applied to the each of the nodes. The indices of co-ordinates are applied in the following order

1. displacement in $x_1$ direction, $u_1$;
2. displacement in $x_2$ direction, $u_2$;
3. displacement in $x_3$ direction, $u_3$;
4. rotation around $x_1$ axis, $\theta_1 = \frac{\delta u_2}{\delta x_3} - \frac{\delta u_3}{\delta x_2}$;
5. rotation around $x_2$ axis, $\theta_2 = \frac{\delta u_3}{\delta x_1} - \frac{\delta u_1}{\delta x_3}$;
6. rotation around $x_3$ axis, $\theta_3 = \frac{\delta u_1}{\delta x_2} - \frac{\delta u_2}{\delta x_1}$;

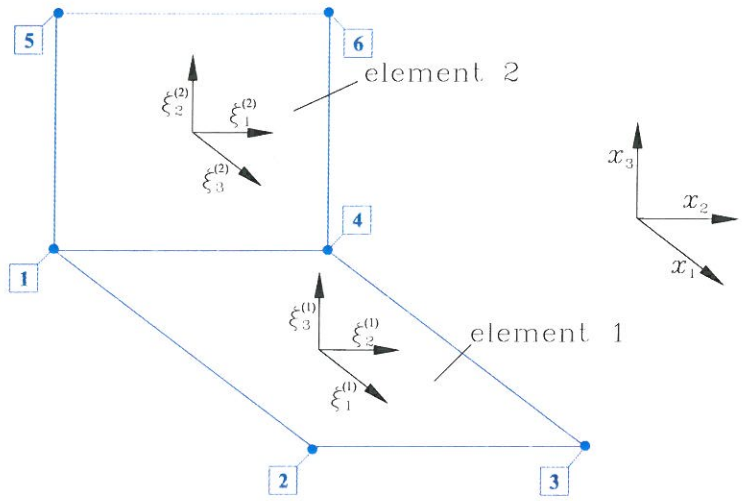


**Figure 4.1**: Example of hierarchical FEM model; elements, nodes, systems of co-ordinates (global and element's natural).

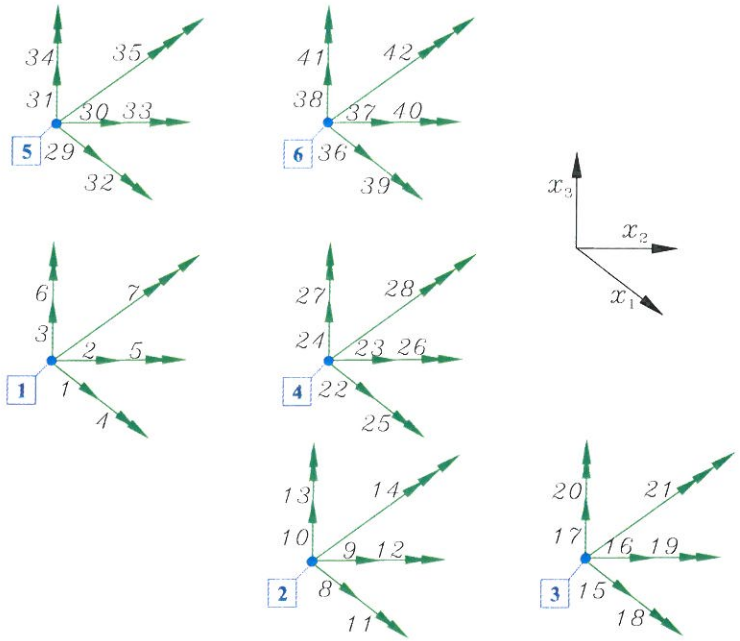


**Figure 4.2**: Position of nodal co-ordinates for the two element model in the system of co-ordinates. Single arrowheads symbolize displacement co-ordinates, double arrowheads symbolize rotational co-ordinates and triple arrowheads symbolize the second derivative of displacement.

**Table 4.1**: Position of co-ordinates of the elements in the co-ordinate set of the system for the two element model.

| Element | Co-ordinates in plane of the element | | | | | | | | | | | |
|---|---|---|---|---|---|---|---|---|---|---|---|---|
| No. (e) | $q_1^{(e)}$ | $q_2^{(e)}$ | $q_3^{(e)}$ | $q_4^{(e)}$ | $q_5^{(e)}$ | $q_6^{(e)}$ | $q_7^{(e)}$ | $q_8^{(e)}$ | $q_9^{(e)}$ | $q_{10}^{(e)}$ | $q_{11}^{(e)}$ | $q_{12}^{(e)}$ |
| 1 | *1* | *2* | *6* | *8* | *9* | *13* | *15* | *16* | *20* | *22* | *23* | *27* |
| 2 | *2* | *3* | *4* | *23* | *24* | *25* | *37* | *38* | *39* | *30* | *31* | *32* |

| Element | Co-ordinates out of plane of the element | | | | | | | | | | | | | | | |
|---|---|---|---|---|---|---|---|---|---|---|---|---|---|---|---|---|
| No. (e) | $q_{13}^{(e)}$ | $q_{14}^{(e)}$ | $q_{15}^{(e)}$ | $q_{16}^{(e)}$ | $q_{17}^{(e)}$ | $q_{18}^{(e)}$ | $q_{19}^{(e)}$ | $q_{20}^{(e)}$ | $q_{21}^{(e)}$ | $q_{22}^{(e)}$ | $q_{23}^{(e)}$ | $q_{24}^{(e)}$ | $q_{25}^{(e)}$ | $q_{26}^{(e)}$ | $q_{27}^{(e)}$ | $q_{28}^{(e)}$ |
| 1 | *3* | *5* | *4* | *7* | *10* | *12* | *11* | *14* | *17* | *19* | *18* | *21* | *24* | *26* | *25* | *28* |
| 2 | *1* | *6* | *5* | *7* | *22* | *27* | *26* | *28* | *36* | *41* | *40* | *42* | *29* | *34* | *33* | *35* |

7. second derivative of displacement, $\Theta = \frac{\partial^2 u_1}{\partial x_2 \partial x_3} + \frac{\partial^2 u_2}{\partial x_3 \partial x_1} + \frac{\partial^2 u_3}{\partial x_1 \partial x_2}$.

The co-ordinates are numbered consequently from node 1, so that the co-ordinates for node $n$ would have indices from $7(n-1)+1$ up to $7(n-1)+7$.

Figure 4.2 presents the co-ordinate numbers for the case of the two elements. These nodal co-ordinates can now be used to extract the co-ordinates of each of elements. This is done by comparison of the node and co-ordinate numbering scheme presented in Sections 3.1.1 and 3.1.2 (see figures 3.2 and 3.5) with the set of co-ordinates of the system (see Figure 4.2). The co-ordinates for the two element model are presented in Table 4.1. It can be seen from Table 4.1 that some of the nodal co-ordinates are present in sets of co-ordinates corresponding to both elements so that the continuity conditions for nodal co-ordinates are fulfilled.

The procedure of extracting co-ordinates of the elements from the system set of co-ordinates is performed in the algorithm automatically. Also, in the case of multiple elements shearing one node, the co-ordinate corresponding to $\Theta$ in this node is automatically removed, as explained in Section 3.2.1.

### 4.1.2 Internal co-ordinates

The internal co-ordinates are grouped in sets corresponding to each of elements and added after all nodal co-ordinates are included in the co-ordinate set.

In the example of two elements the order of interpolation in elements 1 and 2 can be set to 6 and 5, respectively, and equal for each of the directions. The number of internal co-ordinates in elements can be calculated as $N_{int}^{(1)} = 20(6^2 - 16)$ for element 1 and $N_{int}^{(2)} = 9(5^2 - 16)$ for element 2. Consequently, the internal co-ordinates of

element 1 are given by system co-ordinates *43* to *62* and internal co-ordinates of element 2 are given by system co-ordinates *63* to *71*.

To simplify the inverse transformation of indices of internal co-ordinates and shape functions (from single index to double index, as defined in (3.11) the 3-D topology array $\mathbf{T}_{int}$ is used. First two dimensions are used to indicate each of the double indices (corresponding to the order of 1-D shape functions used for definition of the 2-D shape function). The third dimension is used for each of the elements. The entrance $(k, l, n)$ of $\mathbf{T}_{int}$ gives the index of system co-ordinate. The topology matrix for element 1, $\mathbf{T}_{int}(k, l, 1)$ and 2, $\mathbf{T}_{int}(k, l, 2)$ have the form:

$$\mathbf{T}_{int}(k,l,1) = \begin{bmatrix} | & | & | & | & 48 & 58 \\ | & | & | & | & 49 & 59 \\ | & | & | & | & 50 & 60 \\ | & | & | & | & 51 & 61 \\ 43 & 44 & 45 & 46 & 47 & 62 \\ 52 & 53 & 54 & 55 & 56 & 57 \end{bmatrix};$$

$$\mathbf{T}_{int}(k,l,2) = \begin{bmatrix} | & | & | & | & 68 \\ | & | & | & | & 69 \\ | & | & | & | & 70 \\ | & | & | & | & 71 \\ 63 & 64 & 65 & 66 & 67 \end{bmatrix}$$

The empty four by four corner of $\mathbf{T}_{int}$, corresponds to the nodal co-ordinates.

The proper definition of elements co-ordinates in terms of the system co-ordinates allows for simple assembly of system matrices from the element matrices. This is a standard FEM procedure and does not require explanation here.

### 4.1.3 Imposing boundary and continuity conditions

Continuity conditions, see equations (3.19) to (3.26) are defined in terms of elements co-ordinates. These can be easily transformed to the set of co-ordinates of the system by the use of array $\mathbf{T}_{\mathbf{int}}$.

The boundary conditions are defined in terms of nodal co-ordinates, so that the transformation to the system co-ordinates is much simpler. If there are continuity conditions defined along edges then the topology matrix should be used in a similar way as for th continuity conditions.

All the system co-ordinates that are included in continuity conditions can be listed in two variables. The co-ordinates that should be removed from the active

co-ordinates (including the clamped co-ordinates and dependent co-ordinates) are collected in a vector $\boldsymbol{q}_{red}$. The second group of boundary conditions that relates two co-ordinates by the constant is listed in a matrix $\boldsymbol{\chi}_{cont}$. The $\boldsymbol{\chi}_{cont}$ stores the independent co-ordinate in the first row, the dependent co-ordinate in the second row and the constant that relates the two in the third row. The number of columns of the $\boldsymbol{\chi}_{cont}$ corresponds to the number of relations of type (3.19).

The condensation of the system matrices can be performed as described in Section 3.2.4. For the structure considered the continuity conditions between internal co-ordinates will have the form (see (3.24) to (3.26))

$$q^{(2)}_{r,1} \equiv 0; \qquad \text{for } r = 5 \ldots K^{(2)}_1; \tag{4.2}$$

$$q^{(1)}_{1,s} \equiv 0; \qquad \text{for } s = 5 \ldots K^{(1)}_2; \tag{4.3}$$

$$q^{(2)}_{r,2} = q^{(1)}_{2,s}; \quad \text{for } r = s = 5 \ldots min(K^{(2)}_1, K^{(1)}_2). \tag{4.4}$$

The numerical values are $K^{(1)}_1 = K^{(1)}_2 = 6$, $K^{(2}_1 = K^{(2)}_2 = 5$ and the continuity conditions between elements 1 and 2 in terms of co-ordinates of the system will read

$$q_{68} \equiv 0; \; q_{48} \equiv 0; \; q_{64} = q_{49}. \tag{4.5}$$

From the definition of co-ordinates of the system it follows that the original size of the matrices will have the size $71 \times 71$. By removing three co-ordinates, namely *48, 49* (dependent co-ordinates) and *68* the size of condensed matrices is $68 \times 68$.

## 4.2 Validation of the Hierarchical FEM

The performance of the hierarchical formulation developed in the proceeding section can be tested by comparison with analytical results, references and the standard FEM code. First the convergence of mode shapes and natural frequencies is checked based on two examples: the rectangular plate and two plates corner. In the latter part of this section the hierarchical energy flow model is compared with the standard FEM results.

### 4.2.1 Convergence of natural frequencies

#### Rectangular plate

The free vibration analysis of a rectangular plate has been presented in [2] where the comparison of different results from [64,67] and authors own calculations is presented and forms a benchmark for current analysis. The nondimensional frequency

parameter $\Omega_i$ used in [2] is defined as:

$$\Omega_i^2 = \frac{\rho h a^4 \omega_i^2}{B} \tag{4.6}$$

with the symbols defined in section 3.1.2. The cases considered here are:

- plate with free boundary conditions along all edges (F-F-F-F), according to Bardell's terminology [2]), FFFFPLA$i$ where $i$ signifies the number of elements along the edge;
- plate clamped along one edge and free along other edges, (C-F-F-F), denoted by CFFFPLA$i$;
- plate clamped along two opposite edges, free at one edge and simply-supported at one edge, (C-S-C-F), denoted by CSCFPLA$i$.

The case of simply supported plate will be considered in the next section where the two coupled plates are analysed.

Two cases of length-to-width aspect ratio are considered, namely a/b=1 and a/b=2/5, as in [2]. The mode sequence in the two cases might differ, but the frequencies of the four lowest natural modes are included in Tables 4.2–4.4. Only the mode shapes for the square plate are plotted in Tables 4.2–4.4. The hierarchical model used in [2] consists of single element. The convergence of natural frequencies for plate simply supported along all edges (S-S-S-S) is presented as achieved by increasing the order of interpolation functions ($p$-convergence). No remark is given for the $h$-convergence achieved by decreasing the size of elements.

In other work on hierarchical FEM for plates in [3] both $p$-convergence and $h$-convergence have been validated. The results are presented in terms of natural frequency estimates of simply supported plate. The number of natural frequencies that converge to the exact solution within 1% and 2% error are compared. Both the element mesh and the order of interpolation are varied and the results are compared for systems with equal total number of DOF. The conclusion has been reached that [3]:

> (...) for a given total number of DOF the number of eigenfrequencies calculated with given accuracy in most cases larger when large elements and many hierarchical functions are considered, instead of small elements and few hierarchical functions.

In order to study both $p$-convergence and $h$-convergence models with two element meshes, namely model with single element and model with $4 \times 4$ elements are studied, and the order of interpolation is varied in each of the models. It should be noted that because of the in-plane DOF-s the use of more elements introduces additional

DOF-s whose presence will not be visible at present. That is because the in-plane modes are not presented here.

The plate with free boundary conditions is analysed first. Six rigid-body modes exist in this case as opposite to three rigid-body modes listed in [2] because in present case the in-plane motions are included. Therefore, the modes from mode 7 are taken into consideration. The results for F-F-F-F plate are summarized in Table 4.2.

**Table 4.2**: Convergence study for the F-F-F-F plate

| Mode Shape (a/b=1) | Natural Frequencies | | | |
|---|---|---|---|---|
| | MODEL | $N_{int}$ | Non-dim. Freq. | |
| | | | $a/b = 1$ | $a/b = 2/5$ |
| Mode 7 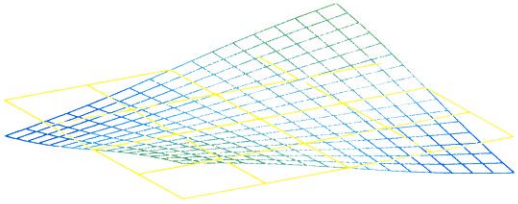 | LEISSA | — | 13.489 | 3.463 |
| | BARDELL | $10^2$ | 13.468 | 3.433 |
| | FFFFPLA1 | 0 | 13.656 | 4.091 |
| | FFFFPLA1 | 20 | 13.505 | 3.434 |
| | FFFFPLA1 | 33 | 13.505 | 3.433 |
| | FFFFPLA1 | 84 | 13.474 | 3.433 |
| | FFFFPLA4 | 0 | 14.250 | 3.439 |
| | FFFFPLA4 | 20 | 13.713 | 3.434 |
| | FFFFPLA4 | 33 | 13.697 | 3.433 |
| | FFFFPLA4 | 84 | 13.530 | 3.433 |
| | MODEL | $N_{int}$ | Non-dim. Freq. | |
| | | | $a/b = 1$ | $a/b = 2/5$ |
| Mode 8 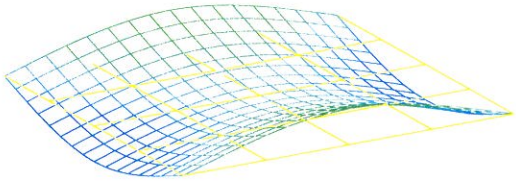 | LEISSA | — | 19.789 | 5.288 |
| | BARDELL | $10^2$ | 19.596 | 5.278 |
| | FFFFPLA1 | 0 | 22.451 | 5.329 |
| | FFFFPLA1 | 20 | 19.606 | 5.290 |
| | FFFFPLA1 | 33 | 19.598 | 5.290 |
| | FFFFPLA1 | 84 | 19.597 | 5.280 |
| | FFFFPLA4 | 0 | 19.623 | 5.937 |
| | FFFFPLA4 | 20 | 19.599 | 5.449 |
| | FFFFPLA4 | 33 | 19.597 | 5.434 |
| | FFFFPLA4 | 84 | 19.597 | 5.322 |

*continued on next page*

Mode Shape (a/b=1)

Mode 9

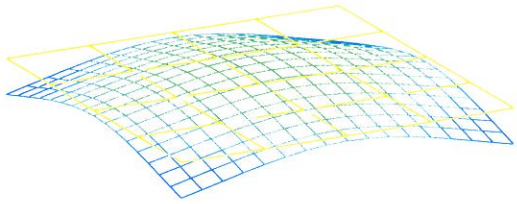

Natural Frequencies

| MODEL | $N_{int}$ | Non-dim. Freq. $a/b = 1$ | Non-dim. Freq. $a/b = 2/5$ |
|---|---|---|---|
| LEISSA | — | 24.432 | 9.622 |
| BARDELL | $10^2$ | 24.270 | 9.541 |
| FFFFPLA1 | 0 | 30.592 | 13.124 |
| FFFFPLA1 | 20 | 24.290 | 9.573 |
| FFFFPLA1 | 33 | 24.274 | 9.571 |
| FFFFPLA1 | 84 | 24.272 | 9.542 |
| FFFFPLA4 | 0 | 24.32 | 9.626 |
| FFFFPLA4 | 20 | 24.277 | 9.551 |
| FFFFPLA4 | 33 | 24.274 | 9.546 |
| FFFFPLA4 | 84 | 24.271 | 9.542 |

Mode 10

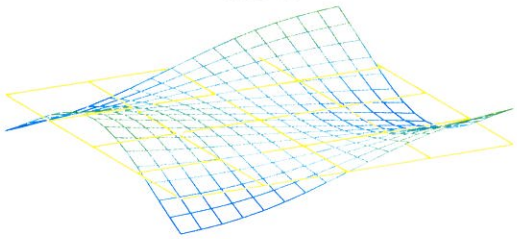

| MODEL | $N_{int}$ | Non-dim. Freq. $a/b = 1$ | Non-dim. Freq. $a/b = 2/5$ |
|---|---|---|---|
| LEISSA | — | 35.024 | 11.437 |
| BARDELL | $10^2$ | 34.801 | 11.329 |
| FFFFPLA1 | 0 | 39.232 | 13.934 |
| FFFFPLA1 | 20 | 34.919 | 11.407 |
| FFFFPLA1 | 33 | 34.893 | 11.367 |
| FFFFPLA1 | 84 | 34.822 | 11.343 |
| FFFFPLA4 | 0 | 36.301 | 13.022 |
| FFFFPLA4 | 20 | 35.183 | 11.685 |
| FFFFPLA4 | 33 | 35.121 | 11.581 |
| FFFFPLA4 | 84 | 34.897 | 11.410 |

Results for the C-F-F-F plate are summarized in Table 4.3. The results of present hierarchical formulation converge well to the values indicated in references.

**Table 4.3**: Convergence study for the C-F-F-F plate

| Mode Shape (a/b=1) | Model | $N_{int}$ | Natural Frequencies Non-dim. Freq. $a/b=1$ | $a/b=2/5$ |
|---|---|---|---|---|
| Mode 1 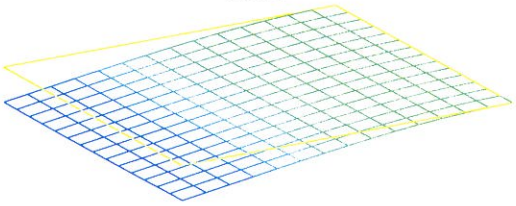 | Leissa | — | 3.49 | 3.51 |
| | Liew | — | 3.47 | 3.51 |
| | Bardell | $10^2$ | 3.47 | 3.50 |
| | CFFFpla1 | 0 | 3.52 | 3.53 |
| | CFFFpla1 | 33 | 3.48 | 3.50 |
| | CFFFpla1 | 84 | 3.47 | 3.50 |
| | CFFFpla4 | 0 | 3.48 | 3.50 |
| | CFFFpla4 | 33 | 3.47 | 3.49 |
| | CFFFpla4 | 84 | 3.47 | 3.49 |
| | Model | $N_{int}$ | Non-dim. Freq. $a/b=1$ | $a/b=2/5$ |
| Mode 2 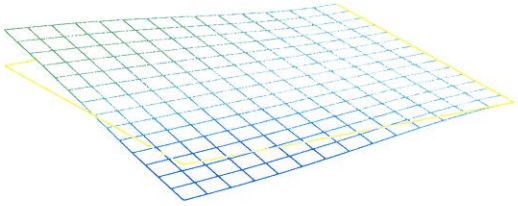 | Leissa | — | 8.52 | 4.49 |
| | Liew | — | 8.54 | 4.80 |
| | Bardell | $10^2$ | 8.51 | 4.77 |
| | CFFFpla1 | 0 | 8.95 | 4.88 |
| | CFFFpla1 | 33 | 8.53 | 4.78 |
| | CFFFpla1 | 84 | 8.52 | 4.77 |
| | CFFFpla4 | 0 | 8.95 | 5.05 |
| | CFFFpla4 | 33 | 8.62 | 4.83 |
| | CFFFpla4 | 84 | 8.53 | 4.78 |
| | Model | $N_{int}$ | Non-dim. Freq. $a/b=1$ | $a/b=2/5$ |
| Mode 3 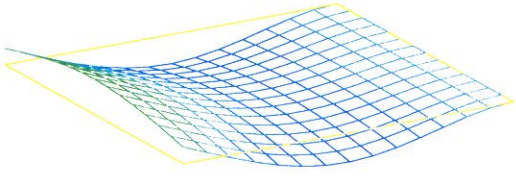 | Leissa | — | 21.43 | 8.11 |
| | Liew | — | 21.33 | 8.19 |
| | Bardell | $10^2$ | 21.29 | 8.07 |
| | CFFFpla1 | 0 | 28.88 | 9.23 |
| | CFFFpla1 | 33 | 21.35 | 8.09 |
| | CFFFpla1 | 84 | 21.31 | 8.08 |
| | CFFFpla4 | 0 | 21.41 | 8.85 |
| | CFFFpla4 | 33 | 21.30 | 8.18 |
| | CFFFpla4 | 84 | 21.29 | 8.10 |

*continued on next page*

| Mode Shape (a/b=1) | Natural Frequencies | | | |
|---|---|---|---|---|
| | MODEL | $N_{int}$ | Non-dim. Freq. | |
| | | | $a/b = 1$ | $a/b = 2/5$ |
| Mode 4 | LEISSA | — | 27.33 | 13.88 |
| | LIEW | — | 27.81 | 13.91 |
| | BARDELL | $10^2$ | 27.20 | 13.81 |
| | CFFFPLA1 | 0 | 37.41 | 18.53 |
| | CFFFPLA1 | 33 | 27.25 | 13.82 |
| | CFFFPLA1 | 84 | 27.22 | 13.82 |
| | CFFFPLA4 | 0 | 27.76 | 15.09 |
| | CFFFPLA4 | 33 | 27.30 | 13.91 |
| | CFFFPLA4 | 84 | 27.23 | 13.84 |

**Table 4.4**: Convergence study for C-S-C-F plate

| Mode Shape (a/b=1) | Natural Frequencies | | | |
|---|---|---|---|---|
| | MODEL | $N_{int}$ | Non-dim. Freq. | |
| | | | $a/b = 1$ | $a/b = 2/5$ |
| Mode 1 | LEISSA | — | 23.46 | 22.54 |
| | LIEW | — | 23.41 | 22.51 |
| | BARDELL | $10^2$ | 23.38 | 22.49 |
| | CSCFPLA1 | 9 | 23.90 | 22.95 |
| | CSCFPLA1 | 33 | 23.52 | 22.61 |
| | CSCFPLA1 | 84 | 23.44 | 22.54 |
| | CSCFPLA4 | 0 | 23.66 | 22.59 |
| | CSCFPLA4 | 33 | 23.40 | 22.50 |
| | CSCFPLA4 | 84 | 23.37 | 22.49 |
| | MODEL | $N_{int}$ | Non-dim. Freq. | |
| | | | $a/b = 1$ | $a/b = 2/5$ |
| Mode 2 | LEISSA | — | 35.61 | 24.30 |
| | LIEW | — | 35.64 | 24.30 |
| | BARDELL | $10^2$ | 35.56 | 24.27 |
| | CSCFPLA1 | 9 | 36.84 | 24.87 |
| | CSCFPLA1 | 33 | 35.88 | 24.42 |
| | CSCFPLA1 | 84 | 35.69 | 24.32 |
| | CSCFPLA4 | 0 | 36.73 | 24.66 |
| | CSCFPLA4 | 33 | 35.66 | 24.32 |
| | CSCFPLA4 | 84 | 35.56 | 24.27 |

*continued on next page*

| Mode Shape (a/b=1) | Natural Frequencies | | | |
|---|---|---|---|---|
| | MODEL | $N_{int}$ | Non-dim. Freq. | |
| | | | $a/b = 1$ | $a/b = 2/5$ |
| Mode 3 | LEISSA | — | 63.13 | 28.34 |
| | LIEW | — | 63.02 | 28.63 |
| | BARDELL | $10^2$ | 62.89 | 28.32 |
| | CSCFPLA1 | 9 | 80.70 | 30.09 |
| | CSCFPLA1 | 33 | 64.53 | 28.53 |
| | CSCFPLA1 | 84 | 63.13 | 28.40 |
| | CSCFPLA4 | 0 | 63.83 | 29.53 |
| | CSCFPLA4 | 33 | 62.90 | 28.43 |
| | CSCFPLA4 | 84 | 62.86 | 28.34 |
| | MODEL | $N_{int}$ | Non-dim. Freq. | |
| | | | $a/b = 1$ | $a/b = 2/5$ |
| Mode 4 | LEISSA | — | 66.81 | 35.35 |
| | LIEW | — | 66.74 | 35.42 |
| | BARDELL | $10^2$ | 66.77 | 35.31 |
| | CSCFPLA1 | 9 | — | 42.07 |
| | CSCFPLA1 | 33 | 67.54 | 35.74 |
| | CSCFPLA1 | 84 | 67.01 | 35.42 |
| | CSCFPLA4 | 0 | 68.43 | 37.19 |
| | CSCFPLA4 | 33 | 66.75 | 35.42 |
| | CSCFPLA4 | 84 | 66.63 | 35.33 |

The convergence studies of natural frequency estimates for the rectangular plates show that the $p$-convergence is monotonic for each of the considered case of the boundary conditions. This does not hold for the $h$-convergence. For the case of $N_{int} = 0$ (only nodal co-ordinates considered) all the estimated natural frequencies for $4 \times 4$ mesh are lower than these for single element (except for seventh mode of free plate, see Table 4.2. However, if higher order interpolation is considered and natural frequency estimates are compared for different meshes then there is no clear tendency for the convergence.

The lack of monotonic $h$-convergence can be a result of several factors:

- the 2-D internal shape functions are formed from mode shapes of clamped beam and in result in some cases correspond well with the mode shapes in the particular case of boundary conditions. The 2-D nodal shape functions do not behave in a similar way and therefore better convergence might be achieved with one 2-D internal shape function than if six 2-D nodal shape functions are used. This should not be a problem for the high order modes because in that case the internal co-ordinates dominate the response;

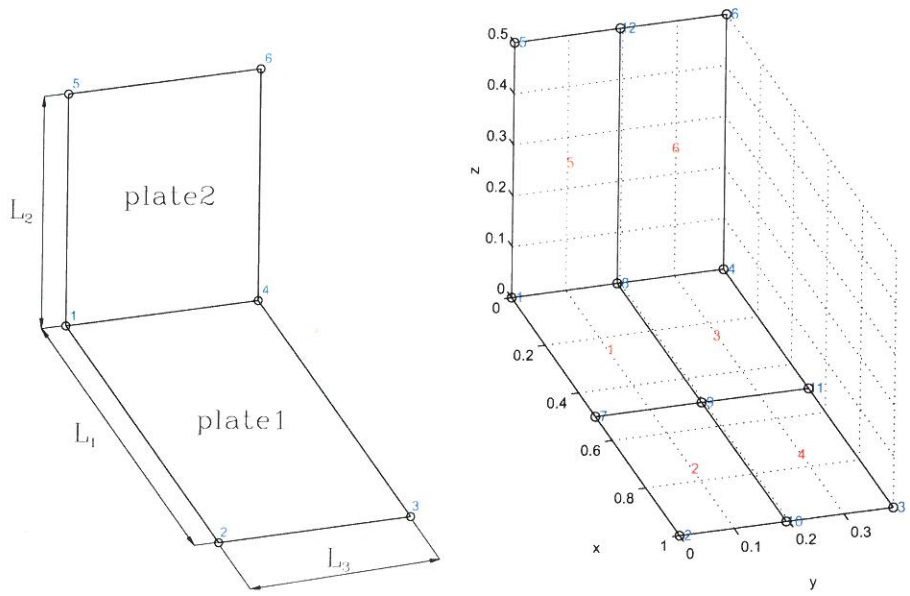


**Figure 4.3**: a) Geometry of two plate corner; b) Mesh of model FCORNER1.

- the definition of boundary conditions can cause additional perturbations in the convergence. That is because introduction of additional nodes requires additional co-ordinates to be included in the definition of boundary conditions;
- the continuity conditions for the displacement field require that some nodal co-ordinates must be excluded from calculations if more than one element is present at the node. These co-ordinates correspond to 2-D shape functions defined as the second derivative of displacement with respect to both directions in plane of element (see Section 3.1.2 for more explanation).

### Two plate corner

Two plate corner is the second example where the convergence of natural frequency estimations is presented. The problem of two plates joined at right angle has been studied previously in several studies [29, 93, 95, 102]. The scheme of the two plate corner is presented in Figure 4.3a).

The material properties and geometry defined in [29] have been used in the present analysis. The numerical values used in analysis for the two plate corner are: $L_1$=1$m$, $L_2$=0.5 $m$, $L_3$=0.39 $m$, thickness 0.01 m. Material data: Young's modulus 4.9 $\times 10^9$ $N/m^2$, Poisson ratio 0.25, density 1180 $kg/m^3$. The plates are simply supported along all edges, including the common edge, so that the transmission from plate 1 to plate 2 is possible through rotational motions.

The comparison of natural frequency estimates between standard FEM and hierarchical FEM is presented in Table 4.5. Three element meshes for standard FEM models are used as well as three element meshes for hierarchical FEM. In addition the order of interpolation is varied in hierarchical FEM. The details of models used in the analysis are summarized in Table 4.6.

**Table 4.5**: Convergence study for the two plate corner

| Mode Shape | Model | $N_{int}$ | Frequency [Hz] |
|---|---|---|---|
| 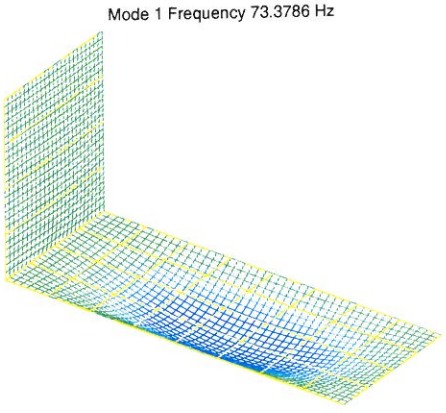 | FEM1 | — | 74.41 |
| | FEM2 | — | 73.62 |
| | FEM3 | — | 73.02 |
| | FCORNER1 | 0 | 74.08 |
| | FCORNER1 | 33 | 73.24 |
| | FCORNER1 | 84 | 73.17 |
| | FCORNER2 | 0 | 74.53 |
| | FCORNER2 | 9 | 73.64 |
| | FCORNER2 | 65 | 73.21 |
| | FCORNER3 | 0 | 74.18 |
| | FCORNER3 | 33 | 73.37 |
| | FCORNER3 | 65 | 73.25 |
| 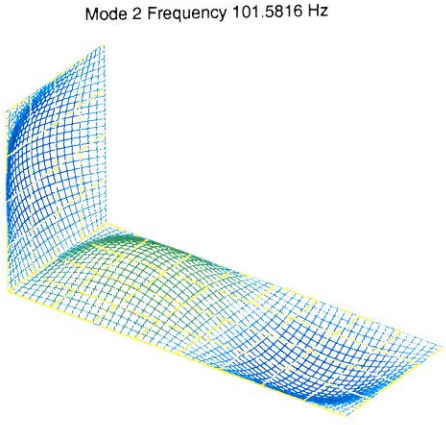 | Model | $N_{int}$ | Frequency [Hz] |
| | FEM1 | — | 102.00 |
| | FEM2 | — | 101.17 |
| | FEM3 | — | 100.38 |
| | FCORNER1 | 0 | 129.12 |
| | FCORNER1 | 33 | 102.15 |
| | FCORNER1 | 84 | 101.45 |
| | FCORNER2 | 0 | 104.64 |
| | FCORNER2 | 9 | 102.18 |
| | FCORNER2 | 65 | 101.12 |
| | FCORNER3 | 0 | 104.08 |
| | FCORNER3 | 33 | 101.58 |
| | FCORNER3 | 65 | 101.23 |

*continued on next page*

| Mode Shape | Natural Frequencies | | |
|---|---|---|---|
| Mode 3 Frequency 110.7255 Hz 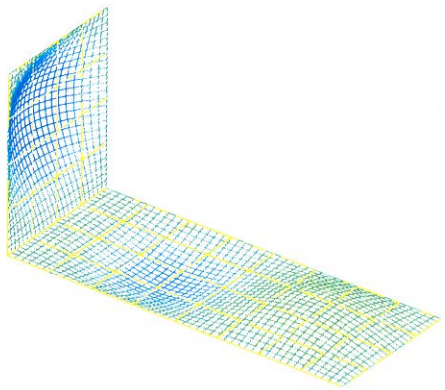 | Model | $N_{int}$ | Frequency [Hz] |
| | FEM1 | — | 111.35 |
| | FEM2 | — | 110.48 |
| | FEM3 | — | 109.61 |
| | FCORNER1 | 0 | 120.41 |
| | FCORNER1 | 33 | 110.82 |
| | FCORNER1 | 84 | 110.35 |
| | FCORNER2 | 0 | 112.67 |
| | FCORNER2 | 9 | 110.76 |
| | FCORNER2 | 65 | 110.22 |
| | FCORNER3 | 0 | 113.69 |
| | FCORNER3 | 33 | 110.72 |
| | FCORNER3 | 65 | 110.41 |
| Mode 4 Frequency 155.161 Hz 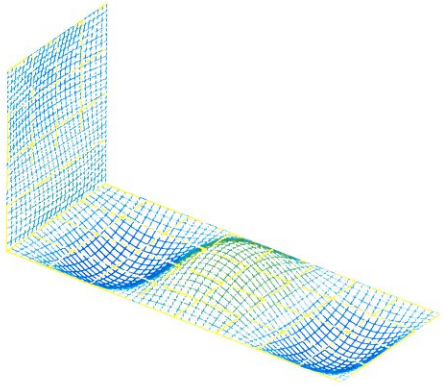 | Model | $N_{int}$ | Frequency [Hz] |
| | FEM1 | — | 156.91 |
| | FEM2 | — | 155.16 |
| | FEM3 | — | 153.41 |
| | FCORNER1 | 0 | 221.72 |
| | FCORNER1 | 33 | 155.01 |
| | FCORNER1 | 84 | 154.43 |
| | FCORNER2 | 0 | 161.58 |
| | FCORNER2 | 9 | 155.93 |
| | FCORNER2 | 65 | 154.47 |
| | FCORNER3 | 0 | 160.39 |
| | FCORNER3 | 33 | 155.16 |
| | FCORNER3 | 65 | 154.66 |
| Mode 5 Frequency 216.6028 Hz 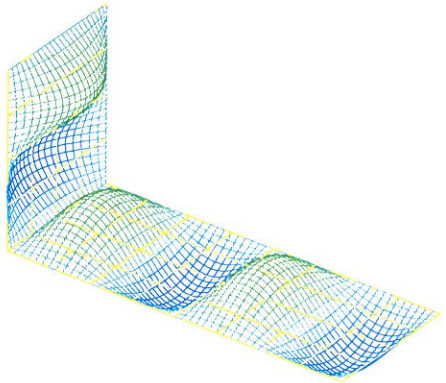 | Model | $N_{int}$ | Frequency [Hz] |
| | FEM1 | — | 222.71 |
| | FEM2 | — | 218.74 |
| | FEM3 | — | 214.76 |
| | FCORNER1 | 0 | 288.52 |
| | FCORNER1 | 33 | 220.26 |
| | FCORNER1 | 84 | 216.52 |
| | FCORNER2 | 0 | 261.61 |
| | FCORNER2 | 9 | 221.09 |
| | FCORNER2 | 65 | 216.39 |
| | FCORNER3 | 0 | 224.78 |
| | FCORNER3 | 33 | 216.60 |
| | FCORNER3 | 65 | 216.00 |

*continued on next page*

Mode Shape

Natural Frequencies

Mode 6 Frequency 240.7106 Hz

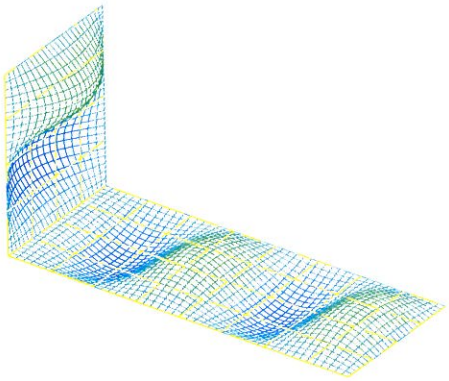

| Model | $N_{int}$ | Frequency [Hz] |
|---|---|---|
| FEM1 | — | 250.43 |
| FEM2 | — | 244.82 |
| FEM3 | — | 239.33 |
| FCORNER1 | 0 | — |
| FCORNER1 | 33 | 243.91 |
| FCORNER1 | 84 | 240.47 |
| FCORNER2 | 0 | 283.98 |
| FCORNER2 | 9 | 244.68 |
| FCORNER2 | 65 | 240.45 |
| FCORNER3 | 0 | 249.29 |
| FCORNER3 | 33 | 240.71 |
| FCORNER3 | 65 | 240.19 |

Mode 7 Frequency 261.2241 Hz

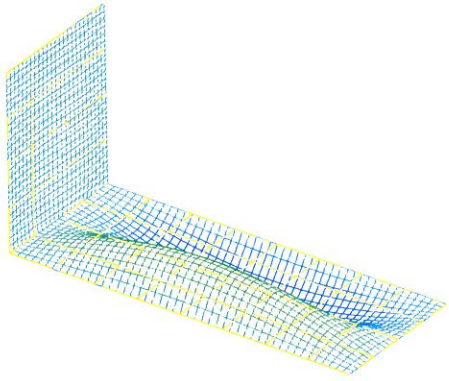

| Model | $N_{int}$ | Frequency [Hz] |
|---|---|---|
| FEM1 | — | 286.05 |
| FEM2 | — | 271.99 |
| FEM3 | — | 262.52 |
| FCORNER1 | 0 | 290.32 |
| FCORNER1 | 33 | 261.61 |
| FCORNER1 | 84 | 261.20 |
| FCORNER2 | 0 | 291.59 |
| FCORNER2 | 9 | 263.21 |
| FCORNER2 | 65 | 261.24 |
| FCORNER3 | 0 | 263.32 |
| FCORNER3 | 33 | 261.22 |
| FCORNER3 | 65 | 261.07 |

Mode 8 Frequency 290.0604 Hz

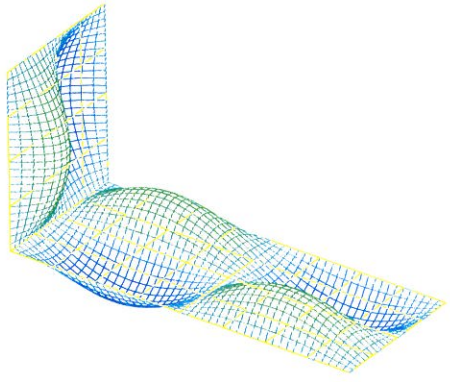

| Model | $N_{int}$ | Frequency [Hz] |
|---|---|---|
| FEM1 | — | 312.20 |
| FEM2 | — | 298.88 |
| FEM3 | — | 289.75 |
| FCORNER1 | 0 | — |
| FCORNER1 | 33 | 293.27 |
| FCORNER1 | 84 | 291.15 |
| FCORNER2 | 0 | 328.13 |
| FCORNER2 | 9 | 294.18 |
| FCORNER2 | 65 | 289.94 |
| FCORNER3 | 0 | 295.32 |
| FCORNER3 | 33 | 290.06 |
| FCORNER3 | 65 | 289.58 |

**Table 4.6**: Models of coupled plates used in convergence study.

| MODEL | $N_{int}$ | Elements along | | | Sum of | Total | Active |
|---|---|---|---|---|---|---|---|
| | | $L_1$ | $L_2$ | $L_3$ | Elements | DOF | DOF |
| FEM1 | — | 18 | 9 | 7 | 189 | 1344 | — |
| FEM2 | — | 24 | 12 | 10 | 360 | 2442 | — |
| FEM3 | — | 48 | 24 | 20 | 1440 | 9198 | — |
| FCORNER1 | 0 | 2 | 1 | 2 | 6 | 107 | 38 |
| FCORNER1 | 33 | 2 | 1 | 2 | 6 | 306 | 158 |
| FCORNER1 | 84 | 2 | 1 | 2 | 6 | 612 | 386 |
| FCORNER2 | 0 | 4 | 2 | 2 | 12 | 188 | 77 |
| FCORNER2 | 9 | 4 | 2 | 2 | 12 | 297 | 135 |
| FCORNER2 | 65 | 4 | 2 | 2 | 12 | 969 | 607 |
| FCORNER3 | 0 | 8 | 4 | 4 | 48 | 584 | 295 |
| FCORNER3 | 33 | 8 | 4 | 4 | 48 | 2169 | 1291 |
| FCORNER3 | 65 | 8 | 4 | 4 | 48 | 3705 | 2435 |

Table 4.5 clearly shows the advantages of the hierarchical FEM in comparison to the standard FEM in the case of the thin plates assemblies providing the high number of internal co-ordinates is used. For example the comparison of standard FEM estimations of natural frequencies in model FEM2 (with more than 2400 DOF) and hierarchical model FCORNER2-65 (with less than 1000 DOF) shows that the estimates given by the hierarchical FEM are lower than these of standard FEM at all considered frequencies.

### 4.2.2 Power flow calculation

The example of two plate corner described above will be used to compare the energy flow models from standard FEM and hierarchical FEM. The accuracy of the results requires that the displacement field of the structure is approximated accurately by the shape functions of the numerical model. In the $h$-version of FEM this is usually translated into the number of elements of certain order per wavelength ($\lambda$) of elastic deformation of the structure. For the first order interpolation functions (4-node plate element) the minimum number of elements is usually taken as 8. In the following it is required that the model has at least 8 first order elements per wavelength. Thin plate can support three types of elastic waves, namely quasi-

longitudinal waves (denoted by subscript $L$), shear waves (denoted by subscript $S$) and bending waves (denoted by subscript $S$). The wavelengths for the three types of waves in plate under harmonic motions of frequency $f$ are given by [21]:

$$\lambda_L = \frac{1}{f}\sqrt{\frac{E}{(1-\nu^2)\rho}}\ ;\ \lambda_S = \frac{1}{f}\sqrt{\frac{E}{2(1+\nu)\rho}}\ ;\ \lambda_B = \sqrt{\frac{2\pi}{f}}\sqrt[4]{\frac{Eh^2}{12(1-\nu^2)\rho}} \tag{4.7}$$

where $E$ is the modulus of elasticity, $\nu$ is the Poisson ratio, $\rho$ is the mass density and $h$ is the plate thickness. It can be seen from (4.7) that the shear waves have wavelengths shorter than the longitudinal waves, and therefore the wavelength of a shear wave should be used for the comparison with the finite element interpolation in plane of the plate.

The FEM models consist of rectangular four node thin plate elements (S4R5 in ABAQUS element library). Therefore, the criteria of 8 elements per wavelength will be used in comparison with the shortest of wavelengths. The hierarchical models consist of rectangular hierarchical elements with third order interpolation functions in nodal set and variable number of internal co-ordinates $N_{int}$ for modelling of out-of-plane (bending) displacement, and third order interpolation functions for in-plane (longitudinal and shear) displacement. Therefore, the global mesh of elements have to fulfil the 4 element/wavelength criteria for the shear waves $\lambda_S$ (equivalent to 8 elements of first order), and the order of interpolation function for out-of-plane component can be adjusted for the wavelength of bending waves $\lambda_B$.

Two frequency ranges, namely 10-600 Hz and 10-2200 Hz are considered. The wavelengths $\lambda_B$ and $\lambda_S$ at frequency 600 Hz can be calculated as $\lambda_B = 0.25$m; $\lambda_S = 2.15$m, and at frequency 2200 Hz as $\lambda_B = 0.12$m; $\lambda_S = 0.52$m. At these frequencies standard FEM models FEM2 and FEM3 as defined in Table 4.6 fulfil the convergence criteria. For the hierarchical models the FCORNER2 is used for the lower frequency range, FCORNER3 is used for the higher frequency range, see Table 4.6. Each of the hierarchical models is used with variable order of interpolation functions, and the number of interpolation functions is indicated by $N_{int}$ as FCORNER3-$N_{int}$.

The first comparison regards the space average energies of plates 1 and 2 forming the corner, see Figure 4.3 at frequencies below 600 Hz when excited by the unit harmonic point force acting at the centre of plate 1 normal to the surface. The results for the energy plate one ($E_1$), plate two ($E_2$) and energy ratio ($E_2/E_1$) are compared in Figure 4.4. There is generally a good agreement between standard FEM and hierarchical FEM results below 200 Hz. Above 200 Hz the hierarchical model with third order interpolation functions is not reliable. Increasing the order to fourth and fifth one improves the convergence of natural frequencies considerably, when comparing with the FEM model. Both hierarchical models have below ten times less DOF than FEM model and result in good energy estimations at frequency of interest (in fact better than FEM considering the convergence of natural frequencies).

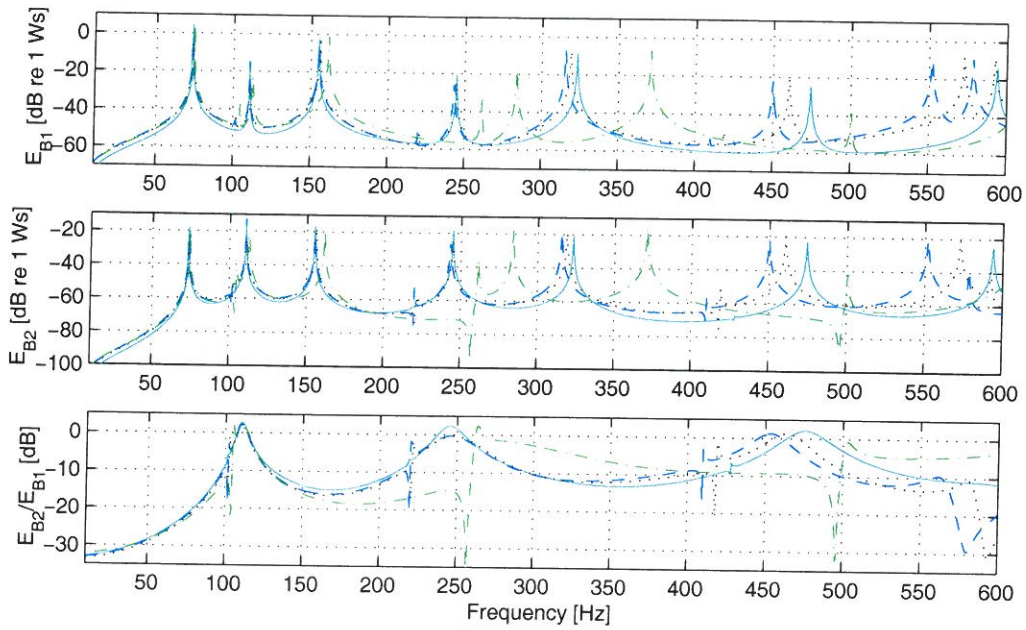


**Figure 4.4**: Kinetic energy of plates 1 and 2 (only out-of-plane motions) in two-plate-corner, comparison of different results for frequency range 10-600 Hz. — FEM2; — · — FCORNER2-0; · · · FCORNER2-9; - - - FCORNER2-20.

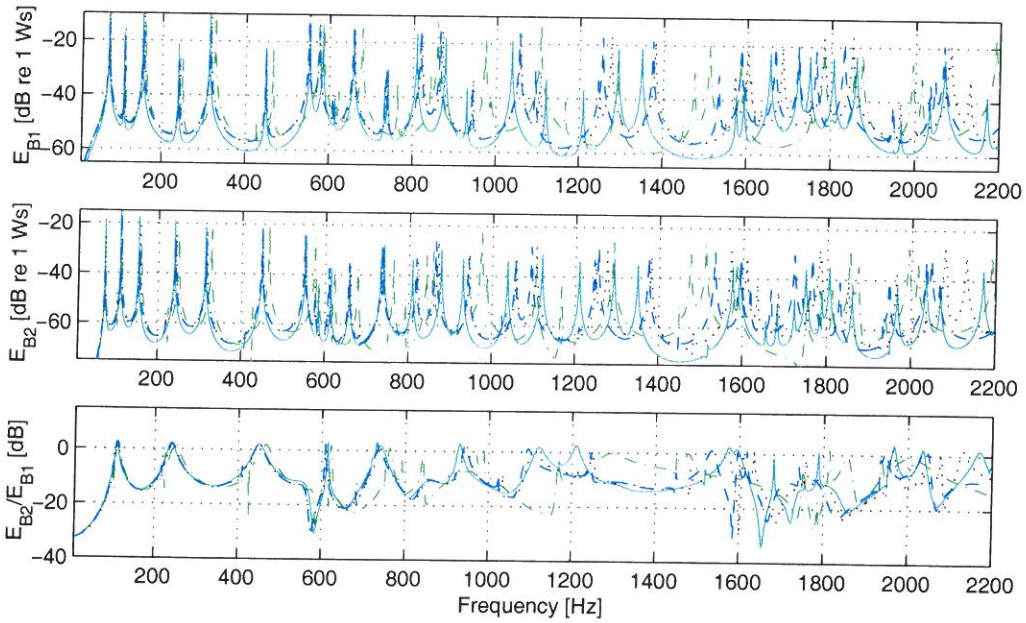


**Figure 4.5**: Kinetic energy of plates 1 and 2 (only out-of-plane motions) in two-plate-corner, comparison of different results for frequency range 10-2200 Hz. — FEM3; — · — FCORNER3-0; · · · FCORNER3-9; - - - FCORNER3-20.

In the second example the frequency range is increased to 2200 Hz.The comparison of energy ratios between energy in driven plate and energy in receiving plate is presented in Figure 4.5. The improvement in the predictions follows the increase of the order of interpolation functions (compare results for c-Hfem2-3, c-Hfem2-4 and c-Hfem2-5). Again the use of hierarchical FEM reduces the number of DOF by the factor of 10.

## 4.3 Summary of Chapter 4

In this chapter the implementation of the hierarchical FEM introduced in previous chapter has been presented. The assembly procedure involving implementation of continuity and boundary conditions was of main interest as it differs considerably from the standard FEM.

In the second part the method has been validated in the case of free and forced vibrations. Good agreement has been found between results from hierarchical FEM as compared with other results (mainly of standard FEM).

# Chapter 5

# Hybrid FEM-SEA for Plate Assemblies

The hierarchical formulation for the plates developed in the previous chapter can now be used to formulate the hybrid FEM-SEA approach. The basic assumptions of hybrid FEM-SEA have been described in Section 2.5. The example of application of the approach to the coupled rod problem has been presented in Section 2.6.4. The partition of co-ordinates that leads to the hybrid formulation can now be considered.

## 5.1 Partition of Co-ordinates

The partition of co-ordinates introduced in (2.52) is a crucial point in the hybrid formulation. It is performed to account for the different types of behaviour in different members of the built-up structure.

### 5.1.1 Modal overlap criteria

The 'smoothness' of the response function depends on the modal overlap factor $\mathcal{M}$ (see Section 2.3.2) that is defined in (2.51) as a product of modal density and half-power bandwidth. In the case of low modal overlap ($\mathcal{M} < 1$) the response of the structure depends on the relation between frequency of excitation and natural frequencies of the system. If the system is excited in the vicinity of resonance (within half-power bandwidth) the response will be much stronger than if it was excited between resonances. The resonant frequencies are distinct even if an ensemble averaged response function (or narrowband frequency averaged response function) is considered. At low frequencies the modal overlap is generally low, depending on the damping and modal density of the structure.

For the 1-D example considered in Section 2.6 the modal density (of the axially vibrating rod) was constant, so that the modal overlap increased proportionally to $\eta\omega$ and for small damping values modes had not overlapped, see for example Figure 2.12. The modal overlap could have been increased by increasing the damping loss factor, see for example Figure 2.14, where the response curve is much smoother than in Figure 2.12.

In built-up complex structures the modal density of different components can change in different way with frequency. This is an additional factor that causes the major differences in modal overlap among components.

The reason for considering modal overlap in details is that modal overlap is one of the basic assumptions of SEA, see Section 2.3.1. In the view of hybrid FEM-SEA assumptions, concerning partition of co-ordinates (modes), the local co-ordinates should only be used to describe the motions in high modal overlap conditions. Therefore, the modal overlap can be used as a criterion for the partition of co-ordinates in the system. The value of the modal overlap factor necessary to fulfil the SEA assumptions is usually taken as $\mathcal{M} > 1$ [19, 68]. If this condition is fulfilled the response should not diverge from the average value given by SEA calculations.

At the frequency where the modal overlap reaches the minimum value for application of SEA the transition from the deterministic description to the statistical description can be performed. This frequency will be called the 'transition frequency' of the subsystem, denoted by $\omega^{(s)}_{trans}$ where the superscript indicates the subsystem. The differences in the modal density and damping among subsystems cause differences in the value of 'transition frequencies' among subsystems. In other words, at certain frequency $\omega$ some subsystems will be described in a deterministic way (by FEM) and some in a statistical way (by SEA).

### 5.1.2 Global and local set of co-ordinates

The co-ordinates partition scheme requires that there is a correspondence between shape functions and wavelengths that leads to the correspondence between co-ordinates and frequency. In the hierarchical FEM there is such a correspondence. The nodal shape functions correspond to the longest wavelengths (the lowest frequency response), whereas the internal shape functions contribute to the response higher in frequency, depending on the order of interpolation. Therefore, it is necessary to include all nodal co-ordinates in the global set $\boldsymbol{q}_g$, see (2.52). The global co-ordinate set can be enriched, if necessary, by appropriate number of internal co-ordinates in each of the subsystems. The algorithm of the co-ordinate partition can be summarized as follows:

- include all nodal co-ordinates in the global set,

- perform division of the structure into SEA subsystems based on their gross parameters (according to SEA assumptions),
- calculate the 'transition frequency' for each of subsystems and corresponding wavelengths of displacement field $\lambda_{trans}^{(s)}$ and wave numbers $k_{trans}^{(s)}$,
- extract internal co-ordinates of elements in each subsystem with wavelength longer than the wavelength of deformation and include in the global set.

With the global co-ordinates defined the global mass and stiffness matrices can be defined either by assembly of the global matrices or by extraction of the elements corresponding to global matrices from the previously assembled matrices with all co-ordinates present. The first method is better from a calculation point of view. The second method can better serve for the purpose of presenting the partition scheme, and will be used in the following.

### 5.1.3 Partition of system matrices

To illustrate the procedures of the system partition an example will be given. A simple model with only two elements, each being a separate subsystem, is considered. The properties of the elements are not important at the moment, apart from the fact that in each element a high number of internal co-ordinates is used. This simple model is sufficient to clarify at least some of the issues in connection with the co-ordinate partition scheme. Only the stiffness matrix of the system will be taken into consideration. The mass matrix has similar properties.

The system of equations corresponding to full set of co-ordinates, i.e. before partition defined as $\mathbf{DQ} = \mathbf{F}$ is used for comparison. The nonzero entries of the stiffness matrix of this system are presented in Figure 5.1 a). On the diagonal of the matrix four square areas can be seen, two smaller ones in the upper left corner and to bigger ones in the middle and in the lower right corner. The first two (small) correspond to nodal variables and their sizes are fixed for an element. The remaining two correspond to the internal co-ordinates in each of the two elements. It can be seen that the internal co-ordinates of the two elements are nearly orthogonal despite of the few co-ordinates that are coupled (giving rise to the nonzero entries in the system matrices that correspond to internal co-ordinates from two different subsystems). These follow the definition of continuity conditions, see equations (3.19) to (3.26). It should be noted that the matrices considered are the condensed matrices, i.e. after imposing of the continuity conditions as described in Section 3.2.4.

First the case when no internal co-ordinates are included in the global set $\boldsymbol{q}_g$ (global set contains only nodal co-ordinates) will be considered. The local co-ordinate set $\boldsymbol{q}_l$ is built from the 'remaining' co-ordinates of the hierarchical model, and in this case all internal co-ordinates are taken to the local set. Each subsystem

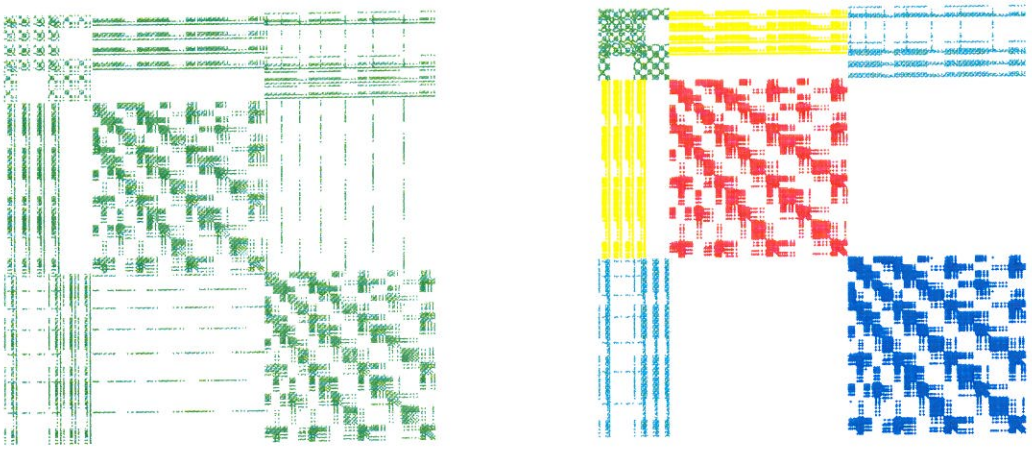

a) b)

**Figure 5.1**: Stiffness matrix of the examples system. Two elements, two subsystems; a) the condensed stiffness matrix of hierarchical FEM, + entries of $K_{gg}$ denotes nonzero entries in deterministic description; b) the stiffness matrix of hybrid formulation with only nodal co-ordinates in global set of co-ordinates. + nonzero entries of $K_{gg}$, + nonzero entries of $K_{gl^1}$ and $K_{l^1g}$, + nonzero entries of $K_{gl^2}$ and $K_{l^2g}$, + nonzero entries of $K_{l^1l^1}$, + nonzero entries of $K_{l^2l^2}$.

should be considered separately, so that there is a subset of local co-ordinates for each subsystem, $\boldsymbol{q}_{l^1}$ and $\boldsymbol{q}_{l^2}$.

In the example of coupled rods the coupling between global and local co-ordinates was only present within the subsystem, see Section 2.6.4. That was because the internal co-ordinates were defined as mode shapes of a clamped element. The use of clamped modes was permissible because of the point connection between rods. Only one variable was necessary (the co-ordinate in the node) to describe the coupling. In effect the local co-ordinates did not participate in energy transmission through the junction and there was a separate SEA model for each subsystem with no net flow but only injection and dissipation of power. In the 2-D problem the number of coupling points is infinite because the junctions are continuous. Therefore, the nodal co-ordinates are not sufficient to define the motions at the edges. The internal co-ordinates must also influence the edges of the elements. Because the continuity condition must be obeyed some of the internal co-ordinates have to be coupled through the junction of elements. This implies that also some of the internal co-ordinates are coupled through the junction between subsystems, and the energy can be transferred between subsystems. In the FEM the continuity conditions are defined by displacement field transformed into the co-ordinates of the FEM model,

see Section 3.2.

Since the local co-ordinates are considered in SEA calculations, the fact that there is energy flow among subsystems implies that there will be net power flow in the system. However, in the view of SEA the energy transfer should take place based on SEA assumption of power flow proportionality to the energy difference, see (2.46) and the CLF. In SEA the continuity conditions are defined by CLF and by the ratio of energy in subsystems across the junction. Consequently, the continuity conditions defined on local co-ordinates belonging to different subsystems should be disregarded in the hierarchical FEM. Otherwise, the continuity conditions would be imposed twice, once in the deterministic description and once in the statistical description. This can be seen as a sort of boundary conditions transformation.

The transformation of the continuity conditions among the local co-ordinates removes the phase information about the incident and transmitted waves taking the mean value of this quantity. This is a standard approach while calculating CLFs for the SEA. Since the uncertainties in the structure prohibit the accurate calculation of the phases this approach introduces averaging in the analysis and therefore takes into account the uncertainties in the local properties.

Figure 5.1 b) presents the partition of the stiffness matrix of the system in the case where the only contribution to the global stiffness matrix $K_{gg}$ is from the nodal co-ordinates. The part of the matrix corresponding to global co-ordinates is plotted in green to indicate that this part is solved in deterministic sense. The red and blue colours are used to plot the local matrices of subsystem 1 ($K_{l^1l^1}$) and subsystem 2 ($K_{l^2l^2}$). The yellow and cyan are used to indicate the matrices $K_{gl^1}$ and $K_{gl^2}$, respectively.

Comparison of figures 5.1 a) and b) gives more insight in the partitioning scheme. The first difference is the lack of the cross products between local co-ordinates from the two subsystems. This corresponds to the transformation of continuity conditions defined in terms of displacement variables to the conditions defined in terms of energy variables.

If the global set includes the internal co-ordinates then the continuity conditions as defined in Section 3.2 should be imposed, but only on co-ordinates included in the global set, i.e. the parameters $K_1^{(n)}$ and $K_2^{(n)}$ in equations (3.19) to (3.26) for each element should be reduced to account only for internal co-ordinates in the global set. The examples of extended stiffness matrices for two cases are presented in Figure 5.2. Part a) presents the system where only few internal co-ordinates are included in the global set. This corresponds to the case of for example higher damping. Part b) of Figure 5.2 corresponds to the case of lower damping in the structure. The decrease of the damping level decreases the modal overlap and therefore more co-ordinates is necessary in the global description, as comparing to the case a). It is also clear from figures 5.1 and 5.2 that the continuity conditions are imposed on

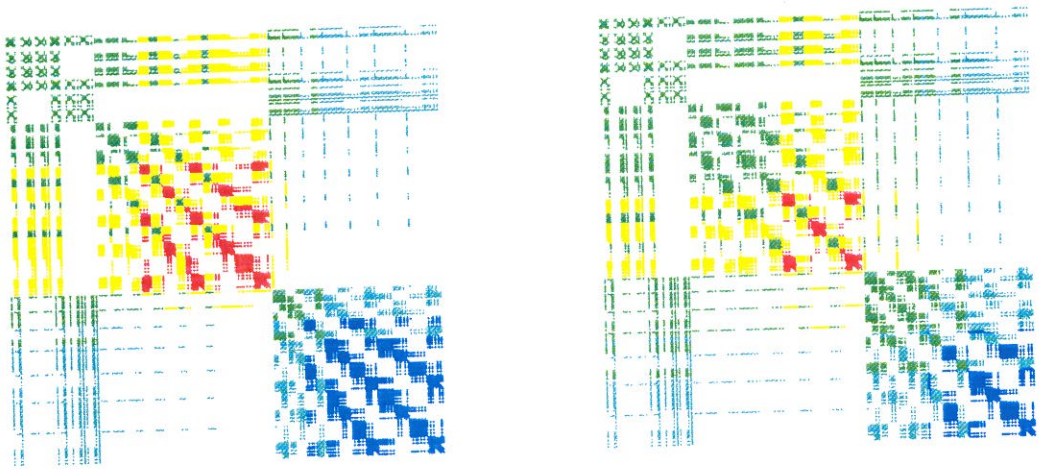

a) b)

**Figure 5.2**: Stiffness matrices of hybrid formulation for two cases where internal co-ordinates are included in global set of co-ordinates. Marks as in Figure 5.1.

the internal co-ordinate pairs from different subsystems, if these are included in the global set. Those are the nonzero entries of the matrices on the interface between internal co-ordinates of the two subsystems.

## 5.2 Global Equation of Motion

The global EOM is defined in equation 2.54 as:

$$[\mathbf{D}_{gg} - \mathbf{D}_{gl}\mathbf{D}_{ll}^{-1}\mathbf{D}_{gl}^{T}]\ \mathbf{Q}_g = \mathbf{F}_g - \mathbf{D}_{gl}\mathbf{D}_{ll}^{-1}\mathbf{F}_l \Rightarrow [\mathbf{D}_{gg} - \Delta\mathbf{D}]\ \mathbf{Q}_g = \mathbf{F}_g - \Delta\mathbf{F}.$$

The reduction of the size of the global equation in comparison with the original equation depends on the modal overlap conditions. This can be seen by comparing figures 5.2 a) and b). The reduction of problem size is only one of the advantages of the hybrid formulation. The other advantage is the use of statistical description of the response in the conditions of modal overlap, where the uncertainties of the structure prohibit the use of deterministic approach. This statistical information, in terms of mean value is included in the additional terms controlling the coupling between deterministic and statistical description. The evaluation of coupling terms i.e. $\Delta\mathbf{D}$ and $\Delta\mathbf{F}$ is the main task in the application of the hybrid method.

### 5.2.1 Additional dynamic stiffness matrix

The definition of additional stiffness matrix is given by $\Delta\mathbf{D} = \mathbf{D}_{gl}\mathbf{D}_{ll}\mathbf{D}_{gl}^T$. For the case of orthogonal local dynamic stiffness matrix of subsystem $s$, where it was possible to substitute the $j^{\text{th}}$ diagonal entry of $D_{l^s l^s}$ by the contribution from the $j^{\text{th}}$ 'local mode' of subsystem $s$, and the off-diagonal terms are all zero, see (2.55):

$$(D_{l^s l^s})_{jj} = \frac{1}{(\omega_j^s)^2(1+i\eta_s) - \omega^2}. \tag{5.1}$$

However, in the current case the local dynamic stiffness matrix of a subsystem is not orthogonal. The local matrices are orthogonal between subsystems, so that the partition of the local dynamic stiffness matrix is possible in the following form (see Figures 5.1 b) and 5.2):

$$\mathbf{D}_{ll} = \begin{bmatrix} \mathbf{D}_{l^1 l^1} & 0 & \cdots & 0 \\ 0 & \mathbf{D}_{l^2 l^2} & \cdots & 0 \\ \vdots & \vdots & \ddots & \vdots \\ 0 & 0 & \vdots & \mathbf{D}_{l^s l^s} \end{bmatrix} \tag{5.2}$$

and the inverse of the $\mathbf{D}_{ll}$ can therefore be calculated separately for each of sub-elements of the matrix, i.e.

$$\mathbf{D}_{ll}^{-1} = \begin{bmatrix} \mathbf{D}_{l^1 l^1}^{-1} & 0 & \cdots & 0 \\ 0 & \mathbf{D}_{l^2 l^2}^{-1} & \cdots & 0 \\ \vdots & \vdots & \ddots & \vdots \\ 0 & 0 & \vdots & \mathbf{D}_{l^s l^s}^{-1} \end{bmatrix} \tag{5.3}$$

This can be proved by taking the product $\mathbf{D}_{ll}\mathbf{D}_{ll}^{-1}$ that should give a unity matrix. The contribution from each of the subsystems can therefore be considered separately. The additional dynamic stiffness term defining contribution from subsystem $s$, $\Delta\mathbf{D}^{(s)}$, is given by:

$$\Delta\mathbf{D}^{(s)} = \mathbf{D}_{gl^s}\mathbf{D}_{l^s l^s}^{-1}\mathbf{D}_{gl^s}^T \tag{5.4}$$

Equation (5.4) describes the coupling that the local co-ordinates exhibit on the global co-ordinates. It will not be further considered at present, so that the solution is strictly deterministic, providing there is a sufficient amount of co-ordinates to describe the local motions of the subsystem. The uncertainties of the structure have main influence on the high-frequency behaviour of the structure. This could be taken into account by introducing certain distribution of parameters and averaging of the local dynamic stiffness over $i$ members taken from the ensemble of nominally identical structures. This would give an ensemble average local dynamic stiffness matrix for the subsystem $s$ denoted by $\langle \mathbf{D}_{l^s l^s} \rangle_i$ and the average could be used in the calculations. In this procedure level of uncertainty could be varied among subsystem.

### 5.2.2 Additional loading vector

The additional loading vector corresponds to the direct loading of the local co-ordinates that is transmitted to the global co-ordinates through the coupling. It is defined in (2.54) as

$$\Delta \mathbf{F} = \mathbf{D}_{gl}\mathbf{D}_{ll}^{-1}\mathbf{F}_l = \sum_{s=1}^{N_{sub}} \mathbf{D}_{gl^s}\mathbf{D}_{l^s l^s}^{-1}\mathbf{F}_{l^s} \tag{5.5}$$

where the orthogonality of local dynamic stiffness matrices has been used.

In the example of coupled rods in Section 2.6.4 the additional loading vector has been calculated using the 'blocked' response of the subsystem to the applied load, $\mathbf{U}_s^B = \mathbf{D}_{l^s l^s}^{-1}\mathbf{F}_{l^s}$. This was calculated from the analytical solution for the response of the clamped rod to the point load.

Using the same approach in the current case would require solving the EOM of the thin plate with the boundary conditions related to the definition of internal co-ordinates. The internal co-ordinates of the hierarchical plate element correspond to the case of the boundary conditions characterized as a 'clamped nodes' (see definition of internal shape functions in Section 3.1.2).

In fact the closed-form solution for the plate excited by the point force exist only in the case of an infinite plate or a special cases of circular plates, which are of less interest. In this case there is an axial symmetry in the problem and the displacement due to the acting force depends only on the distance from the excitation point. The use of the solution for the infinite plate could be justified by the assumption of strong damping in the system. In that case the attenuation of wave amplitude reduces the effects of the reflections from the boundaries of the element. Otherwise, the reflection at the boundaries occurs. The interference between the incident and reflected waves results in resonances and anti-resonances. However, in the conditions of modal overlap these effects should be insignificant. For these reasons the possibility of expressing the additional loading vector $\Delta\mathbf{F}$ could be proposed for further examination.

### 5.2.3 Comments to the solution of global equation

At the current stage of development of the hybrid FEM-SEA approach as presented in this thesis the additional stiffness matrix $\Delta\mathbf{D}$ and the additional loading vector $\Delta F$ should be calculated from the high-order internal co-ordinates of the hierarchical FEM. For this reason the order of internal co-ordinates taken in the original MDOF system should correspond to the proper interpolation of the displacement field at the frequency considered. The reduction of the system matrices, as described in Section 5.1 should be performed to yield the appropriate sub-matrices either in terms of additional stiffness matrices or in terms of mass and stiffness matrices.

The advantages of solving the global EOM over the solution of EOM in its original form, i.e. where the full set of co-ordinates has been used include:

- The partition of local dynamic stiffness matrix of the system in several dynamic stiffness matrices. Inversion of the partitioned matrix is much more efficient computationally.
- The possibility of using the solution for the infinite plate in the case of point load acting on the local structure (this approach has not been applied yet).
- It will be shown in the next section that even if the additional terms are calculated in deterministic sense, the use of the local description of power dissipation and power transfer among subsystems implies that the uncertainties in the system are taken into consideration.

The energy of each of the subsystems can be calculated according to (2.21). It is, however, only the part of energy corresponding to the global description. An additional portion of energy of each subsystem is carried by the local co-ordinates. The total energy consists of the sum of the two contributions.

## 5.3 Local Equations

The local equation of motion defined in (2.56) has the form:

$$\mathbf{D}_{gl}^T \mathbf{Q}_g + \mathbf{D}_{ll} \mathbf{Q}_l = \mathbf{F}_l \tag{5.6}$$

It should be solved after the equation (2.54) has been solved. The term $\mathbf{D}_{gl}^T \mathbf{Q}_g$ is then known and can be regarded as the known load for the local modes.

Introduction of further partition of the co-ordinates into co-ordinates corresponding to $s$ subsystems reads $\mathbf{Q}_l = [\mathbf{Q}_{l^1}\ \mathbf{Q}_{l^2}\ \cdots\ \mathbf{Q}_{l^s}]^T$ where the superscript is used to denote the subsystem. Using this partition and making use of the orthogonality of local co-ordinates (as described in previous section) among subsystems allows to transform equation (2.56) as follows:

$$\begin{bmatrix} \mathbf{D}_{gl^1}^T \\ \mathbf{D}_{gl^2}^T \\ \vdots \\ \mathbf{D}_{gl^s}^T \end{bmatrix} \mathbf{Q}_g + \begin{bmatrix} \mathbf{D}_{l^1l^1} & 0 & \cdots & 0 \\ 0 & \mathbf{D}_{l^2l^2} & \cdots & 0 \\ \vdots & \vdots & \ddots & \vdots \\ 0 & 0 & \vdots & \mathbf{D}_{l^sl^s} \end{bmatrix} \begin{bmatrix} \mathbf{Q}_{l^1} \\ \mathbf{Q}_{l^2} \\ \vdots \\ \mathbf{Q}_{l^s} \end{bmatrix} = \begin{bmatrix} \mathbf{F}_{l^1} \\ \mathbf{F}_{l^2} \\ \vdots \\ \mathbf{F}_{l^s} \end{bmatrix} \tag{5.7}$$

Left-hand side multiplication by the velocity vector $\dot{\boldsymbol{q}}_l = i\omega \mathbf{Q}_{l^i} e^{i\omega t}$ reads

$$i\omega \mathbf{Q}_{l^i}^T \begin{bmatrix} \mathbf{D}_{gl^1}^T \\ \mathbf{D}_{gl^2}^T \\ \vdots \\ \mathbf{D}_{gl^s}^T \end{bmatrix} \mathbf{Q}_g + i\omega \mathbf{Q}_{l^i}^T \begin{bmatrix} \mathbf{D}_{l^1l^1} & 0 & \cdots & 0 \\ 0 & \mathbf{D}_{l^2l^2} & \cdots & 0 \\ \vdots & \vdots & \ddots & \vdots \\ 0 & 0 & \vdots & \mathbf{D}_{l^sl^s} \end{bmatrix} \begin{bmatrix} \mathbf{Q}_{l^1} \\ \mathbf{Q}_{l^2} \\ \vdots \\ \mathbf{Q}_{l^s} \end{bmatrix} = i\omega \mathbf{Q}_{l^i}^T \begin{bmatrix} \mathbf{F}_{l^1} \\ \mathbf{F}_{l^2} \\ \vdots \\ \mathbf{F}_{l^s} \end{bmatrix}. \tag{5.8}$$

Introducing the time-average over $t = [0,\ 2\pi/\omega]$, denoted by $\langle\ \rangle_t$, results in power balance for subsystem $i$ in the form

$$\langle i\omega \mathbf{Q}_{l^i}^T \mathbf{D}_{gl^i}^T \mathbf{Q}_g \rangle_t + \langle i\omega \mathbf{Q}_{l^i}^T \mathbf{D}_{l^i l^i} \mathbf{Q}_{l^i} \rangle_t + \sum_{j=1, j\neq i}^{s} \langle i\omega \mathbf{Q}_{l^i}^T \mathbf{D}_{l^i l^j} \mathbf{Q}_{l^j} \rangle_t = \langle i\omega \mathbf{Q}_{l^i}^T \mathbf{F}_{l^i} \rangle_t. \quad (5.9)$$

This power balance corresponds to the power balance for subsystem in SEA. The elements of (5.9) can be identified as:

- $\langle i\omega \mathbf{Q}_{l^i}^T \mathbf{D}_{gl^i}^T \mathbf{Q}_g \rangle_t$ - time-average power input by the global motions to the local motions through the coupling DSM ($\mathbf{D}_{gl^i}$) between global co-ordinates and local co-ordinates of subsystem $i$,
- $\langle i\omega \mathbf{Q}_{l^i}^T \mathbf{D}_{l^i l^i} \mathbf{Q}_{l^i} \rangle_t$ - power dissipated by the subsystem $i$,
- $\langle i\omega \mathbf{Q}_{l^i}^T \mathbf{D}_{l^i l^j} \mathbf{Q}_{l^j} \rangle_t$ - power exchanged between subsystems $i$ and $j$,
- $\langle i\omega \mathbf{Q}_{l^i}^T \mathbf{F}_{l^i} \rangle_t$ power supplied by external forces to subsystem $i$.

Solution to (5.9) can be found in terms of SEA after calculating the elements of (5.9).

### 5.3.1 Power input to local subsystems

As discussed in Section 2.3.1 the power input from the external loading is defined as the product of force and velocity vectors (2.42). Specifically, in the case of harmonic point load acting on the subsystem, the power input is given by (2.43).

Two sources of external power input are present in this case. One due to the load acting directly on the local subsystem, and one due to the coupling with global co-ordinates. These sources cannot be considered separately, since the cross-terms might exist that should be accounted for. Of the main importance is the phase shift between the generalized forces acting on each of local co-ordinates. Forces acting in-phase with each other will add, whereas acting out of phase will subtract their contribution. Since the loading on the structure, defined in the current analysis as a harmonic load, excites both global and local co-ordinates, the correlation between the two components will be relevant. For that reason the generalized forces acting on local co-ordinates should first be combined and the power input calculation should follow.

Taken together the two contribution yield the loading vector $\mathbf{F}_{l^i}^{tot}$ for subsystem $i$ in the form:

$$\mathbf{F}_{l^i}^{tot} = \mathbf{F}_{l^i} + \mathbf{D}_{gl^i}^T \mathbf{Q}_{gl^i}. \quad (5.10)$$

The sign change between (5.9) and (5.10) has been introduced because the product $\mathbf{D}_{gl^i}^T \mathbf{Q}_{gl^i}$ signifies the response of the global structure due to the load from the local one, and the forces acting on the local structure have opposite sign.

Thus, the time-average external power input to the subsystem $i$, according to (5.9) is given by

$$\langle \Pi_i^{ext} \rangle_t = \langle i\omega \mathbf{Q}_{l^i}^T \mathbf{F}_{l^i}^{tot} \rangle_t \tag{5.11}$$

which is undetermined, because the local motions defined by $\mathbf{Q}_{l^i}$ are unknown. These can, however, be approximated by considering the local motions separately from the global motions, and therefore considering the forces acting on the local structure as an external load and solving

$$\mathbf{D}_{l^i l^i} \mathbf{Q}_l^i = \mathbf{F}_{l^i}^{tot} \tag{5.12}$$

for the local co-ordinates. Combining (5.11) and (5.12) yields:

$$\langle \Pi_i^{ext} \rangle_t = \langle i\omega [(\mathbf{D}_{l^i l^i})^{-1} \mathbf{F}_{l^i}^{tot}]^T \mathbf{F}_{l^i}^{tot} \rangle_t. \tag{5.13}$$

### 5.3.2 Power dissipated by the local subsystems

The term $\langle i\omega \mathbf{Q}_{l^i}^T \mathbf{D}_{l^i l^i} \mathbf{Q}_{l^i} \rangle$ has been identified as the power dissipated by the subsystem. In the time-average sense the potential and kinetic energies, (see (2.21) are almost equal to each other and equal to half of the total energy $E_i$. Then the expression under consideration can be reduced as:

$$\langle i\omega \mathbf{Q}_{l^i}^T \mathbf{D}_{l^i l^i} \mathbf{Q}_{l^i} \rangle_t = i\omega \left[ 2W^{(i)} - 2T^{(i)} + i\eta_i 2W \right] = -\omega \eta_i E_i. \tag{5.14}$$

which is the same result as in the standard SEA , see (2.44).

### 5.3.3 Power exchange between subsystems

The expression $\sum_{j=1, j\neq i}^{s} \langle i\omega \mathbf{Q}_{l^i}^T \mathbf{D}_{l^i l^j} \mathbf{Q}_{l^j} \rangle_t$ cannot be used to calculate the power transfer between subsystems. As explained previously, the cross terms between local modes of two different subsystems follow the definition of continuity between subsystems. Since these have been exchanged from the displacement to the energy ratio, the matrix $\mathbf{D}_{l^i l^j}$ has all entries equal to zero. However, the transformation of the continuity conditions means that the power transfer between subsystems should be modelled as in SEA, using equation (2.46).

The power flow between subsystems in SEA is dominated by the resonating modes. This means that the transfer of energy can only take place if there are resonating modes in the local subsystems. This condition holds above the 'transition' frequency of the subsystem. Below the 'transition' frequency of subsystem the CLF's between this subsystem and any other subsystem should be forced to zero. In that case the power balance for this subsystem consists of the external power input and power dissipation within the subsystem.

Once the elements of (5.9) are known the power balance for the subsystems can be set up and solved for the energies in the local description.

## 5.4 Overview of the Algorithm

This section presents the algorithm that has been implemented in Matlab [106] for the analysis of plate assemblies by the hybrid FEM-SEA. The steps of the algorithm are as follows.

### FREQUENCY INDEPENDENT PART

PREPARATION OF INPUT DATA The preprocessing includes the definition of geometry and material properties (including damping loss factor) of the structure. The preprocessing is performed in a separate module of the programme using graphical user interface. It also includes tools for mesh generation, definition of properties of hierarchical finite elements (order of interpolation), properties of subsystems as well as boundary conditions. The continuity conditions for internal co-ordinates are generated automatically.

DEFINITION OF LOAD The point harmonic load can be applied to the system at arbitrary position. The load vector $\mathbf{F}$ is calculated using (2.10) to (2.12). The load can be applied at multiple positions and with a phase shift between loads.

DEFINITION AND ASSEMBLY OF TOTAL SYSTEM MATRICES The generation of elements mass and stiffness matrices for the hierarchical version of FEM has been described in Sections 3.1.1 and 3.1.2. The continuity conditions for nodal co-ordinates and internal co-ordinates have been described in Section 3.2. Finally, the assembly procedure of the system mass and stiffness matrices (before partition of co-ordinates) has been described in Section 4.1.

PARTITION OF CO-ORDINATES The partition of co-ordinates is based on the wavelength criteria, as described in Section 5.1. The co-ordinate vector $\boldsymbol{q}$ is divided into vector of global co-ordinates $\boldsymbol{q}_g$ and a vector of local co-ordinates for each subsystem $\boldsymbol{q}_{l^s}$.

CONTINUITY AND BOUNDARY CONDITIONS The reduction of continuity conditions involving pairs of local co-ordinates belonging to different subsystems is performed first. The continuity conditions are imposed by condensation of matrices as described in Section 3.2.4. The vector of active global co-ordinates is extracted from $\boldsymbol{q}_g$ by removing the co-ordinates that are removed either by definition of continuity conditions or boundary conditions. In a similar way the vectors of active local co-ordinates $\boldsymbol{q}_{l^s}$ for each subsystem are defined.

GLOBAL AND LOCAL MATRICES The global and local matrices are extracted from the total condensed matrices using the vectors of active global and local co-ordinates. At this stage the global matrices $\mathbf{M}_{gg}$, $\mathbf{K}_{gg}$, $\mathbf{F}_g$, local matrices for each of subsystem $\mathbf{M}_{l^s l^s}$, $\mathbf{K}_{l^s l^s}$, $\mathbf{F}_{l^s}$ and the coupling matrices between global co-ordinates and local co-ordinates of each subsystem $\mathbf{M}_{gl^s}$, $\mathbf{K}_{gl^s}$ are known.

### FREQUENCY DEPENDENT PART

SOLUTION OF GLOBAL EQUATION The dynamic stiffness matrices (global and local for each subsystem) can be calculated from proper mass and stiffness matrices. The contribution from each of the subsystems to the additional dynamic stiffness matrices is calculated using equation (5.4), and to the additional loading vector using equation (5.5). The global EOM (2.54) can be solved at this stage for the global co-ordinates. These are used to calculate energy of the global motions as well as to calculate the power input to the local co-ordinates.

SOLUTION OF LOCAL EQUATIONS The SEA power balance for the structure is set up, see equation (2.48). The power input to the subsystem is calculated using (5.13). The damping loss factors are defined by the user. The CLF's are calculated for the junction of two plates with only bending waves present (as only bending waves are described by local co-ordinates). The power transfer is only allowed between resonating subsystems, i.e. subsystems with the 'transition frequency' lower than the actual frequency. Solution of power balance gives the energies of local motions.

### FREQUENCY INDEPENDENT PART

POST PROCESSING OF THE RESULTS The results in terms of energy of subsystems, can be saved to the result file, printed etc. The frequency averaging can also be performed if necessary.

## 5.5 Example of Hybrid FEM-SEA Analysis

An example of the hybrid FEM-SEA based on the hierarchical FEM is presented in this section. In the example the two plate model is considered, as described in Section 4.2 but the free boundary conditions are used. The numerical values used in the analysis are: $L_1$=1$m$, $L_2$=0.5 $m$, $L_3$=0.39 $m$, thickness 0.01 m, see Figure 5.3. Co-ordinates of the excitation point are: $a$=0.1$m$, $b$=0.1$m$. Material data: Young's modulus 4.9 $\times 10^9$ $N/m^2$, Poisson ratio 0.25, density 1180 $kg/m^3$.

The model used in the analysis (FCORNER2, see Table 4.6) with 12 elements and 105 internal shape functions is used as a base for the analysis. The co-ordinates are then divided and the matrices corresponding to global and local DOF are extracted from the total matrices.

The time-average kinetic energy in plates due to the unit harmonic point force is considered. The energy of the plate consists of the sum of energies of the global and the local co-ordinates. The procedures for calculating the energy of the subsystem have been presented previously.

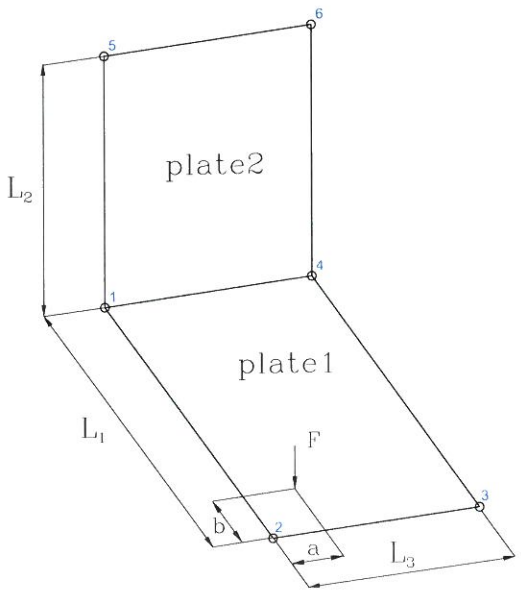


**Figure 5.3**: Geometry of the two plate corner.

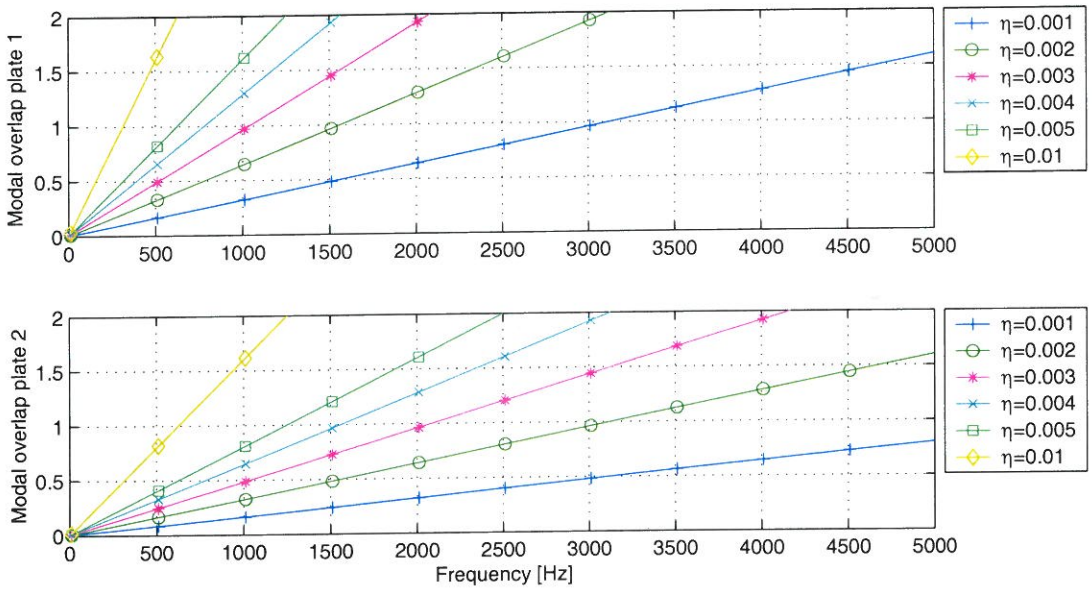


**Figure 5.4**: Modal overlap for two plate corner for different levels of damping loss factor.

**Table 5.1**: 'Transition' frequencies and wavelengths for the two plate corner and different levels of damping loss factor.

| Damping | Plate 1 | | Plate 2 | |
|---|---|---|---|---|
| $\eta$ | $f^{(1)}_{trans}$ [Hz] | $\lambda^{(1)}_{trans}$ [m] | $f^{(2)}_{trans}$ [Hz] | $\lambda^{(2)}_{trans}$ [m] |
| 0.001 | 3116 | 0.11 | 6231 | 0.078 |
| 0.002 | 1558 | 0.16 | 3116 | 0.11 |
| 0.003 | 1038 | 0.19 | 2077 | 0.14 |
| 0.004 | 779 | 0.22 | 1558 | 0.16 |
| 0.005 | 623 | 0.25 | 1246 | 0.17 |
| 0.01 | 311 | 0.35 | 623 | 0.25 |

### Partition of co-ordinates

Because of the geometry and physical properties the approximate modal density of plate 1 is twice as big as the modal density of plate 2. The modal overlap $\mathcal{M}^{(i)}$ of each of the plates is presented in Figure 5.4.

According to the modal overlap criteria the transition from the deterministic to the statistical description of subsystem $s$ can be performed when $\mathcal{M}^{(s)} > 1$. The 'transition frequencies' $f_{trans}$ and the wavelength of deformation at the 'transition frequency', $\lambda_{trans}$ for different levels of damping are presented in Table 5.1.

Three cases will be considered in the following. In the first case both plates have low level of damping, $\eta_1 = 0.001$ (in plate 1) and $\eta_2 = 0.001$ (in plate 2). In the second case the level of damping in the plate 2 is increased (in reality it could be the addition of a layer of damping material) to $\eta_2 = 0.005$ while the damping in plate 1 remains low ($\eta_1 = 0.001$). In the third case both plates have higher damping loss factors, $\eta_1 = 0.004$ and $\eta_2 = 0.01$. The 'transition' frequencies and wavelengths for each of the three cases are summarized in Table 5.2.

In case I the low frequency region spans from 10 Hz to 3 kHz. In this region both plates are modelled in deterministic sense. From 3116 Hz the plate 1 can be modelled in a statistical sense. There is no energy flow between subsystems yet, as there is only one local subsystem with resonating modes. Above 6231 Hz both plates can be modelled statistically and the power transfer might take place between the local modes.

In case II the low frequency ranges up to 1246 Hz. Above that frequency plate 2 has sufficient modal overlap to be described statistically. Above 3116 Hz local modes in both subsystems resonate and the power transfer takes place in both deterministic

and statistical description.

Finally, in case III the high damping in the two plates generates the modal overlap conditions below 1000 Hz for both subsystems (779 Hz for subsystem 1 and 623 Hz for subsystem 2).

The results of the analysis in terms of total energy plate 1 and plate 2 for all three cases in frequency range 10 Hz - 6 kHz are presented in Figure 5.5. The top, medium and bottom plots present energy of plates in case I, II and III, respectively. The plots on the right-hand side present energy in plate 1 (driven). The plots on the left-hand side present energy in plate 2 (receiving).

The narrowband energy spectrum and the moving average of the energy spectrum are presented. Also, the 'transition frequency' of each subsystem is indicated. The influence of the damping level and the frequency on the amplitudes of the resonant peaks (deviation from the mean) can be clearly seen in Figure 5.5. It can serve as an indication of how precise the SEA estimation would be in the case considered.

The frequency-averaged values are combined in Figure 5.6. Upper plot presents energies in each of the plates separately. Lower plot presents the total energy in the system. In cases I and II the damping of plate 1 is kept constant. The comparison of curves for energy in plate 1 in cases I and II shows the influence of the damping factor of plate 2 on the energy of plate 1. As expected the energy of plate 1 in case 2 is smaller, because there is less energy in the combined system.

Figure 5.7 presents the comparison of the energy in plate 1 in the low frequency range (10 to 600 Hz), i.e. below 'transition frequency' in any of the cases. There is a good agreement between the results of the three cases in the stiffness controlled and in the mass controlled bands. In the damping controlled frequency bands the differences between three cases are also properly modelled.

It can be seen be comparison of the results from cases I and II that despite the same level of damping in the plate 1, the energy of plate 1 at the resonances in case I is higher than in case II. This difference is more readable at some natural

**Table 5.2**: 'Transition' frequencies and wavelengths for the three cases of damping values considered in the two plate corner.

| Case | Plate 1 | | | Plate 2 | | |
|---|---|---|---|---|---|---|
| | $\eta_1$ | $f^{(1)}_{trans}$ [Hz] | $\lambda^{(1)}_{trans}$ [m] | $\eta_2$ | $f^{(2)}_{trans}$ [Hz] | $\lambda^{(2)}_{trans}$ [m] |
| I | 0.001 | 3116 | 0.11 | 0.001 | 6231 | 0.078 |
| II | 0.001 | 3116 | 0.11 | 0.005 | 1246 | 0.17 |
| III | 0.004 | 779 | 0.22 | 0.01 | 623 | 0.25 |

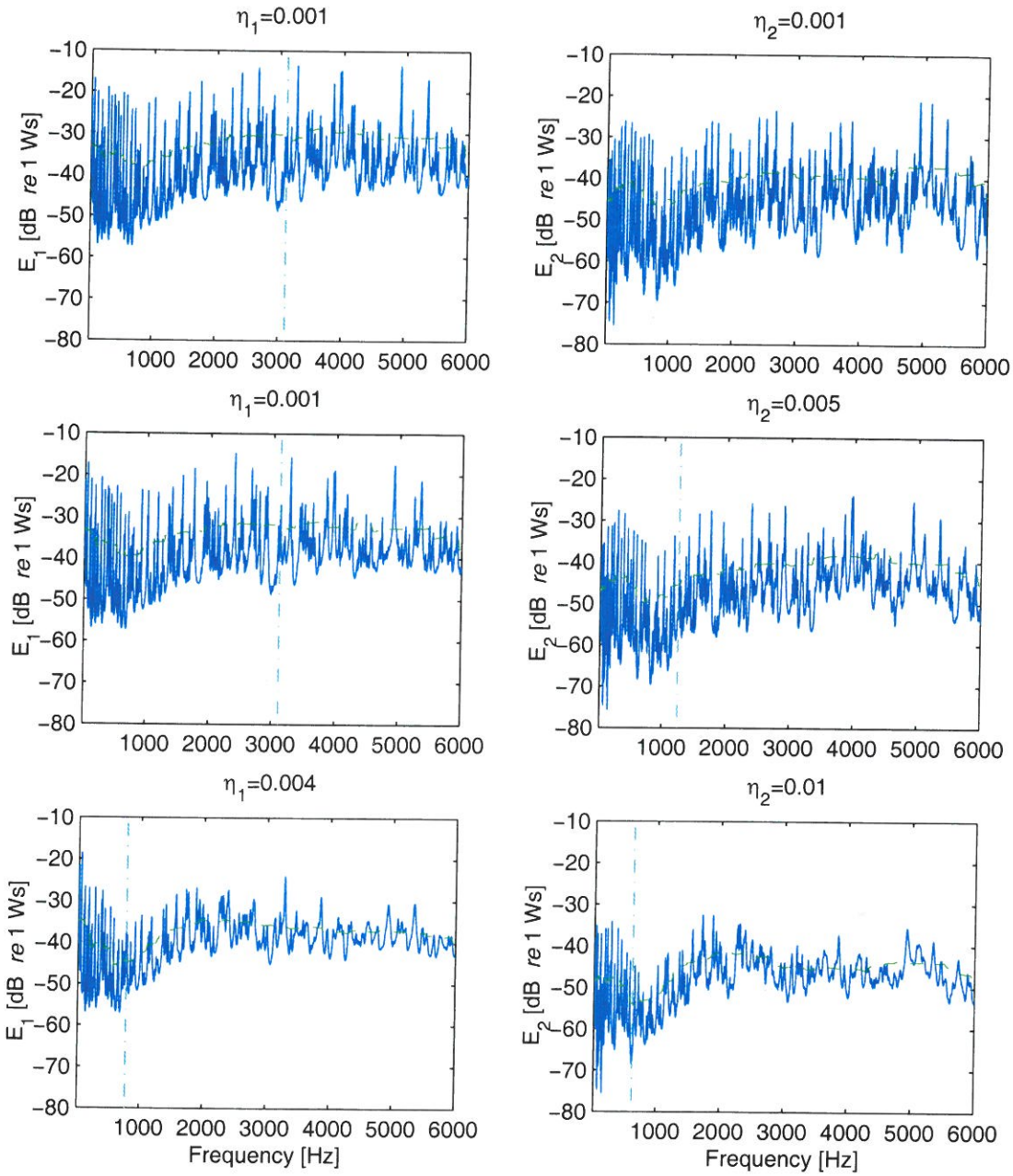


**Figure 5.5**: Energies in plate 1 (left-hand side) and plate 2 (right-hand side) in case I (top), case II (middle) and case III (bottom). — energy of the subsystem, - - - frequency averaged energy (moving average), - · - 'transition frequency' of subsystem.

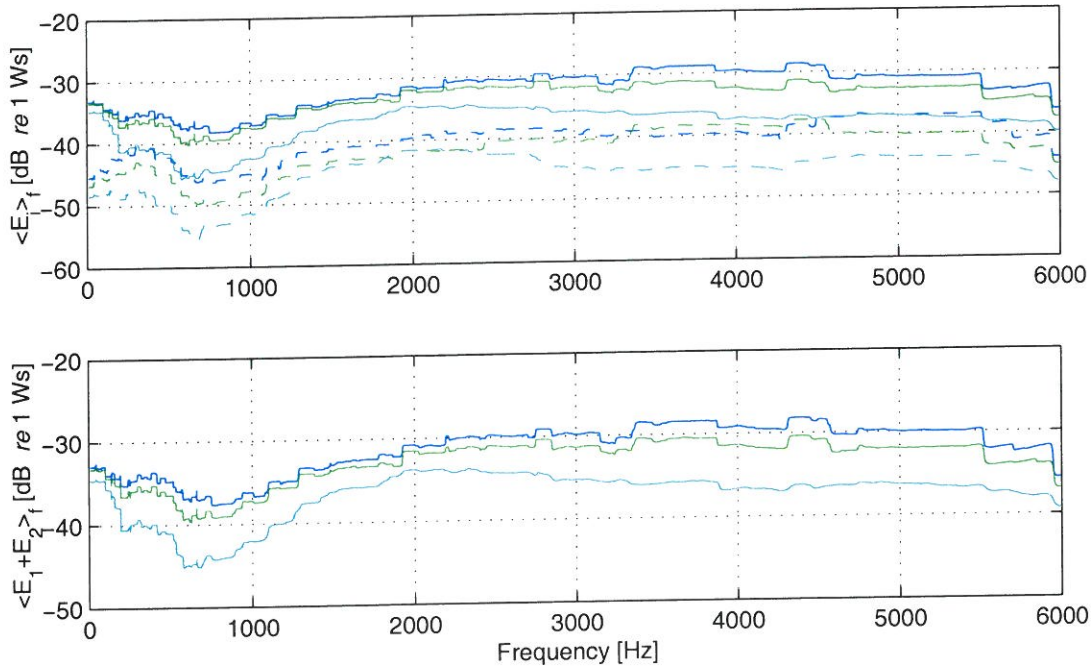


**Figure 5.6**: Frequency averaged energies in plates 1 and 2 in all three cases (top) and combined energy of the system (bottom). Results for case I: — $< E_1 >_f$, - - - $< E_2 >_f$; results for case II: — $< E_1 >_f$, - - - $< E_2 >_f$; results for case III: — $< E_1 >_f$, - - - $< E_2 >_f$

frequencies than in the others. That is because some modes of the plate corner involve nearly equal participation of both plates whereas some modes have local behaviour and the energy depends on the local properties. Similar comparison for the energy estimations in plate 2 are presented in Figure 5.8.

The results for the frequency range 2010-2600 Hz are presented in figures 5.9 and 5.10. This frequency range is a low frequency range for case I, medium frequency range for case II and high frequency range for case III. Despite the differences in the damping that influences the energy level (the heights of resonant peaks), the results of case I and II are very similar as compared to the results in the case III. That is because in cases I and II the load acts on the plate described by FEM and there is no energy flow between local subsystems. In case III the power is injected to both global and local co-ordinates and, since both local subsystems are resonating, there is also the power transfer between them, as described by SEA equations.

Finally, figures 5.11 and 5.12 present the results for the frequency range from 5010 Hz to 5600 Hz. Both case II and case III are in the high frequency range, case I is in medium frequency range.

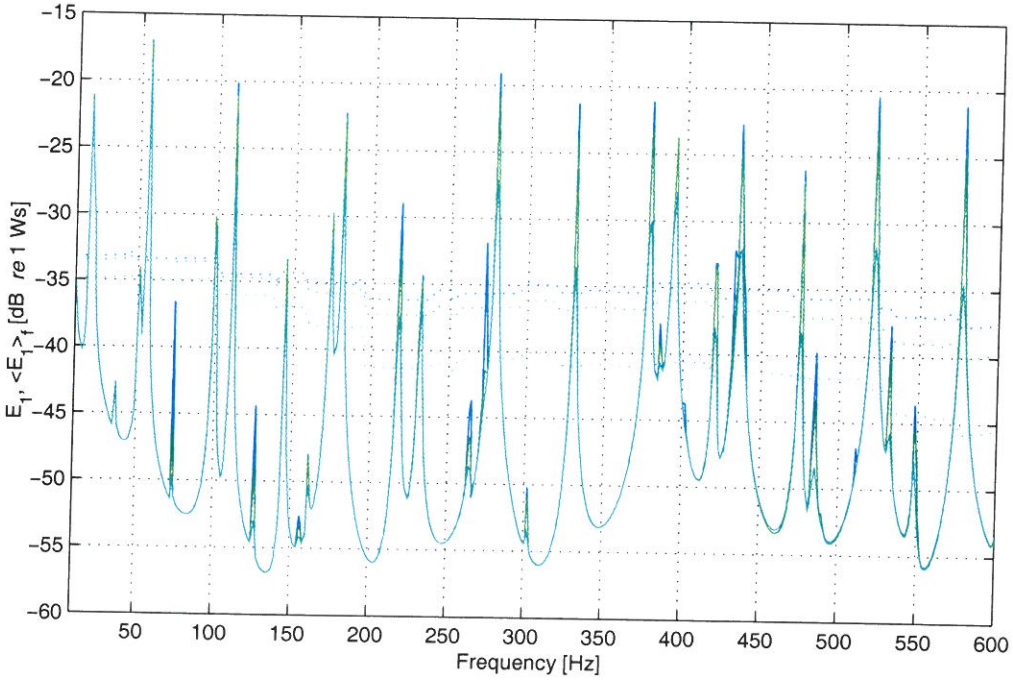


**Figure 5.7**: Energies in plate 1 in all three cases, frequency 10-600 Hz. Results for case I: — $E_1$, - - - $< E_1 >_f$; results for case II: $E_1$, - - - $< E_1 >_f$; results for case III: — $E_1$, - - - $< E_1 >_f$

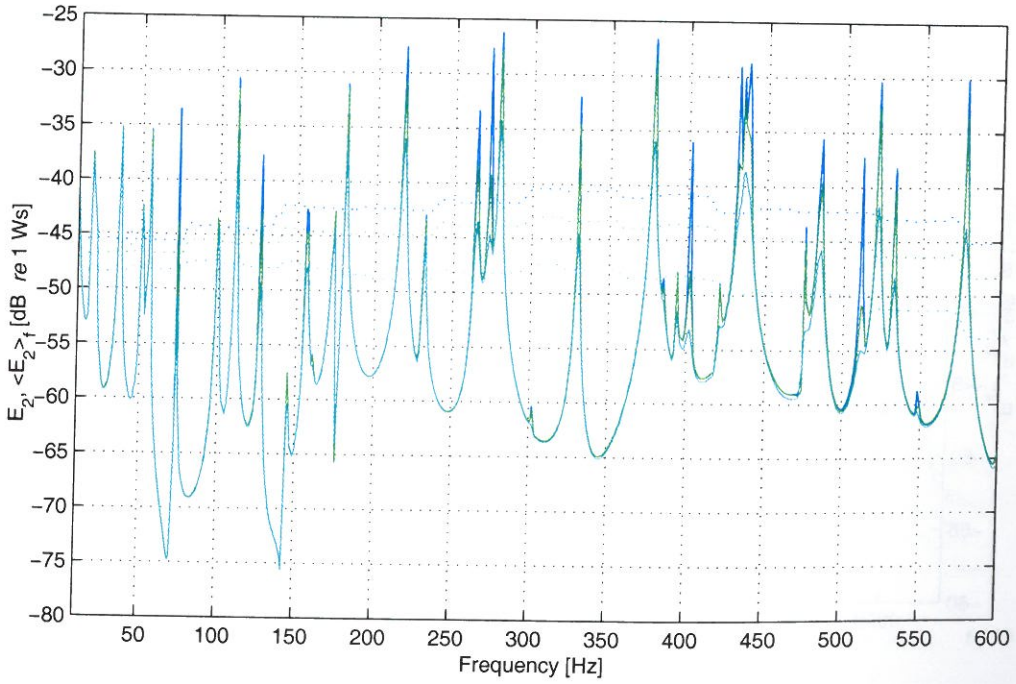


**Figure 5.8**: Energies in plate 2, 10-600 Hz. Labels as in Figure 5.7

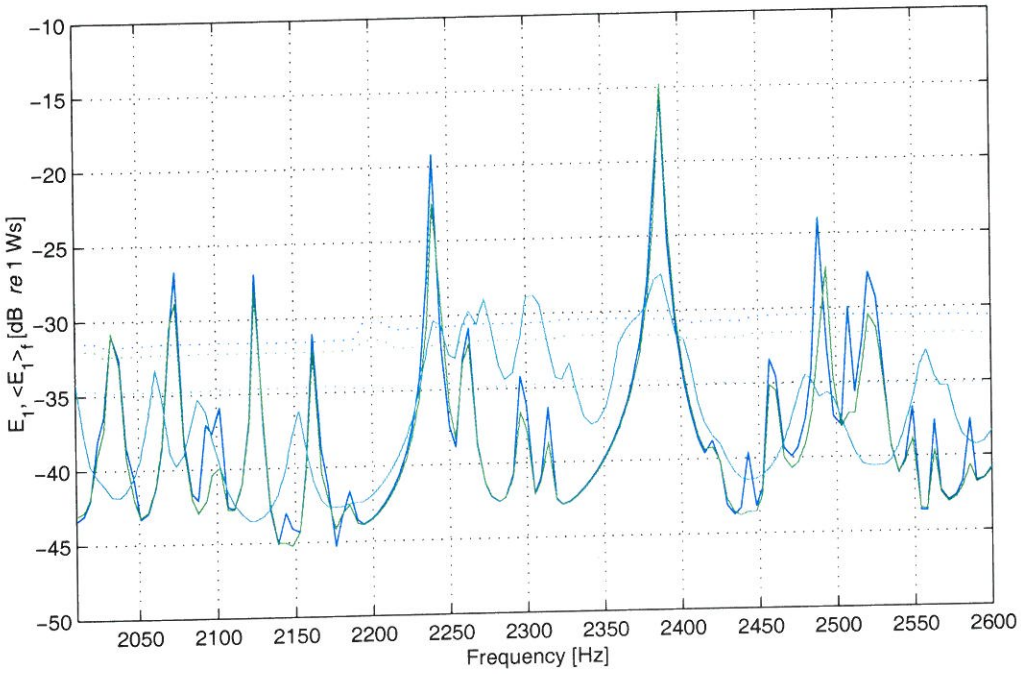


**Figure 5.9**: Energies in plate 1 in all three cases, frequency 2010-2600 Hz. Results for case I: — $E_1$, - - - $< E_1 >_f$; results for case II: $E_1$, - - - $< E_1 >_f$; results for case III: — $E_1$, - - - $< E_1 >_f$

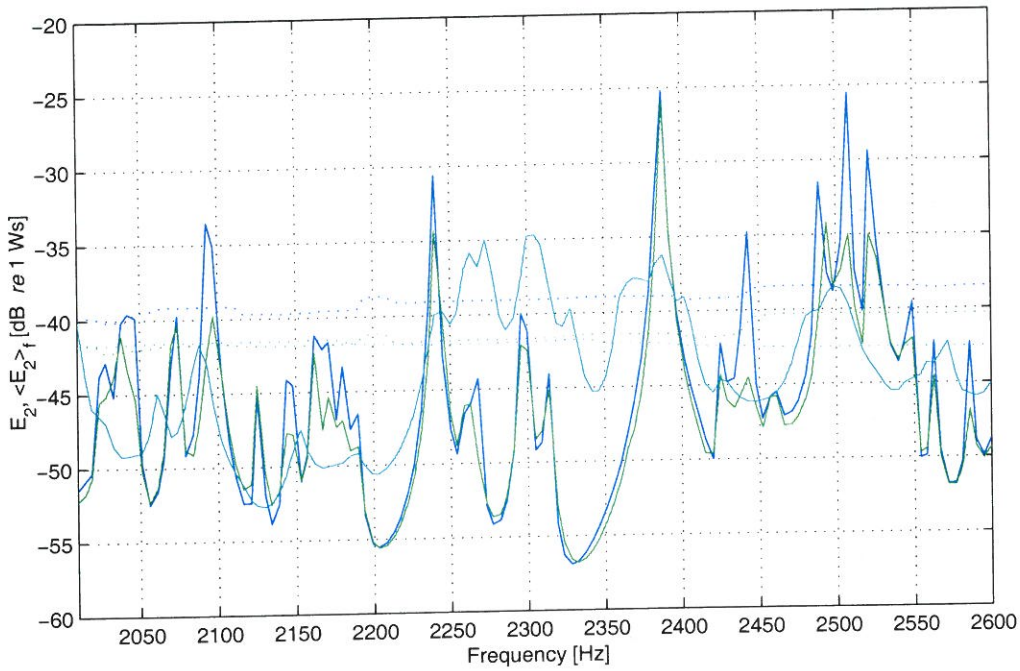


**Figure 5.10**: Energies in plate 2, 2010-2600 Hz. Labels as in Figure 5.9

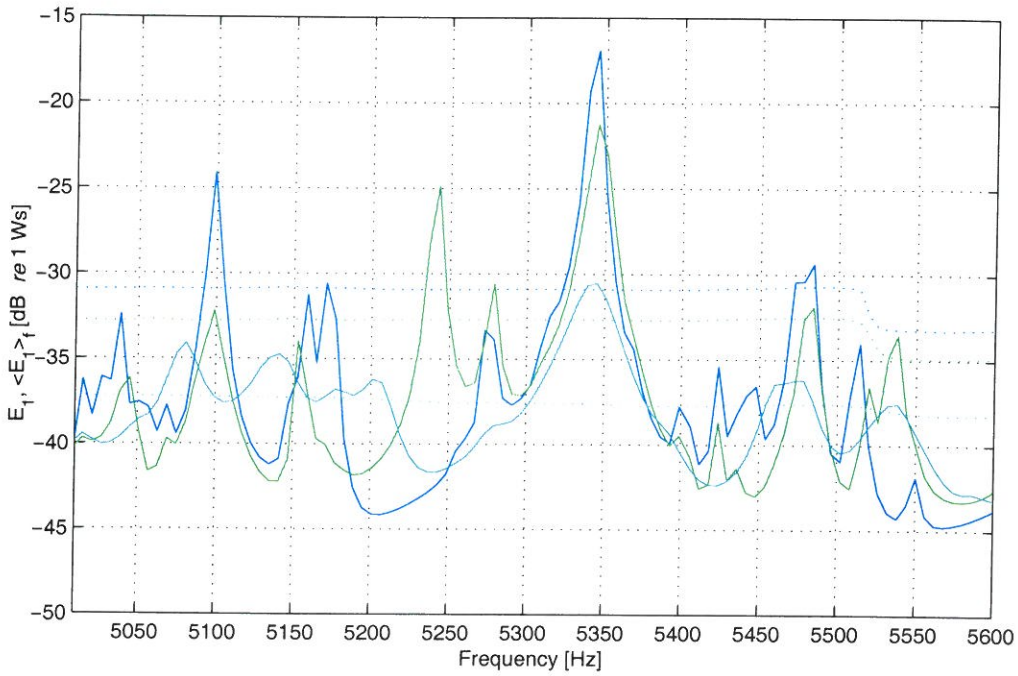


**Figure 5.11**: Energies in plate 1 in all three cases, frequency 5010-5600 Hz. Results for case I: — $E_1$, - - - $< E_1 >_f$; results for case II: $E_1$, - - - $< E_1 >_f$; results for case III: — $E_1$, - - - $< E_1 >_f$

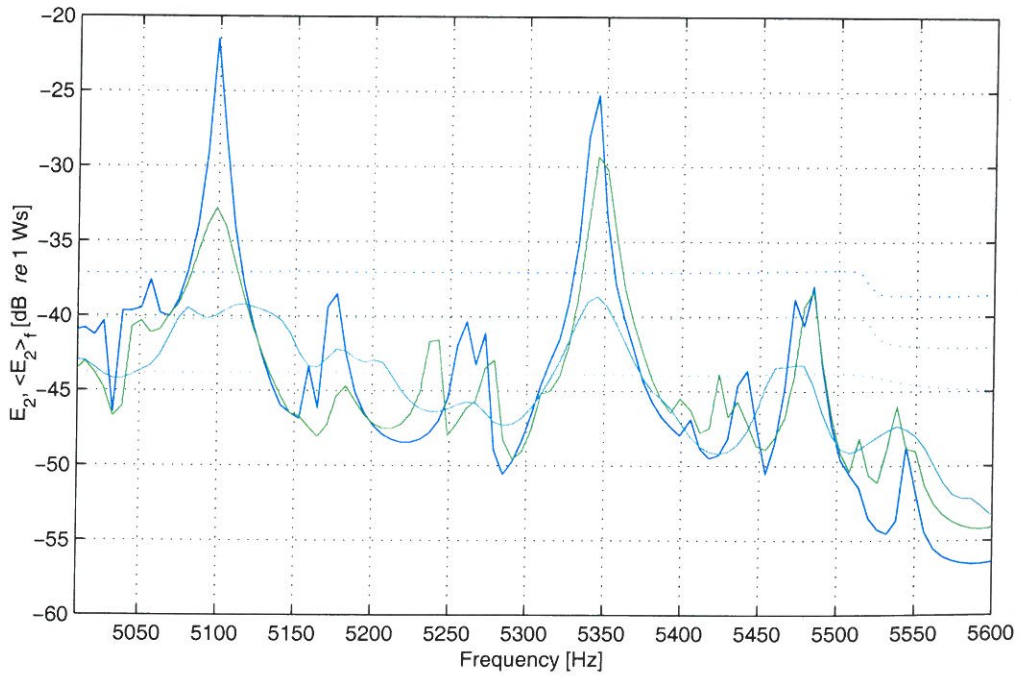


**Figure 5.12**: Energies in plate 2, 5010-5600 Hz. Labels as in Figure 5.11

From the comparison of the results in figures 5.7 to 5.12 it can be seen that although the modal density of thin plate in bending is constant, there is less and less visible separate resonances in the same frequency range as the frequency increase. That is because the modes overlap. Another effect of the overlapping modes is the increase of the energy content between resonances, also visible in the results.

## 5.6 Summary of Chapter 5

In this chapter the implementation of the hybrid FEM-SEA approach to the problem of coupled thin plates has been presented. The co-ordinate partition scheme, based on the modal overlap criteria, has been discussed in Section 5.1.

The transformation of the continuity conditions, from the displacement-based, to energy based, has been introduced. This allows for uncoupling of the local matrices that describe different subsystems.

The contribution from the subsystems to the coupling terms (additional dynamic stiffness and additional load) can in this way be separated. The expressions for the additional terms are presented in Section 5.2. these can be used to solve the global EOM. In Section 5.3 the power balance for the local subsystems is considered. The terms describing power input, power transfer and power dissipation are presented. The algorithm of the calculations is summarized in Section 5.4 and in Section 5.5 an example of hybrid FEM-SEA analysis is presented.

Benefits from applying the hybrid approach at the current stage of development can be seen in the partition of the local dynamic stiffness matrix accordingly to the subsystems. The inversion of the separate matrices is more efficient computationally then the inversion of the full matrix. The second advantage can be seen in applying the continuity conditions between subsystems in terms of energy ratio. This description of continuity conditions is more suitable at high frequencies because of the uncertainties in the structure, which cause the deterministic description to be inaccurate.

# Chapter 6

# Conclusions

This thesis has been concerned with the analysis of power flow in built-up structures. For two reasons the focus has been on the assemblies of thin plates. The first reason is that in the structure made of thin plates there is a big difference between the dynamic properties when considering the in-plane motions and the out-of-plane motions. Since the coupling of in-plane and out-of-plane motions appears at the junctions between coupled plates the structure need to be analysed accordingly to the dynamic properties of both types of motions. The second reason for analysing the plate assemblies is that for the structure-borne noise analysis the plates are of importance due to the radiation properties.

In the first part of the thesis different techniques of power flow calculations have been presented and the limits of the approaches were pointed out. The idea of coupling the two techniques, FEM and SEA, has been chosen as the possibility for the analysis of built-up structures.

In order to apply the hybrid FEM-SEA approach to the thin plates assemblies the hierarchical version of FEM has been developed and implemented. The use of hierarchical FEM simplifies the calculations as the modal analysis of the structural components is not required. The original co-ordinates of the hierarchical FEM posses the properties required by the hybrid FEM-SEA, namely there is a correspondence between the order of interpolation function and the frequency where it contributes to the response. The differences in the dynamic properties of the thin plates manifest in the differences of the wavelengths of different wave types. The in-plane waves are longer then the out-of-plane waves and therefore only the out-of plane displacement field has been described in the hierarchical formulation. This definition allows to use only a necessary amount of DOF to model in-plane and out-of -plane motions. In the standard FEM the amount of DOF is usually adjust at the same proportions to describe the in-plane and to the out-of-plane motions resulting unnecessary DOFs. From the point of view of computational efficiency the hierarchical FEM is therefore preferable.

The hybrid FEM-SEA approach has been implemented in the latter part of the thesis. The modal overlap criteria has been chosen as the indicator of the frequency range for the deterministic (FEM) and for the statistical (SEA) description. The hierarchical formulation of FEM allows for adjusting the sets of co-ordinates to the frequency of interest, and to use the local co-ordinates as an indication of coupling forces between the two descriptions.

A transformation of continuity conditions has been introduced. The continuity conditions for the local co-ordinates that describe interaction between subsystems have been removed. The SEA balance between the energy levels of the subsystems has been used instead. As a result the energy transfer between subsystems does no longer include the information of the phase shift at the junction. This can be seen as the application of the mean transfer coefficient of an ensemble instead of applying exact conditions for the model with nominal, not real, properties. The second result of the transformation of continuity conditions is the possibility to uncouple the local matrices describing different subsystems. It has a remarkable computational advantage as the inverse of the dynamic stiffness matrix can be calculated in parts corresponding to subsystems.

The new contribution in this thesis are, to the author's knowledge is summarized below.

- The formulation of hierarchical FEM for thin plates that includes in-plane and out-of-plane contribution, that include the definition and implementation of continuity conditions between plates in different planes.
- The definition of the co-ordinate partition scheme based on the modal overlap criteria and the transformation of continuity conditions that allows for efficient calculations of coupling terms between the global and local co-ordinates.
- The implementation of the hybrid FEM-SEA approach to the assemblies of thin plates using the hierarchical formulation of FEM.

The following areas can be suggested for further research.

- The estimation of the coupling terms between global and local co-ordinates in the cases of distributed or stochastic loads.
- Further study of the possibility to describe the local modes in more compact way than presented in this thesis.
- The validation of the modal overlap criteria (the required value for the SEA description) and definition of alternative criteria for the partition of co-ordinates.

# Bibliography


[1] J.D. Achenbach. *Wave Propagation in Elastic Solids.* North-Holland Publishing Company, 1976.

[2] N.S. Bardell. Free vibration analysis of a flat plate using the hierarchical finite element method. *Journal of Sound and Vibration*, 151(2):263–289, 1991.

[3] M. Barrette, A. Berry, and O. Beslin. Vibration of stiffened plates using hierarchical trigonometric functions. *Journal of Sound and Vibration*, 235(5):727–747, 2000.

[4] K. J. Bathe. *Finite Element Procedures.* Prentice Hall, Upper Saddle River, New Jersey 07458, 1996.

[5] L.S. Beale and M.L. Accorsi. Power flow in two and three-dimensional frame structures. *Journal of Sound and Vibration*, 185(4):685–702, 1995.

[6] A.K. Belyaev. Parabolic equation for modelling wave propagation in complex structures. *Proceedings, Seventh International Congress on Sound and Vibration*, pages 1107–1114, 2000.

[7] A.N. Bercin. Analysis of orthotropic plate structures by the direct dynamic stiffness method. *Mechanics Research Comunications*, 22(5):461–466, 1995.

[8] A.N. Bercin and R.S. Langley. Application of the dynamic stiffness technique to the in-plane vibrations of plate structures. *Computers & Structures*, 59(5):869–875, 1996.

[9] M. Beshara and A. J. Keane. Vibrational energy flows in beam networks with compliant and dissipative joints. *Journal of Sound and Vibration*, 203(2):321–339, 1997.

[10] O. Beslin and J. Nicolas. A hierarchical functions set for predicting very high order plate bending modes with any boundary conditions. *Journal of Sound and Vibration*, 202(5):633–655, 1997.

[11] V.V. Bolotin. *Random Vibrations of Elastic Systems.* Martinus Nijhoff Publishers, 1984.

[12] O.M. Bouthier and R.J. Bernhard. Simple models of energy flow in vibrating membranes. *Journal of Sound and Vibration*, 182(1):129–147, 1995.

[13] O.M. Bouthier and R.J. Bernhard. Simple models of the energetics of transversely vibrating plates. *Journal of Sound and Vibration*, 182(1):149–164, 1995.

[14] A. Carcaterra and Adamo L. Thermal analogy in wave energy transfer: Theoretical and experimental analysis. *Journal of Sound and Vibration*, 226(2):253–284, 1999.

[15] S Chen, M. Geradin, and E. Lamine. An improved dynamis stiffness method and modal analysis for beam-like structures. *Computers & Structures*, 60(5):725–731, 1996.

[16] R.D. Cook, D.S. Malkus, and M.E. Plesha. *Concepts and Applications of Finite Element Analysis.* John Wiley & Sons, 1989.

[17] R.R. Jr. Craig. *Structural Dynamics, an Intoduction to Numerical Methods.* John Wiley & Sons, 1981.

[18] R.R. Jr. Craig. Substructure methods in vibration. *Transactions of ASME, Journal of Vibration and Acoustics*, 117(50th Anniversary Design Issue):207–213, 1995.

[19] R.J.M. Craik. *Sound Transmission through Buildings Using Statistical Energy Analysis.* Gower, 1996.

[20] R.J.M. Craik, J.A. Steel, and D.I. Evans. Statistical energy analysis of structure-borne sound transmission at low frequencies. *Journal of Sound and Vibration*, 144(1):95–107, 1991.

[21] L. Cremer, M. Heckl, and E.E. Ungar. *Structure-Borne Sound.* New York Springer-Verlag; second edition, 1988.

[22] H.G. Davies and M.A. Wahab. Ensemble averages of power flow in randomly excited coupled beams. *Journal of Sound and Vibration*, 77(3):311–321, 1981.

[23] F.J. Fahy. Statistical energy analysis: a critical overview. *Statistical Energy Analysis, an Overview with Applications in Structural Dynamics*, pages 1–18, 1994.

[24] F.J. Fahy and P.P. James. A study of the kinetic energy impulse response as an indicator of the strength of coupling between sea subsystems. *Journal of Sound and Vibration*, 190(3):363–386, 1996.

[25] F.J. Fahy and A.D. Mohammed. A study of uncertainty in applications of sea to coupled beam and plate systems, part i: Computational experiments. *Journal of Sound and Vibration*, 158(1):45–67, 1992.

[26] F.Y. Fahy. *Sound and Structural Vibration. Radiation, Transmission and Response.* Academic Press, 1987.

[27] P Fischer, A.K. Belyaev, and H. Pradlwarter. Combined integral and fe analysis of broad-band random vibration in structural members. *Probablistic Engineering Mechanics*, 10:241–250, 1995.

[28] C.R. Fredø. *Statistical Energy Analysis and the Indyvidual Case.* PhD thesis, Chalmers University of Technology, June 1995.

[29] C.R. Fredö. Sea-like approach for derivation of energy flow coefficients with finite element method. *Journal of Sound and Vibration*, 199(4):645–666, 1997.

[30] L. Gavrić and G. Pavić. Finite element model for computation of structural intensity by the normal mode approach. *Journal of Sound and Vibration*, 164(1):29–43, 1993.

[31] R.G. Ghanem and P.D. Spanos. *Stochastic Finite Elements: a Spectral Approach.* Springer-Verlag, New York, 1991.

[32] K.F. Graff. *Wave Motion in Elastic Solids.* Dover Publications, INC., 1975.

[33] R.M. Grice and R.J. Pinnington. Vibration analysis of a thin-plate box using a finite element model which accommodates only in-plane motion. *Journal of Sound and Vibration*, 232(2):449–471, 2000.

[34] S.A. Hambric. Power flow and mechanical intensity calcutations in structural finite elements. *Transactions of ASME, Journal of Vibration and Acoustics*, 112:542–549, 1990.

[35] S.A. Hambric. Comparison of finite element predictions and experimental measurements of structure-borne powers in a t-shaped beam. *Inter-Noise 95*, 1995.

[36] S.A. Hambric and P.D. Taylor. Comparison of experimental and finite element structure-borne flexural power measurements for a straight beam. *Journal of Sound and Vibration*, 170(5):595–605, 1994.

[37] H. Hassis. Proposition of a new approach for the substructure method. *Journal of Sound and Vibration*, 232(4):659–668, 2000.

[38] M. Heckl and M. Lewit. Statistical energy analysis as a tool for quantifying sound and vibration transmission paths. *SEA, an Overwiev with Applications in Structural Dynamics, Keane and Price (eds.)*, pages 19–34, 1997.

[39] K.H. Heron. Advanced statistical energy analysis. *Statistical Energy Analysis, an Overview with Applications in Structural Dynamics*, pages 71–80, 1994.

[40] K.H. Heron. Predictive statistical energy analysis: A fifty plate case study. *CEAS/AIAA Aeroacoustic Conference (16th AIAA), Munich, Germany*, 1995.

[41] C.H. Hodges and J. Woodhouse. Noise and vibration transmission in complex structures. *Reports on Progress in Physics*, 49(1):107–170, 1986.

[42] J.L. Horner and R.G. White. Prediction of vibrational power transmission through bends and joints in beam-like structures. *Journal of Sound and Vibration*, 147(1):87–103, 1991.

[43] A. Houmat. An alternative hierarchical finite element formulation applied to plate vibrations. *Journal of Sound and Vibration*, 206(2):201–215, 1997.

[44] C. T. Hugin. Power transmission between two finite beams at low modal overlap. *Journal of Sound and Vibration*, 212(5):829–854, 1998.

[45] C.T. Hugin. Energy distribution of structure-borne sound in tree-dimensional structures. *Report no 67, 1996, Department of Acoustic Technology, Technical Universiy of Denmark*, 1996.

[46] P. Hynnä, P. Klinge, and J. Vuoksinen. Prediction of structure-borne sound transmission in large welded ship structures using statistical energy analysis. *Journal of Sound and Vibration*, 180:583–607, 1995.

[47] Waterloo Maple Inc. *Maple 6. User's Manual.* 2000.

[48] P.P. James and F.J. Fahy. A technique for the assessment of strength of coupling between sea subsystems: Experiments with two coupled plates and two coupled rooms. *Journal of Sound and Vibration*, 203(2):265–282, 1997.

[49] C.W. Jen, D.A. Johnson, and F. Dubois. Numerical modal analysis of structures based on revised substructure synthesis approach. *Journal of Sound and Vibration*, 180(2):185–203, 1995.

[50] A.J. Keane and W.G. Price. Statistical energy analysis of strongly coupled systems. *Journal of Sound and Vibration*, 117(2):363–386, 1987.

[51] A.J. Keane and W.G. Price. A note on the power flowing between two conservatively coupled multi-modal subsystems. *Journal of Sound and Vibration*, 144(2):185–196, 1991.

[52] R.S. Langley. Application of the dynamic stiffness method to the free and forced vibrations of aircraft panels. *Journal of Sound and Vibration*, 135(2):319–331, 1989.

[53] R.S. Langley. A general derivation of statistical energy analysis equations for coupled dynamic systems. *Journal of Sound and Vibration*, 141(2):207–219, 1989.

[54] R.S. Langley. Analysis of power flow in beams and frameworks using the direct stiffness method. *Journal of Sound and Vibration*, 136:439–452, 1990.

[55] R.S. Langley. A derivation of coupling loss factors used in statistical energy analysis. *Journal of Sound and Vibration*, 141(2):207–219, 1990.

[56] R.S. Langley. A dynamic stiffness/boundary element method for the prediction of interior noise levels. *Journal of Sound and Vibration*, 163(2):207–230, 1993.

[57] R.S. Langley. Elastic wave transmission coefficients and coupling loss factors for structural junctions between curved panels. *Journal of Sound and Vibration*, 169(3):297–317, 1994.

[58] R.S. Langley. Spatially averaged frequency response envelopes for one and two dimensional structural components. *Journal of Sound and Vibration*, 178(4):483–500, 1994.

[59] R.S. Langley. Wave motion and energy flow in cylindrical shells. *Journal of Sound and Vibration*, 169(1):26–42, 1994.

[60] R.S. Langley. The frequency band-averaged wave transmission coefficient of a periodic structure. *The Journal of the Acoustical Society of America*, 100(1):304–311, 1996.

[61] R.S. Langley. A non-poisson model for the vibration analysis of uncertain dynamic systems. *Proceedings of the Royal Society of London*, 455:3325–3349, 1999.

[62] R.S. Langley and N.S. Bardell. A review of current analysis capabilities applicable to the high frequency vibration prediction of aerospace structures. *The Aeronautical Journal*, 102:287–297, 1998.

[63] R.S. Langley and P. Bremner. A hybrid method for the vibration analysis of complex structural-acoustic systems. *The Journal of the Acoustical Society of America*, 105(3):1657–1671, 1999.

[64] A.W. Leissa. The free vibration of rectangular plates. *Journal of Sound and Vibration*, 31:257–293, 1973.

[65] A.Y.T. Leung. *Dynamic Stiffness and Substructures.* Springer-Verlag, Berlin, 1993.

[66] A.Y.T. Leung and Chan J.K.W. Fourier p-element for analysis of beams and plates. *Journal of Sound and Vibration*, 212(1):179–185, 1998.

[67] K.M. Liew, K.Y. Lam, and S.T. Chow. Free vibration analysis of rectangular plates using orthogonal plate function. *Computers and Structures*, 34(1):79–85, 1990.

[68] R. Lyon and R. De Jong. *Theory and Application of Statistical Energy Analysis.* Butterworth-Heinemann, 313 Washington Street Newton, 2 edition, 1995.

[69] R. Lyon and G. Maidanik. Power flow between linearly coupled oscillators. *The Journal of the Acoustical Society of America*, 34(5):623–639, 1962.

[70] B.R. Mace. Power flow between two continuous one-dimensional subsystems: a wave solution. *Journal of Sound and Vibration*, 154(2):289–319, 1992.

[71] B.R. Mace. On the statistical energy analysis hypothesis of coupling power proportionality and some implications of its failure. *Journal of Sound and Vibration*, 178(1):95–112, 1994.

[72] B.R. Mace. Wave coherence, coupling power and statistical energy analysis. *Journal of Sound and Vibration*, 199(3):369–380, 1997.

[73] B.R. Mace and P.J. Shorter. Energy flow models from finite element analysis. *Journal of Sound and Vibration*, 233(3):369–389, 2000.

[74] C.S. Manohar and S. Adhikari. Statistics of vibration energy flow in randomly parametered trusses. *Journal of Sound and Vibration*, 217(1):43–74, 1998.

[75] L. Maxit and J.L. Guayader. Estimation of sea coupling loss factor using a dual formulation and fem modal information. *Journal of Sound and Vibration*, 239(5):907:948, 2001.

[76] L. Meirovitch. *Analytical Methods in Vibrations.* Collier-Macmillan, 1967.

[77] L. Meirovitch. *Computational Methods in Structural Dynamics.* Sijthoff & Noordhoff, 1980.

[78] L. Meirovitch and H. Baruh. On the inclusion principle for the hierarchical finite element method. *International Journal for Numerical Methods in Engineering*, 19:281–291, 1983.

[79] D.W. Miller and A.H. von Flotow. A travelling wave approach to power flow in structural networks. *Journal of Sound and Vibration*, 128(1):145–162, 1989.

[80] C. Morales. Rayleigh-ritz based sustructure synthesis for multiply supported structures. *Transactions of ASME, Journal of Vibration and Acoustics*, 122:2–6, 2000.

[81] D.J. Nefske and S.H. Sung. Power flow finite element analysis of dynamic systems:basic theory and application to beams. *Trasactions of the ASME, Journal of Vibration adn Acoustics*, 111:94–100, 1989.

[82] S.R.K. Nielsen. *Vibration Theory, Vol.1. Linear Vibration Theory.* Aalborg tekniske Universitetsforlag, 1998.

[83] R Ohayon and Ch. Soize. *Structural Acoustics and Vibration.* Academic Press Limited, 24-28 Oval Road Londod NW1, 1998.

[84] M. Ohlrich and A. Nø jgaard. Vibrational power flow and structural wave intensity: Measurements and limitations at low frequencies. *Journal of Low Frequency Noise & Vibration*, 10(2):45–53, 1991.

[85] D.-H. Park, S.-Y. Hong, H.-G. Kil, and J.-J. Jeon. Power flow models and analysis of in-plane waves in finite coupled thin plates. *Journal of Sound and Vibration*, 244(4):651–668, 2001.

[86] Y. Ren and C.F. Beards. On substructure synthesis with frf data. *Journal of Sound and Vibration*, 185(5):845–866, 1995.

[87] T.D. Scharton and R.H. Lyon. Power flow and energy sharing in random vibration. *The Journal of the Acoustical Society of America*, 43(6):1332–1343, 1968.

[88] M. Scheble, C.N. Strizzolo, and J. Converti. A reyleigh-ritz substructure synthesis method in physical coordinates for dynamic analysis of structures. *Journal of Sound and Vibration*, 213(1):193–200, 1998.

[89] W. Seemann. Transmission and reflection coefficients for longitudinal waves obtained by a combination of refined rod theory and fem. *Journal of Sound and Vibration*, 197:571–587, 1996.

[90] K. Shankar and A. J. Keane. Energy flow predictions in a structure of rigidly joined beams using receptance theory. *Journal of Sound and Vibration*, 185(5):867–890, 1995.

[91] K. Shankar and A. J. Keane. A study of the vibrational energies of two coupled beams by finite element and green function (receptance) methods. *Journal of Sound and Vibration*, 181(5):801–838, 1995.

[92] K. Shankar and A. J. Keane. Vibration energy flow analysis using a substructure approach: the application of receptance theory to fem and sea. *Journal of Sound and Vibration*, 201:491–513, 1997.

[93] P. Shorter. *Combining Finite Elements and Statistical Energy Analysis.* PhD thesis, University of Auckland, July 1998.

[94] J. Signoprelli and A.H. von Flotow. Wave propagation, power flow, and resonance in a truss beam. *Journal of Sound and Vibration*, 126(1):127–144, 1988.

[95] C. Simmons. Structure-borne sound transmission through plate junctions and estimates of sea coupling loss factors using finite element method. *Journal of Sound and Vibration*, 144(2):215–227, 1991.

[96] E. Skudrzyk. The mean-value method of predicting the dynamic response of complex vibrators. *The Journal of the Acoustical Society of America*, 67(4):1105–1135, 1980.

[97] J.A. Steel. The prediction of structural vibration transmission through a motor vhicle using ststistical energy analysis. *Journal of Sound and Vibration*, 193(3):691–703, 1996.

[98] J.A. Steel and R.J.M. Craik. Statistical energy analysis of structure-borne sound transmission by finite element methods. *Journal of Sound and Vibration*, 178(4):553–561, 1994.

[99] Yung-Chang Tan, M.P. Castanier, and C. Pierre. Modal approximations of power flow between coupled component structures. *Proceedings ICSV-6, Copenhagen, Denmark*, pages 2315–2322, 1999.

[100] A.G. Troshin and M.A. Sanderson. Structural energy flow in a resiliently coupled t-shaped beam by wave intensity and mobility approaches. *Acustica, Acta Acustica*, 84:860–869, 1998.

[101] T.K. Tso and D.J. Norwood. Vibratory power transmission through three-dimensional beam junctions. *Journal of Sound and Vibration*, 185(4):595–607, 1995.

[102] N Vlahopoulos, X Zhao, and T Allen. An approach for evaluating power transfer coefficients for spot-welded joints in an energy finite element formulation. *Journal of Sound and Vibration*, 220(1):135–154, 1999.

[103] E.C.N. Wester and B.R. Mace. Statistical energy analysis of two edge-coupled rectangular plates: Ensamble averages. *Journal of Sound and Vibration*, 193(4):793–822, 1996.

[104] A. Wilson. Extended frequency range for finite element based vibration analysis. Master's thesis, Chalmers University of Technology, 1997.

[105] J.P. Wolf. *Finite-Element Modelling of Unbounded Media.* John Willey & Sons, 1996.

[106] The Math Works. *Matlab. The Language of Technical Computing*, volume Version 6. 2000.

# Power Flow and Structure-Borne Noise in Medium Frequency Range

**Marcin Wachulec**

*Thesis accepted for public defence in partial fulfillment of the degree of Doctor of Philosophy, PhD Aalborg University, September 27, 2002*

The present thesis deals with methods for power flow estimation that could be applied in the medium frequency range. Coupling of standard Finite Element Method (FEM) and the Statistical Energy Analysis (SEA) in a hybrid formulation is explored. The hybrid formulation requires partition of co-ordinates into sets corresponding with global and local motions. The hierarchical formulation of FEM is used to implement the hybrid approach. This gives the possibility to modify the calculations without making changes in the model. The hierarchical formulation has also additional properties that the high order co-ordinates behave in similar manner as the high order normal modes. The hierarchical formulation developed in this thesis allows for modelling plate assemblies in an efficient way.

Department of Civil Engineering ♦ Aalborg University ♦ Sohngaardsholmsvej 57 ♦ DK-9000 Aalborg

ISSN 1395-7953 R2002-1